

WHOLE-BODY BIOMECHANICAL LOAD MONITORING FROM ACCELEROMETRY IN TEAM SPORTS

NIELS JENSBY NEDERGAARD

A thesis submitted in partial fulfilment of the requirements of
Liverpool John Moores University for the degree of Doctor of Philosophy

November 2016

Abstract

Contemporary research into training load in team sports primarily focusses on the physiological load demands, whereas the biomechanical load still remains largely unexplored. While the former refers to the work-energy relationship when the players move around the pitch, the latter refers to the external forces the players are exposed to from their movements around the pitch. Monitoring of the biomechanical load helps practitioners estimate the stresses on an athlete's musculoskeletal structures as a consequence of the external forces acting on their body. Monitoring of the biomechanical load is currently restricted to laboratory settings, but the recent introduction of GPS devices with integrated accelerometers in team sports may enable practitioners to monitor whole-body biomechanical load during training sessions and match-play. The aim of this thesis was therefore to explore if body-worn accelerometry can be used for whole-body biomechanical load monitoring in team sports.

The first study of this thesis showed that although a linear relationship exists between body-worn accelerometry (e.g. from GPS integrated accelerometers) and whole-body accelerations, the linear relationship based on Newton's second law of motion is weak regardless of accelerometer location (trunk, pelvis or tibia). Body-worn accelerometry only measures the acceleration of the segment it is attached to and is therefore inadequate to measure the complex multi-segment dynamics of the whole body during team sports movements. The second study of this thesis did however offer a potential solution to that problem, and it was demonstrated that the complex multi-segment dynamics of the body and the associated ground reaction forces (GRF), a surrogate for whole-body biomechanical load, can be estimated with a mass-spring-damper model (MSD-model). Nonetheless, the MSD-model's accuracy to estimate GRF slightly decreases for sharp changes of direction at high intensities, because the absorption of energy and generation

of energy are decoupled. Finally, a novel approach to estimate GRF from the combination of trunk-mounted accelerometry and a MSD-model was introduced in this thesis. This approach showed that trunk accelerometry data has the potential to generate the eight model parameters required to estimate GRF from a MSD-model, though further work is required in particular towards improving the model's ability to estimate GRF across a wide range of activities.

The novel approach introduced in this thesis has the potential to give practitioners in team sports the opportunity to monitor whole-body biomechanical load due to player-ground interaction in the field, a necessity if they wish to predict the consequent musculoskeletal structural adaptations of training sessions and match-play.

Acknowledgement

John, Paul, George and Ringo are known as the Fab Four of Liverpool, but *Jos, Mark, Barry and Paulo* will for me always stand out as the fab four supervisor team of my PhD journey. I would like to take this opportunity to show my greatest appreciation for your support, feedback, enthusiasm and dedication in my work over the past three years.

Firstly, I would like to give my sincere appreciation to *Dr. Jos Vanrenterghem* and *Dr. Mark Robinson*. I appreciate the confidence you have shown in me as an individual and in my work and I am grateful that I have had the opportunity to observe and experience your dedication to biomechanics, research and your students. I would also like to thank my co-supervisors *Professor Barry Drust* for our informal meetings and reflections about training load and beyond, and *Professor Paulo Lisboa* for your ability to translate your mathematical knowledge to a level suitable for my mathematical abilities.

I would also like to acknowledge the Football Exchange for funding my PhD program. I would also like to express my gratitude to *Dr. Terence Ethcells* for the Matlab mass-spring-damper model script that has played such a central part of my PhD. My gratitude also goes out to *Dr. Ian Poole, Dr. Malcolm Hawken* and *Dr. Mark Lake* for your technical and general guidance on accelerometry. And of course a special thanks to all the postgraduate research students in the biomechanical laboratory, it has been a pleasure to share my PhD rollercoaster ride with all of you and follow your development as biomechanists.

Finally, I want to thank my parents *Vibeke* and *Kurt*, and my brother *Morten* for your endless support and belief in me throughout my life. You were the only ones that believed in me back in 2007 where my dream of a career in sports biomechanics seemed far away. I therefore want to dedicate this thesis to you. Tusind Tak!

Publications

Nedergaard, N.J., et al. (2015). “Player load monitoring from accelerometry in team sports: Is it time to take one step backwards to move two steps forward?” *The Sport & Exercise Scientist*. Issue 45, Autumn 2015.

Nedergaard, N. J., et al. (2016). “The relationship between whole-body external loading and body-worn accelerometry during team sports movements.” *International Journal of Sports Physiology and Performance*. (Epub ahead of print)

Nedergaard, N. J., et al. (*Under Review*). “Generalisability of a mass-spring-damper model to estimate ground reaction forces during team sports related movements.”

Conference publications/presentations

Nedergaard, N. J. “Player load monitoring in sport: Predicting centre of mass acceleration from body-worn accelerometry.” *The annual BASES Biomechanical Interest Group Meeting*, The University of Roehampton, UK, April 8th 2015.
(Award for Best Oral Presentation)

Nedergaard, N. J. “Player load monitoring in football: Does body-worn accelerometry predict centre of mass acceleration in football-related movements?” *The 8th World Congress on Science and Football*, Copenhagen, Denmark, 20th to 23rd of May 2015.
(Poster Presentation)

Nedergaard, N. J. “Player load monitoring in sport: Predicting centre of mass acceleration from body-worn accelerometry.” *The 25th Congress of the International Society of Biomechanics*, Glasgow, Scotland, 12th to 16th of July 2015.
(Poster Presentation)

Nedergaard, N. J. “A new approach to quantify whole-body mechanical load from trunk accelerometry.” *2nd ASPIRE Sport Science Conference “Monitoring Athlete Training Loads – The Hows and Whys”*, Doha, Qatar, 23rd to 25th of February 2016.
(Oral Presentation, Young Investigator Award)

Nedergaard, N. J. “A new approach to quantify whole-body mechanical load from trunk accelerometry.” *Faculty of Engineering & Technology Research Week 2016*, Liverpool, UK, 9th to 13th of May 2016.
(Award for Best Paper and 3rd Best Oral Presentation)

Table of contents

Abstract	ii
Acknowledgement	iv
Publications	v
Table of contents	vi
List of tables	viii
List of figures	x
Glossary of terms and abbreviations	xvii
Background	1
CHAPTER 1 Literature Review	5
1.1. Training load monitoring	6
1.2. Training load monitoring using GPS integrated accelerometry	12
1.3. Spring-mass modelling of the human body	21
1.4. Summary	32
1.5. Aim and objectives	33
CHAPTER 2 Estimating whole-body loading from body-worn accelerometry	34
2.1. Introduction.....	35
2.2. Methods	37
2.3. Results.....	42
2.4. Discussion.....	47
2.5. Conclusion	52
CHAPTER 3 Generalisability of a mass-spring-damper model for team sports movements	53
3.1. Introduction.....	54
3.2. Methods	56
3.3. Results.....	62
3.4. Discussion.....	67
3.5. Conclusion	71

CHAPTER 4 A new approach to predict biomechanical loading from trunk-mounted accelerometry	72
4.1. Introduction.....	73
4.2. Methods	75
4.3. Results.....	80
4.4. Discussion.....	97
4.5. Conclusion	102
CHAPTER 5 General Discussion	103
5.1. Summary.....	104
5.2. The challenges associated with the use of wearable sensor technology.....	105
5.3. Application of biomechanical load monitoring in team sports.....	107
5.4. Potential application in other load related studies	112
5.5. The relationship between external and internal biomechanical load.....	113
5.6. Recommendations for future research	114
5.7. General conclusion	118
References	119
Appendices.....	138
Appendix A: Laboratory accelerometers location relative to the GPS device.....	139
Appendix B: 1g static accelerometer calibration protocol.....	141
Appendix C: Synchronisation of GPS integrated accelerometer	143
Appendix D: Establishing accelerometer filter cut-off frequency in Chapter 2....	145
Appendix E: Definition of the eight natural MSD-model parameters	148
Appendix F: Establishing study specific search parameters.....	150
Appendix G: Effect of filter cut-off frequency on accelerometer/MSD-model	151
Appendix H: Laboratory accelerometer as accelerometer/MSD-model input.....	154
Appendix I: Acceleration from trunk kinematics as MSD-model input.....	159
Appendix J: Sensitivity analysis of fixed model parameters on SSE_{GRF}	166
Appendix K: Sensitivity analysis of changing $GRF_{measured}$ model parameters.....	168
Appendix L: Foot-contact identification from GPS integrated accelerometry	170

List of tables

Chapter 1

Table 1.1: Summary of the findings from the studies validating GPS integrated accelerometry against golden standard GRF measurements..... 18

Chapter 2

Table 2.1: Peak Acc, Loading Rate and Impulse for all tasks (Run, Cut45, Cut90) and approach speeds (2-5 m·s⁻¹) for CoM accelerations and the four body-mounted accelerometers. The values presented are means ± standard deviations and n = 80 trails in total for each task.43

Table 2.2: Within task linear regression values (R²) for Peak Acc, Loading Rate and Impulse between the CoM acceleration and acceleration data from the individual accelerometers and multiple laboratory accelerometers.44

Chapter 3

Table 3.1: Mean ± standard deviation for SSE (N·kg⁻¹·ms⁻¹) for the individual tasks and approach speeds. Mean difference and 98.75% confidence interval (CI) of the difference in SSE between tasks and approach speeds (alpha = 0.0125) obtained from the two-way ANOVA and post-hoc analysis. 62

Table 3.2: Mean ± standard deviation and R² for the extracted GRF variables from the GRF_{measured} and GRF_{model} for the individual tasks and approach speeds..... 64

Table 3.3: Mean ± standard deviation of the eight model parameters for the individual tasks and approach speeds..... 66

Chapter 4

Table 4.1: Mean ± standard deviation for SSE_{Trunk} (g/frames) and SSE_{GRF} (N/kg/frames) for the individual tasks and approach speeds. Trials with SSE_{GRF} above 5000 were removed before mean and standard deviations was calculated for SSE_{GRF}, a total of 82 trials were removed (Run: 19 trials; Cut45: 30 trials; Cut90: 33 trials)..... 81

Table 4.2: Mean difference and 98.75% confidence interval (CI) of the difference in SSE_{Trunk} (g/frames) between tasks and approach speeds (alpha = 0.0125) obtained from the one-way ANOVA post-hoc analysis. 84

Table 4.3: Mean \pm standard deviation of the eight model parameters from the accelerometer/MSD-model for the individual tasks and approach speeds. 85

Table 4.4: Mean \pm standard deviation for SSE_{GRF} (N/kg/frames) for $GRF_{modelNP3}$, $GRF_{modelNP4}$ and $GRF_{modelNP5}$ across the individual tasks and approach speeds. Trials with SSE_{GRF} above 100 were removed before mean and standard deviations were calculated, the number of trials removed are indicated in brackets. 90

Table 4.5: Correlation (R^2) values from the linear regression analysis between the GRF variables from $GRF_{measured}$ and GRF_{NP3} and GRF_{NP5} respectively..... 93

Table 4.6: Mean \pm standard deviation for the GRF loading variables from $GRF_{measured}$ (bold font), GRF_{NP3} and GRF_{NP5} for the individual tasks and approach speeds..... 95

Appendices

Table A.1: Resultant peak accelerations measured with the GPS integrated accelerometer and the two laboratory accelerometers located on the anterior and posterior side of the GPS device..... 140

Table D.1: Resultant peak accelerations from the three laboratory accelerometers (Trunk, Pelvis and Tibia) with low-pass filter cut-off frequencies between 20-100Hz applied to the acceleration signal for the Run, Cut45 and Cut90 at 2 and 5 $m \cdot s^{-1}$ 146

Table L.1: Mean \pm standard deviations of the gravity corrected acceleration values (g) at touch down and take off from the GPS integrated accelerometers..... 170

List of figures

Background

Figure 1: Car analogy used to illustrate the difference between physiological and biomechanical load monitoring. The permission to reproduce the human skeletal images has been granted by iStock/LindaMariaB. 3

Chapter 1

Figure 1.1: The training load monitoring circle illustrating how subjective (coach) and objective (sports scientist) analysis is used to make decisions on training planning, match selection etc. 7

Figure 1.2: Remake of the model presented in Dye (2005) illustrating the relationship between tissue loading and structural adaption. The grey area illustrates the zone of supraphysiological overload which is reached with the right level of load volume and impact load. 9

Figure 1.3: Illustration of the attempt to separate the external and internal load of physiological and biomechanical load from each other and the associated adaptations (taken from Vanrenterghem et al., Under Review). 10

Figure 1.4: Example of a GPS device (MinimaxX S4, Catapult Sports) and its location on the upper trunk within a small pocket of a tight fitted vest. 13

Figure 1.5: Illustration of the simple spring-mass model, where l is the natural length of the spring, Δy is the displacement of the mass (m) and $l - \Delta y$ is the length of the compressed spring. 22

Figure 1.6: Illustration of the linear relationship between displacement of the mass (dashed grey line) and the GRF acting on the spring-mass model (black line). 23

Figure 1.7: Measured GRF (solid black line) and GRF estimated from a simple spring-mass model (dotted black line) for running and change of direction of 45° and 90°. The shared grey area illustrates the differences between the measured and modelled GRF. 26

Figure 1.8: Illustration of the MSD-model used by Derrick et al. (2000) to estimate GRF patterns and an example of the simulated GRF from this model (dotted black line) and the measured GRF (solid black line) for running. 28

Figure 1.9: The displacement, velocity and acceleration of the upper and lower mass for two running examples (example A: dotted grey line and example B: dotted black line). The bottom row display the measured GRF (solid black line) and simulated MSD-model GRF (dotted grey line) from the two examples.30

Chapter 2

Figure 2.1: Pictures displaying the position of the four body-mounted accelerometers, the red circles display the location of the three laboratory accelerometers (Trunk, Pelvis and Tibia).39

Figure 2.2: Representative examples of the resultant CoM acceleration and resultant acceleration from the Catapult and Trunk accelerometer for the Run, Cut45 and Cut90 at $5 \text{ m}\cdot\text{s}^{-1}$. All curves are normalised over the stance phase (%).42

Figure 2.3: SPM1D regression analysis of the Run task for the four body-worn accelerometers, all curves are normalised over the stance phase (%). The top row shows a representative acceleration from the four approach speeds and accelerometer locations for one participant. The second row shows the CoM acceleration, coloured according to the peak acceleration from the same participant for all trials. The third row shows the β curves from all participants. The specific β curve generated from the data in the second row is shown in black. The bottom row shows the statistical relationship (SPM{t}) between Peak Acc and CoM acceleration across the entire stance phase. Shaded areas indicate a significant relationship ($p < 0.0125$) between Peak Acc from the accelerometer and CoM acceleration.45

Figure 2.4: SPM1D regression analysis of the Cut45 task for the four body-worn accelerometers, all curves are normalised over the stance phase (%). See Figure 2.3 for a detailed explanation of the data displayed in the individual rows.46

Figure 2.5: SPM1D regression analysis of the Cut90 task for the four body-worn accelerometers, all curves are normalised over the stance phase (%). See Figure 2.3 for a detailed explanation of the data displayed in the individual rows.47

Chapter 3

Figure 3.1: Illustration of the MSD-model and a free-body diagram of the model.57

Figure 3.2: Flow-chart of the purpose built gradient descent optimisation routine used to estimate $\text{GRF}_{\text{model}}$59

Figure 3.3: The top row display the SSE history from the gradient descent optimisation. The second row display $GRF_{measured}$ and GRF_{model} calculated from the initial search parameters (ISparam) and the model parameters from iteration 0, 100, 300 and 500 (Itera). The polar plots in the bottom row display the model parameter history from the initial search parameters to iteration step 500 (in scaled dimensionless values). 60

Figure 3.4: Representative example of $GRF_{measured}$ (solid black line) and GRF_{model} (dotted grey line) and the associated SSE for the conditions investigated in this study. 63

Figure 3.5: Results from the Bland-Altman analysis, showing the mean difference (marker) and 95% limits of agreements (error bar) for the Run (solid square), Cut45 (solid circle) and Cut90 (open circle) across the different tasks and approach speeds. 65

Figure 3.6: Polar plots displaying the mean (black line and circles) and standard deviations (dotted grey line) of the model parameters (in scaled dimensionless values) across all conditions and for the individual tasks and approach speeds. 66

Figure 3.7: Examples of the MSD-models ability to estimate the range of different GRF patterns ($GRF_{measured}$ is the solid black line and GRF_{model} is the dotted grey line) observed in this study between participants, tasks and approach speeds. The SSE ($N \cdot kg^{-1} \cdot ms^{-1}$) and polar plots displaying the model parameters (in scaled dimensionless values) for the individual trials. 67

Chapter 4

Figure 4.1: Illustration of the accelerometer/MSD-model, where $TrunkAcc_{measured}$ is used to simulate the acceleration of the upper mass from which the eight natural model parameters are obtained required to predict GRF_{model} 77

Figure 4.2: Flow-chart of the gradient descent optimisation routine from which the eight model parameters were generated when $TrunkAcc_{measured}$ was used as model input. The model parameter sensitivity analysis is displayed with grey dashed lines. 78

Figure 4.3: Example of $TrunkAcc_{measured}$ (black line), a_1 (dashed grey line), $GRF_{measured}$ (black line) and GRF_{model} (dashed grey line) for the Run from a representative participant. The polar plots display the model parameters (in scaled dimensionless values) for the individual trials. 81

Figure 4.4: Example of $\text{TrunkAcc}_{\text{measured}}$ (black line), a_1 (dashed grey line), $\text{GRF}_{\text{measured}}$ (black line) and $\text{GRF}_{\text{model}}$ (dashed grey line) for the Cut45 from a representative participant. The polar plots display the model parameters (in scaled dimensionless values) for the individual trials.	82
Figure 4.5: Example of $\text{TrunkAcc}_{\text{measured}}$ (black line), a_1 (dashed grey line), $\text{GRF}_{\text{measured}}$ (black line) and $\text{GRF}_{\text{model}}$ (dashed grey line) for the Cut90 from a representative participant. The polar plots display the model parameters (in scaled dimensionless values) for the individual trials.	83
Figure 4.6: Polar plots displaying the mean model parameters (in scaled dimensionless values) across all tasks and for the individual tasks. The grey circles display the average model parameters for $\text{TrunkAcc}_{\text{measured}}$ and the black circles display average model parameters for $\text{GRF}_{\text{measured}}$ (Chapter 3).	86
Figure 4.7: Linear regression between $\text{TrunkAcc}_{\text{measured}}$ (horizontal axis) and $\text{GRF}_{\text{measured}}$ (vertical axis) model parameters. Each circle represents the participants mean within task parameters (Run: circle; Cut45: square and Cut90: diamond). Mean within task parameters outside the 95% prediction interval (dashed line) were not included in the regression analysis.	87
Figure 4.8: Displaying the five new model parameter combinations ($\text{GRF}_{\text{modelNP1-5}}$) and histograms of the SSE_{GRF} distribution for the different model parameter combinations. Representative examples of $\text{GRF}_{\text{measured}}$ (black line) and $\text{GRF}_{\text{modelNP1-5}}$ (dashed grey line) for the Run, Cut45 and Cut90 at an approach speed of $4 \text{ m}\cdot\text{s}^{-1}$	89
Figure 4.9: Examples of the $\text{GRF}_{\text{measured}}$ (black line), $\text{GRF}_{\text{modelNP3}}$ (dashed grey line), $\text{GRF}_{\text{modelNP5}}$ (dotted grey line) for the difference tasks and approach speeds from a representative participants. The SSE_{GRF} (N/kg/frames) and polar plots displaying the model parameters of the four model parameters that was not kept constant.	92
Figure 4.10: Results from the Bland-Altman analysis, showing the mean difference (marker) and 95% limits of agreements (error bar) for the Run (Circle), Cut45 (square) and Cut90 (diamond) across the different tasks and approach speeds calculated from $\text{GRF}_{\text{modelNP3}}$ (open marker) and $\text{GRF}_{\text{modelNP5}}$ (filled marker).	96

Chapter 5

Figure 5.1: Resultant gravity corrected trunk acceleration measured from a trunk-mounted accelerometer is displayed in top row, in which the solid black line indicate the individual foot-ground-contacts. The second row display the GRF_{model} predicted from the accelerometer/MSD-model and the bar plots in the bottom row display the sum and average values from player A (black) and B (grey) respectively for Impulse, Impact peak and Active peak..... 109

Appendices

Figure A.1: Pictures of the laboratory accelerometers location on the anterior (picture on the left) and posterior side (picture on the right) of the GPS device..... 139

Figure A.2: Two representative examples of the trunk acceleration measured from the GPS integrated accelerometer (Catapult) and the two laboratory accelerometers (Noraxon) from the single leg drop landing..... 140

Figure B.1: Pictures of the three laboratory accelerometers and two GPS integrated accelerometers mounted inside the calibration box used for the 1g static calibration.. 141

Figure B.2: Illustration of the change in acceleration of 2g when rotating an accelerometer 180° during the static 1g calibration protocol. 142

Figure C.1: Time synchronised (A) and vector scalar product synchronisation (B) example from one trial. 144

Figure C.2: Synchronised acceleration data from a representative example..... 144

Figure D.1: Resultant acceleration from the Trunk, Pelvis and Tibia for a representative Run, Cut45 and Cut90 trial at 5 m·s⁻¹ with different low-pass filter cut-off frequencies applied to the acceleration signal. 145

Figure E.1: Illustration of the MSD-model and its free-body diagram. 148

Figure G.1: Polar plots displaying the mean task model parameters (in scaled dimensionless values) for $GRF_{measured}$ (Chapter 3) and the GPS integrated accelerometer (Catapult) with different cut-off frequencies. 152

Figure G.2: Representative examples of the of the measured trunk acceleration when different low-pass filter cut-off frequencies were applied to the GPS integrated accelerometer data (black line) and a_1 for the associated acceleration signals (dashed grey line).	153
Figure H.1: Representative examples of the measured trunk acceleration from the laboratory accelerometer (black line) and a_1 (dashed grey line).	155
Figure H.2: Polar plots displaying the mean model parameters (in scaled dimensionless values) for the individual conditions. The dark grey squares display the laboratory accelerometer model parameters, the light grey circles display the GPS integrated accelerometer model parameter from Chapter 4 and the black circles display the $GRF_{measured}$ model parameters from Chapter 3.	156
Figure H.3: Linear regression between laboratory accelerometer (horizontal axis) and $GRF_{measured}$ (vertical axis) model parameters. Each circle represents the participants mean within task parameters (Run: circle; Cut45: square and Cut90: diamond). Mean within task parameters outside the 95% prediction interval (dashed line) were not included in the regression analysis.	157
Figure H.4: Representative examples of the $GRF_{measured}$ (black line) and $GRF_{modelNP3}$ when GPS integrated accelerometer data (dashed grey line) and laboratory accelerometer data (dotted grey line) were used as accelerometer/MSD-model input.	158
Figure I.1: Pictures displaying the marker set used to measure the three-dimensional kinematics of the trunk segment. C7, Sternum, Xiphoid process and T8 (red circles) were used as tracking markers.	159
Figure I.2: Representative examples of the vertical trunk acceleration measured from trunk kinematics (black line) and a_1 when trunk kinematics (dashed grey line) and GPS integrated accelerometry (dotted grey line) were used as MSD-model input.	160
Figure I.3: Representative examples of $GRF_{measured}$ (black line) and GRF_{model} (dashed grey line) when vertical trunk acceleration from trunk kinematics was used as MSD-model input.	161

Figure I.4: Polar plots displaying the mean model parameters (in scaled dimensionless values) for the individual conditions. The dark grey squares display the parameters from vertical trunk acceleration, the light grey circles display the GPS integrated accelerometer parameters from Chapter 4 and the black circles display the $GRF_{measured}$ parameters from Chapter 3. 162

Figure I.5: Linear regression between vertical trunk kinematic (horizontal axis) and $GRF_{measured}$ (vertical axis) model parameters. Each circle represents the participants mean within task parameters (Run: circle; Cut45: square and Cut90: diamond). Mean within task parameters outside the 95% prediction interval (dashed line) were not included in the regression analysis. 163

Figure I.6: Representative examples of the $GRF_{measured}$ (black line), $GRF_{modelNP}$ (dotted grey line) and GRF_{model} (dashed grey line) when vertical trunk acceleration measured from trunk kinematics was used as MSD-model input for the difference tasks and approach speeds. 164

Figure J.1: The top row display the new model parameter combinations (NP), where the open circles indicate that the parameters were kept constant using the average task parameters found in Chapter 3, and the open squares indicate that the model parameters were kept constant using the average parameter value of the individual conditions. The second row display the histograms of the SSE_{GRF} distribution and the bottom row display the average SSE_{GRF} across tasks (All) and for the individual tasks. 167

Figure K.1: Displaying the effect of changing one parameter on GRF_{model} for four different GRF patterns from the same participant..... 169

Glossary of terms and abbreviations

a_1:	Acceleration of the mass-spring-damper models upper mass
a_2:	Acceleration of the mass-spring-damper models lower mass
Accelerometer/MSD-model:	Accelerometer mass-spring-damper model
Cut45:	Anticipated 45° open side-cut
Cut90:	Anticipated 90° open side-cut
CoM:	Centre of mass
GPS device:	Wearable global positioning system device with integrated accelerometer used in team sports
GRF:	Ground reaction force
GRF_{measured}:	Measured ground reaction force from a force platform
GRF_{model}:	Estimated ground reaction force from the mass-spring-damper model
GRF_{modelNP}:	Estimated ground reaction force from the accelerometer mass-spring-damper model with new/modified model parameters
m_1:	Mass of the mass-spring-damper models upper mass
m_2:	Mass of the mass-spring-damper models lower mass
MSD-model:	Mass-spring-damper model
p_1:	Position of the mass-spring-damper models upper mass
p_2:	Position of the mass-spring-damper models lower mass
PlayerLoadTM:	Accelerometer derived variable summarising the instantaneous rate of change in acceleration
RPE:	Rate of perceived exertion
Run:	Straight line running
SPM1D:	One-dimensional statistical parametric mapping
SSE:	Sum of square errors
SSE_{GRF}:	Sum of square errors between measured and model ground reaction force
SSE_{trunk}:	Sum of square errors between measured trunk acceleration and the acceleration of the mass-spring-damper models upper mass
TrunkAcc_{measured}:	Resultant gravity corrected acceleration measured from a trunk-mounted accelerometer
v_1:	Velocity of the mass-spring-damper models upper mass
v_2:	Velocity of the mass-spring-damper models lower mass
λ:	Mass ratio of the mass-spring-damper models lower mass relative to the participants total mass
ζ:	Damping ratio of the damper in the mass-spring-damper model
ω_1^2:	Natural frequency of the mass-spring-damper models upper spring
ω_2^2:	Natural frequency of the mass-spring-damper models lower spring

BACKGROUND

Researchers and practitioners have had a longstanding interest in monitoring and understanding athletes' training load (the volume, frequency and intensity of their training). Monitoring training load has in the first place enabled researchers and practitioners to understand how adjustments in training load can lead to improved performance. The first model of the relationship between training load and performance was proposed in the mid 1970's where it was suggested that performance depends on the athlete's fitness and fatigue, and increased fatigue was associated with decreased performance and increased injury risk (Banister et al., 1975). Though the field of training load monitoring has grown substantially since then, modern training load monitoring still builds on the principles suggested by Bannister et al. (1975) where the physiological aspect of training load monitoring is the main focus when pursuing performance enhancement as well as injury prevention.

The physiological aspect of training load monitoring is governed by monitoring the relationship between the work performed by the athletes from voluntary skeletal muscle contractions to move their body around the field and the energy (with or without oxygen uptake) needed to complete the required work. This work-energy relationship has been extensively monitored in professional athletes and more recently gone from heart rate monitoring to GPS position tracking in team sports. GPS data can monitor the external work generated by the athlete (e.g. distance covered and running velocity) and the associated energy demands. In other words, if the body were considered as a car then it monitors fuel consumption based on the athlete's velocity and distance travelled. This can help scientists and practitioners to make sure the athlete is able to cope with the energetic demands and make time for recovery (refuelling) when needed. Despite the introduction of technologies such as GPS, and an increased emphasis on training load monitoring in professional team sports such as basketball, football and rugby, the injury

rates in professional team sports remain unchanged (Dick et al., 2007; Ekstrand et al., 2013; King et al., 2010). Therefore, a shift in focus may be required.

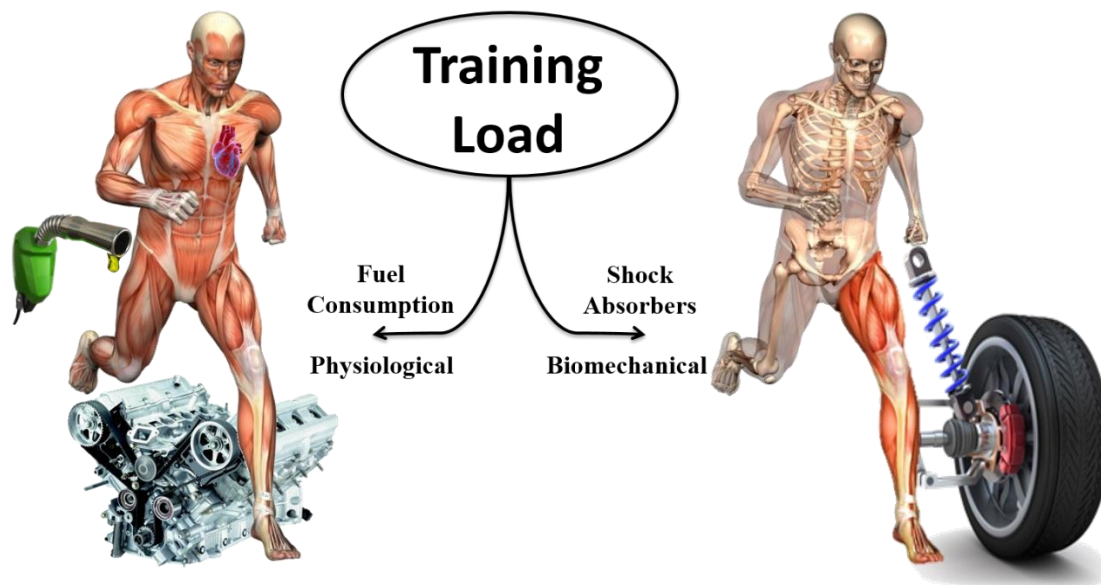


Figure 1: Car analogy used to illustrate the difference between physiological and biomechanical load monitoring. The permission to reproduce the human skeletal images has been granted by iStock/LindaMariaB.

Keeping the car analogy, the athlete's soft tissues (bones, cartilage, muscles, tendons and ligaments) work as shock absorbers for the external forces that athletes are exposed to (Figure B.1). These shock absorbers undergo considerable stresses from the high forces they need to generate against the ground during accelerations and decelerations. Just as a high physiological load leads to an empty fuel tank, a high biomechanical load leads to wear and tear of the shock absorbers, which has been largely unexplored in the team sports. Whilst it seems logical that appropriate levels of biomechanical stress will lead to desirable bone and muscle adaptations, it remains pretty much unknown what constitutes 'appropriate' biomechanical load during training sessions and match-play in team sports. Similarly, excessive accumulated stresses over time with insufficient recovery will lead to undesirable damage of the soft tissues (overload/overuse injuries), or in the worst case scenario to acute injuries when the individual stresses are simply too large for the soft tissues to resist. Monitoring of the biomechanical load to which team sports players are

exposed might therefore help to better understand the dose-response relationship between biomechanical load and overuse injuries in team sports. However, monitoring the biomechanical load imposed on a player's body is currently restricted to laboratory measurements and therefore remains very limited during training sessions and match-play.

A strong candidate for biomechanical load monitoring are accelerometers that can be integrated in the GPS devices worn by the players, considering that Newton's second law of motion ($F = m \cdot a$) offers a linear relationship between forces acting on the body and the net acceleration of the body. As promising as this sounds, it still remains largely unexplored if the accelerations measured with the GPS integrated accelerometers, typically attached to the torso, are related to the net acceleration of the whole body. If a linear relationship does not exist, one might have to explore other methods from which accelerations measured through trunk-mounted accelerometers can be used to monitor the external forces acting on team sports players during training sessions and match-play.

The seed for a highly innovative research venture was planted.

CHAPTER 1
Literature Review

The aim of this literature review is to provide the reader with information regarding the current literature on 1) training load monitoring and the differentiation between physiological and biomechanical load; 2) training load monitoring using GPS integrated accelerometry and its application for biomechanical load monitoring; 3) spring-mass models and the application of these to simulate whole-body acceleration of the human body during running. Finally, the aim and objectives of this thesis are outline at the end of this chapter.

1.1. Training load monitoring

This section of the literature review will cover the basic principles of training load monitoring and introduce the difference between physiological training load and biomechanical training load.

1.1.1. Evidence based training prescription

In team sports, the coaches and team of sports scientists analyse player performances during and after every match or training session, often based on subjective perceptions. The information gained from this analysis is used to make decisions about team selection, training periodisation, the mental and physiological status of the players, etc. (Akenhead and Nassis, 2016; Cummins et al., 2013; Impellizzeri et al., 2004). The coaching team uses this to plan aspects such as intensity, frequency or volume of the following training sessions. This plan is then implemented within an organisational structure and the training load monitoring cycle starts over again (Figure 1.1). The sports scientist's role in the training load monitoring cycle is to provide objective evidence of the players' performance or state. This objective analysis is expected to better inform the coach about changes in a player's performance and minimize some of the uncertainties of the coach's subjective analysis (Akenhead and Nassis, 2016; Cummins et al., 2013). Providing robust

and evidence based training load information is crucial to get the coach's "buy-in", as otherwise the objective analysis from the sports scientist easily becomes redundant.

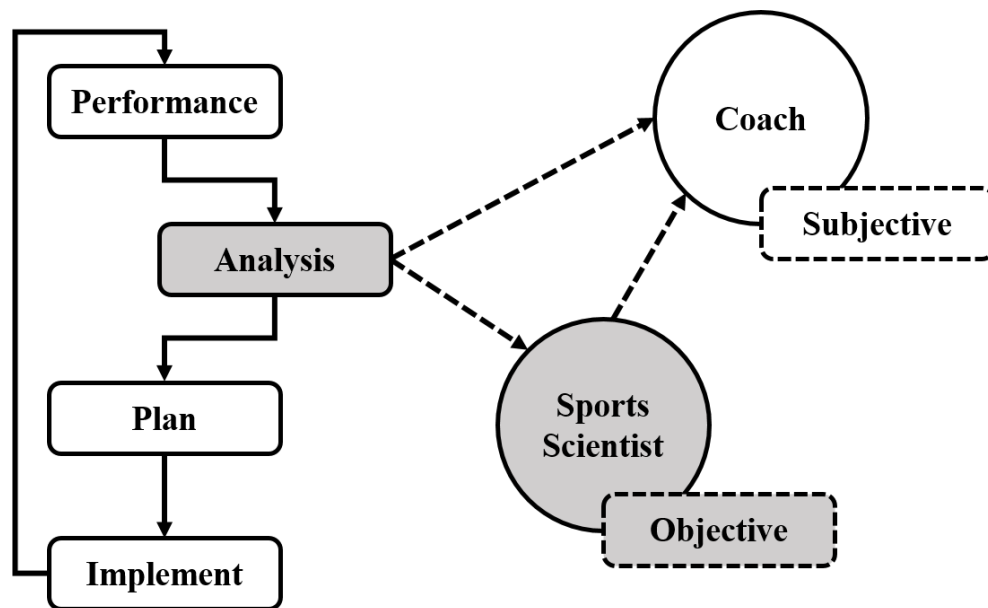


Figure 1.1: The training load monitoring circle illustrating how subjective (coach) and objective (sports scientist) analysis is used to make decisions on training planning, match selection etc.

1.1.2. Dose-response relationship of training

Coaches and sports scientists monitor their players on a daily basis to gain insight into the dose-response relationship of the prescribed training. Where the dose refers to the stresses imposed on the player and the response refers to the adaptation following the prescribed training (Banister et al., 1975; Impellizzeri et al., 2004; Lambert and Borresen, 2010). Understanding the dose-response relationship of training is the first step to provide evidence-based training prescription (Akubat et al., 2014; Busso, 2003). Since the response (adaptations) is dependent on the training dose (e.g. the intensity, frequency or volume), it is important that the level of the dose challenges the players to an appropriate level which will lead to positive adaptations. It is well-known that positive adaptations to the aerobic, cardiovascular and muscular systems follow the supercompensation principle in team sports (Meeusen et al., 2006). The positive adaptations are associated with

improvements in endurance, speed, strength and power, and thereby the player's performance (Busso, 2003). At the same time insufficient or excessive levels of training load can lead to negative adaptations that degenerate the cardiovascular and muscular systems which eventually can result in failure to the system such as injuries and illness (Soligard et al., 2016; Viru and Viru, 2000). Adjusting the training load through appropriate periodization, which combines adequate training stimuli with optimal recovery periods, is therefore of high importance for sports scientists to ensure the players reach the desired response/adaptations. The internal adaptation imposed from training, the so called internal load, is however very difficult to measure directly in the field and is therefore traditionally estimated from the external work completed by the player, the so called external load (Akubat et al., 2014; Impellizzeri et al., 2004). Monitoring the external load is therefore widely accepted as a method to gain insight into the internal load imposed on the body.

1.1.3. Physiological vs. biomechanical load monitoring

The body's soft tissues (bones, cartilage, muscles, tendons and ligaments) follow the same loading principles as the cardiovascular, metabolic, and muscular systems though this seems to have received less attention in training load monitoring. The principle is illustrated in Figure 1.2 where the load volume is dictated by the frequency, duration and intensity, and the impact load is a broad representation of joint load (Dye, 2005; Kibler et al., 1992). The dose-response relationship of training load can lead to undesirable damage to the soft tissues, either leading to overuse/overload injuries because of insufficient recovery, or (subsequently) to acute injuries when the load rapidly increases and the load becomes too large for the tissue. At the same time the right dose will lead to positive adaptations of the tissue (Dye, 2005; Kibler et al., 1992; Soligard et al., 2016).

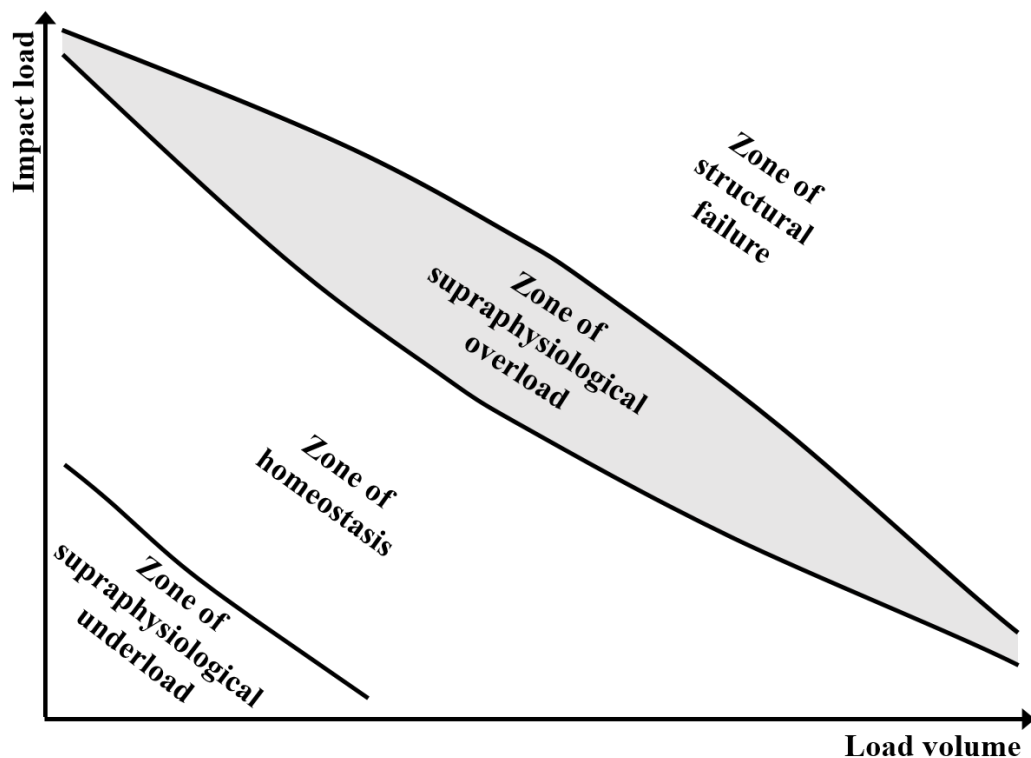


Figure 1.2: Remake of the model presented in Dye (2005) illustrating the relationship between tissue loading and structural adaptation. The grey area illustrates the zone of supraphysiological overload which is reached with the right level of load volume and impact load.

Measures of physiological training load in team sports have traditionally been related to the kinetic energy associated with a player's movement around the pitch. The external physiological training load is practically done by monitoring the distance covered and running velocity from GPS devices or semi-automated video tracking systems providing sports scientists with an estimate of the work done by the player (Cunniffe et al., 2009; Gaudino et al., 2014; Malone et al., 2015). The player's movement is a result of voluntary muscle contraction, where the muscle cells are stimulated with a nerve impulse from the brain resulting in an active muscle contraction. The muscle cells require energy for this contraction, either from energy already stored in the muscle cells or from the cardiovascular system's delivery of oxygen to the muscle cells. Heart rate monitoring has, due to its linear relationship with oxygen uptake (Hopkins, 1991), been used frequently as a measurement of the internal physiological training load in team sports (Drust et al., 2007), primarily through the Training Impulse (TRIMP) combining different measures of

heart rate (maximal, rest, average heart rate) and training duration (Morton et al., 1990). Heart rate is still the most commonly used measurement of the internal physiological training load in a field context despite daily variation (Bagger et al., 2003). Session duration dependent rating of perceived exertion (sRPE) has also been frequently used to estimate the internal physiological load in team sports (Foster, 1998; Gallo et al., 2015; Impellizzeri et al., 2004; Lovell et al., 2013). It appears that a number of methods successfully have been developed and implemented in team sports to monitor the external and internal physiological load in team sports and that researchers and practitioners should explore methods that can monitor the biomechanical load players are exposed to.

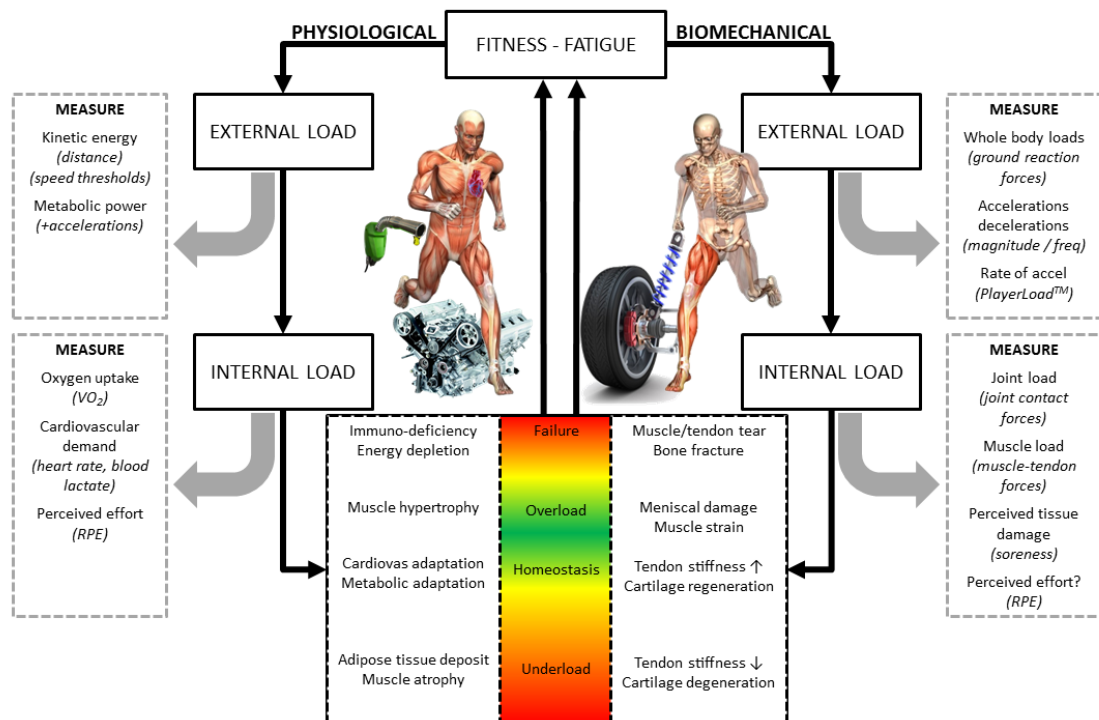


Figure 1.3: Illustration of the attempt to separate the external and internal load of physiological and biomechanical load from each other and the associated adaptations (taken from Vanrenterghem et al., Under Review).

When players move around the pitch they generate forces against the ground to accelerate and decelerate their body, however this comes with a cost because equal and opposite reaction forces from the ground (GRF) are acting on their body imposing a biomechanical load. As a consequence of the external forces from the ground, the body's soft tissues are

imposed to biomechanical stress as they absorb the external forces. The internal biomechanical load associated with external load is the joint contact forces and the muscle tendon forces (Figure 1.3). In vivo measurements of the internal forces are rare, as this will require direct measurements of the joint contact forces from force/pressure sensors integrated in the joint and therefore are seen only in patients with artificial knee or hip joint (D'Lima et al., 2007; Mundermann et al., 2008). The joint contact forces and muscle tendon forces are therefore typically estimated from inverse dynamics in biomechanics using musculoskeletal modelling systems such as AnyBody (Damsgaard et al., 2006) and OpenSim (Delp et al., 2007). However, these modelling systems currently require external measurements of the body's kinematics and/or kinetics to estimate the internal load. Three-dimensional motion capture systems, where a series of optoelectronics cameras are used to measure the movement of retroreflective markers positioned on anatomical landmarks (Winter, 2005), is for instance required to measure the three-dimensional kinematics of the body and therefore limits its application in applied sports settings. Though recent studies have shown promising results in using kinematics from full-body inertial sensor systems as model input in musculoskeletal modelling systems (Koning et al., 2015).

Measurements of the external GRF acting on the human body are typically taken from force transducers inbuilt to the ground (force platforms) which since its introduction in 1938 (Elfmann, 1938) has been considered as the gold standard to measure GRF (Winter, 2005). These are typically restricted to laboratory settings and can only measure the GRF from one foot-ground-contact, making the use of these in the field very limited. Measurements of the external GRF can also be obtained from other techniques such as insole pressure sensors (Jung et al., 2014) and full-body motion capture (Mapelli et al., 2014), but these also come with practical and technical constraints when applied in a field

setting. Another candidate for external biomechanical load monitoring in the field is accelerometry and in particular the GPS integrated accelerometers.

1.2. Training load monitoring using GPS integrated accelerometry

This section of the literature review will cover the use of GPS integrated accelerometry for training load monitoring in the current literature. This includes general information about the GPS integrated accelerometers as well as their current application for physiological and biomechanical training load monitoring.

1.2.1. Micro GPS sensor technology in team sports

Since its introduction in Australian football in the mid-2000s GPS devices has become a common training load monitoring tool in professional team sports. The literature on team sport players' activity profiles including measurements of total distance covered and running velocity (typically through different speed zones) has accordingly increased considerably over the last decade. Whereas the semi-automated video tracking systems such as Prozone are limited to match analysis, GPS technology has made it possible to monitor the energy demands of player's movements during training sessions (Aughey, 2011; Cummins et al., 2013; Dellaserra et al., 2014). The GPS technology is even allowed during games in Australian football and rugby, and more recently the international football federation (FIFA) has also allowed GPS technology in professional football. In other words, it looks like the GPS technology as a training load monitoring tool in professional team sports is here to stay.



Figure 1.4: Example of a GPS device (Minimax S4, Catapult Sports) and its location on the upper trunk within a small pocket of a tight fitted vest.

The GPS device has a total mass of 64 grams, 88 x 50 x 19 mm in dimension and is typically located on the upper trunk between the scapulae within a small pocket of a tight fitted elastic vest, see Figure 1.4. The GPS device's reliability and validity with specific focus on sampling frequency (currently at 10 Hz) has been extensively investigated in the current literature (Akenhead et al., 2014; Aughey, 2011; Coutts and Duffield, 2010; Jennings et al., 2010; Varley et al., 2012). Though the GPS devices have shown acceptable levels of accuracy and reliability of total distance covered during team sports movements (Coutts and Duffield, 2010; Jennings et al., 2010) its accuracy is compromised at high speeds, short distances, accelerations over $4 \text{ m} \cdot \text{s}^{-1}$, and when players frequently change their direction (Akenhead et al., 2014; Varley et al., 2012). Researchers and sports scientists have therefore turned their attention to the inertial measurement unit (IMU) integrated in the GPS device including a tri-axial accelerometer, gyroscope and magnetometer. The IMU can potentially provide better information about high intensity movements, sports specific movements (e.g. jumps and kicking) and the external forces from collisions with other players and from player-ground interaction and even allow monitoring during indoor sports which is not possible from the GPS measurements (Cummins et al., 2013; Dellaserra et al., 2014).

1.2.2. GPS integrated accelerometry

The recent advancement in IMU sensor technology has made it possible to manufacture low cost sensors which has increased the use of IMU to detect sports movements in individual and team sports such as tennis, weightlifting, swimming, baseball, handball and cricket (Chambers et al., 2015; Luteberget and Spencer, 2016). Though the IMU sensor integrated in the GPS device also includes a gyroscope and magnetometer, the accelerometer has gained considerably more attention than the other two sensors. Accelerometers measure the applied accelerations acting along one or three sensing axes, where the former is called a uni-axial accelerometer and the latter a tri-axial accelerometer. Though a number of different accelerometer types exist (e.g. piezo-resistive and piezoelectric accelerometers) the conceptual measuring principles are based on a spring-mass system. A sensing mass is attached to a suspension system, and the applied acceleration in the accelerometer is measured from the displacement of the mass along its reference axis (Mathie et al., 2004; Yang and Hsu, 2010). Accelerometers were first introduced in the 1950s to measure gait velocity and accelerations (Saunders et al., 1953) and have historically been used in physical activity monitoring to estimate energy expenditure, classify different movement patterns in daily life activities, identify risk of falls (Mathie et al., 2004; Yang and Hsu, 2010), or measure tibial shock acceleration during walking, running and jumping activities (Lafortune, 1991).

Accelerometry has been used in a number of ways in team sports, the raw GPS integrated accelerometer and/or gyroscope signal has for instance been used to successfully classify team sports movements (Wundersitz et al., 2015d) whereas contrasting results have been found in its ability to detect tackling/collisions in rugby and Australian football from automatic tackle/collision algorithms (Gabbett, 2013; Gastin et al., 2014; Kelly et al., 2012). Finally, a recent study has shown that raw GPS integrated accelerometer data

cannot be used to measure the average horizontal acceleration during high speed running (Alexander et al., 2016). The latter study confirms the limitation of the GPS integrated accelerometers to monitor players' kinetic energy demands as outlined in Figure 1.3 despite its successful application in physical activity monitoring. The most common use of accelerometry in team sports is to calculate the amount of accelerations as a measure of load, where a number of manufacturers have proposed to summarise the continuous accelerometer signal from the GPS integrated accelerometer as a modified vector magnitude. The different commercial GPS integrated accelerometer companies use different terminologies for the summarised vector magnitude (e.g. PlayerLoadTM from Catapult Sports and Body Load from GPSports Systems) where PlayerLoadTM is most commonly reported in the current literature. PlayerLoadTM is an arbitrary unit vector magnitude value expressed as the square root of the sum of the squared instantaneous rates of change in acceleration along each of the three accelerometer axes, divided by a scaling factor of 100 (Boyd et al., 2011), see Equation 1.1.

$$PlayerLoad^{TM} = \sum \sqrt{\frac{(a_{y1}-a_{y-1})^2+(a_{x1}-a_{x-1})^2+(a_{z1}-a_{z-1})^2}{100}} \quad [Equation 1.1]$$

Where a_x , a_y , a_z , is the instantaneous acceleration from the accelerometer's medial-lateral, anterior-posterior and vertical axis, respectively. Due to the single value nature of the summarised vector magnitude it has its clear advantages in applied team sports because it is very easy to collect and has therefore been used to investigate match and training demands in a range of team sports such as Australian football (Boyd et al., 2013; Kempton et al., 2015; Ritchie et al., 2016), basketball (Montgomery et al., 2010), football (Barrett et al., 2016a; Barron et al., 2014; Dalen et al., 2016), hockey (Polglaze et al., 2015), lacrosse (Polley et al., 2015), netball (Chandler et al., 2014; Cormack et al., 2014; Young et al., 2016) and rugby union (McLaren et al., 2016c). Recent studies have also explored

the relationship between the summarised vector magnitude obtained from the GPS integrated accelerometry and the risk of soft tissue injuries in Australian football (Colby et al., 2014) and football (Bowen et al., 2016; Ehrmann et al., 2016). The downside of the summarised vector magnitude is however that it is very difficult to interpret how the “shaking up” of the body is related to the internal training load. This is confirmed in the contrasting findings from studies exploring the relationship between PlayerLoad™ and fatigue (Barrett et al., 2016b; Page et al., 2015, 2016) and between PlayerLoad™ and external measurements of physiological load such as total distance covered (Casamichana et al., 2013; Polglaze et al., 2015) and internal physiological load such as oxygen uptake, heart rate (Barrett et al., 2014; Highton et al., 2016; Scanlan et al., 2014; Scott et al., 2013; Walker et al., 2016) and session duration dependent rating of perceived exertion (sRPE) (Casamichana et al., 2013; Gallo et al., 2015; Gaudino et al., 2015; Gomez-Piriz et al., 2011; Lovell et al., 2013; Scanlan et al., 2014; Scott et al., 2013). Taking a step backwards exploring the potential of the raw accelerometer data is therefore needed to fulfil the GPS integrated accelerometers prospective in a training load context.

A number of recent studies have explored the GPS integrated accelerometers reliability and validity during laboratory and field tests (Barrett et al., 2014; Boyd et al., 2011; Kelly et al., 2015). The variable PlayerLoad™ has for example shown moderate to high reliability across tasks performed at different speeds (Barreira et al., 2016) and moderate to high within-subject reliability regardless of accelerometer position (upper and lower trunk), whereas large between-subject variance in PlayerLoad™ has been observed, indicating that between-player comparisons should be made with caution (Barreira et al., 2016; Barrett et al., 2014). Recent studies have found contradicting results for the GPS integrated accelerometer’s ability to measure peak accelerations; the GPS integrated accelerometer underestimated peak accelerations when tested against a reference

accelerometer, particularly during high frequency movements (Kelly et al., 2015; Lake et al., 2014), whereas it overestimated peak acceleration when tested against acceleration data obtained from three-dimensional motion analysis systems (Wundersitz et al., 2015a; Wundersitz et al., 2015b; Wundersitz et al., 2015c). The overestimation could be caused by the poor quality “fixing” of the accelerometer to the trunk resulting in unwanted high-frequency artefacts in the data. The application of a low-pass filter has for instance shown to improve the validity though the optimal filtering is yet to be established (Wundersitz et al., 2015a; Wundersitz et al., 2015b; Wundersitz et al., 2015c; Wundersitz et al., 2013).

1.2.3. Biomechanical load monitoring from GPS integrated accelerometry

The use of GPS integrated accelerometry for biomechanical load monitoring in team sports is based on Newton’s second law of motion ($F = m \cdot a$), with a common assumption that the acceleration from the trunk-mounted accelerometer is equal or very similar to the whole body acceleration. Whereas the GPS integrated accelerometer ability to monitoring physiological load has been explored extensively in the current literature, its ability to monitor whole-body biomechanical loading remains largely unexplored. In fact, this is limited to three studies in the current literature, where trunk acceleration from GPS integrated accelerometers has been validated against GRF from force platforms (Table 1.1). In two of these studies vertical and resultant peak acceleration data from GPS integrated accelerometers were compared with GRF measurements during jumping/landing tasks (Tran, 2010) and running/change of direction tasks (Wundersitz et al., 2013). Both studies showed that the GPS integrated accelerometers significantly overestimated peak resultant GRF. Both studies found that the overestimation was reduced when a low-pass filter of 10-25 Hz was applied to the accelerometer data removing high frequency signal noise (likely due to movement of the unit/vest relative to the trunk).

Table 1.1: Summary of the findings from the studies validating GPS integrated accelerometry against golden standard GRF measurements.

Author (year)	Participants (N)	Acceleromete/ Force plate	Task	Dependent variable	Findings
Tran et al. (2010)	10	SPI Pro from GPSports	DLAND from 30, 40 and 50 cm heights	Peak vertical and resultant acceleration	↑ DLAND and CMJ 16.8 – 30.8% (r_p : 0.45 – 0.56)
		A portable force plate (model ACG) from Advanced Mechanical Technologies	CMJ	Filtered acceleration data (20 Hz low-pass filter)	Filtered data ↑ DLAND and CMJ 10.9 – 22.2% (r_p : 0.55 – 0.70)
Wundersitz et al. (2013)	17	SPI Pro from GPSports	Running and COD (45°, 90°, and 180°)	Peak vertical and resultant acceleration	↓ Vertical acceleration for running and all COD (r_s : -0.26 – 0.33)
		In-ground force plate (BP600900) from Advanced Mechanical Technology	Velocities ranged from 2.5 to 7.4 m·s ⁻¹	Filtered acceleration data (10 - 25 Hz low-pass filter)	↑ Resultant acceleration for running and all COD (r_s : 0.00 – 0.48)
					Filtered data ↓ Vertical acceleration for running and all COD (r_s : -0.26 – 0.39)
					↑ Resultant acceleration for running and all COD (r_s : 0.23 – 0.76)
Hollville et al. (2015)	14	MinimaxX S4 from Catapult	General team sports movements		
		One on the upper trunk & one at the lower trunk	A running start	PlayerLoad™	Upper back ↑ 43.3 – 95.6% for all tasks (r_p : 0.74 – 0.90)
		6 individual Kistler force plates (KI 9067) connected in series	A simulated 1x1 All at both high and low intensities		Lower back ↑ 78.7 – 113.8% for all tasks (r_p : 0.77 – 0.93)

↑: Overestimate; ↓: Underestimate; DLAND: Drop landings; CMJ: Countermovement jumps; r_p : Pearson r-value; COD: Change of direction; r_s : Spearman's correlation coefficient.

Contrasting results were however found when vertical acceleration was compared to vertical GRF (vGRF), as it overestimated vGRF for the landing/jumping tasks (Tran, 2010) but underestimated vGRF for the running/change of direction tasks (Wundersitz et al., 2013). These contrasting findings are most likely because the accelerometer measures the acceleration in its own local coordinate system, and although the vertical axis of the accelerometer is the same as the vertical axis of the GRF when the participant is standing still, this would not be the case when the participant is performing changes of directions where the trunk is often leaning forward. Nonetheless, it was concluded that the GPS integrated accelerometers could measure whole-body impact peaks from the collision with the ground during team sports activities with reasonable accuracy when a 10-20 Hz low-pass filter was applied to the accelerometer data (Tran, 2010; Wundersitz et al., 2013). The optimal filtering frequency is yet to be established which can prove to be difficult as the optimal filtering frequency will depend on sports, task and intensity.

In a more recent study the traditional output variable from the GPS integrated accelerometer when used in the field (PlayerLoad™) was compared with PlayerLoad™ calculated from multiple force platforms during typical running related team sports movements (Hollville et al., 2015). Though PlayerLoad™ calculated from the upper trunk accelerometer overestimated PlayerLoad™ calculated from the GRF by as much as 43.3-58.0% for low intensity activity and 52.4-95.6% for high intensity activities, moderate to strong correlations (0.74-0.90) were found between the accelerometer and GRF data. In addition even larger overestimations were found for a GPS integrated accelerometer positioned on the lower part of the trunk, at the level of the posterior superior iliac spines, (78.7-113.8%) but with similar correlations (0.77-0.93) across the different tasks and intensities (Hollville et al., 2015). The higher PlayerLoad™ observed from the lower trunk-mounted accelerometer is similar to observations from previous studies that have

explored the effect of GPS integrated accelerometer location and PlayerLoad™ during 90 minutes of simulated football (Barrett et al., 2014; Barrett et al., 2016b). Similar results were found for treadmill and overground running at different running intensities, when accelerations of the upper and lower trunk were measured with a similar 100 Hz tri-axial accelerometer (Kawabata et al., 2013).

The discrepancy between trunk-mounted accelerometer data and GRF is expected as the impact acceleration from the foot colliding with the ground is attenuated as it travels up along the body (Lafortune et al., 1996). The location of the accelerometer is therefore likely to influence the relationship with whole-body loading. The relationship may also be influenced by the type of activity and intensity of the activity. Accelerometers located at the hip have for example demonstrated an acceptable association with the GRF, during daily life activities (Meyer et al., 2015; Rowlands and Stiles, 2012), and accelerometers located at the hip and tibia have shown a strong association with GRF in vertical jumping (Elvin et al., 2007; Setuain et al., 2016). Not only is the magnitude of the accelerometer signal influenced by the position of the accelerometer, the acceleration pattern also differs. Differences in the medial/lateral acceleration pattern from an upper and lower trunk-mounted accelerometer have also been observed during running (Kawabata et al., 2013). The difference in segmental acceleration from different accelerometer locations and whole-body acceleration from force platforms is therefore a combination of the attenuation of the acceleration magnitude and changes in acceleration pattern. Nonetheless it still remains uncertain which segmental accelerations and accelerometer locations would better relate to whole-body biomechanical loading (GRF) during typical team sports movements.

1.3. Spring-mass modelling of the human body

Spring-mass models has successfully been used to estimate the whole-body acceleration and the associated GRF acting on the human body during running. If a direct relationship does not exist between body-worn accelerometry and whole-body acceleration, researchers might seek inspiration from the biomechanical literature on spring-mass models. A brief literature review on the current use of spring-mass models in sports science is therefore provided in the following section. Though a number of different spring-mass models exist, this literature review will focus on the most commonly used spring-mass models, i.e. consisting of a single mass and a spring, and a mass-spring-damper model consisting of spring-mass model on top of another mass in series with a spring-damper system.

1.3.1. The “bouncing” nature of running

During running the human body follows a spring-like behaviour where elastic energy is absorbed and re-generated as the body’s CoM moves down and up. During the contact phase elastic energy is absorbed and re-generated by the body’s soft tissues (bones, cartilage, ligaments, tendons, muscles), where the energy is absorbed when the tissue is compressed/stretched and returned as it recoils (Cavagna et al., 1964; Farley and Gonzalez, 1996). As the body’s CoM moves downwards during the first half of the stance phase elastic energy is stored in the legs’ soft tissues. In the second half of the stance phase the stored energy is released and the CoM is moved upwards again as the soft tissues recoil the stored energy accelerating the body into the next step (Blickhan, 1989; Farley and Gonzalez, 1996; McMahon and Cheng, 1990). As a result of the storage and return of energy the body bounces along the ground during running, similar to a person hopping on a pogo stick, where the spring stores and returns the mechanical energy.

The spring-like behaviour of the human body is however dependent on movement and frequency of the movement (Farley et al., 1991; McMahon and Cheng, 1990). This is for example the case when hopping at low frequencies because the maximal force is reached before the body reaches its maximal vertical displacement (Farley et al., 1991). This violates the assumption of a 100% elastic system because the storage and return of elastic energy is not equal. Similarly, the body does not follow the spring-like behaviour during walking because the CoM is at its highest at the middle of the stance phase (Cavagna et al., 1976; McMahon and Cheng, 1990).

1.3.2. Spring-mass model

A simple spring-mass model, consisting of a single mass representing the CoM on top of a mass-less linear spring (Figure 1.5), has been successful in describing and predicting CoM movement and GRF of running humans and animals (Alexander, 1984; Blickhan, 1989; McMahon and Cheng, 1990). The force acting on the model is equal to the force in the spring, which according to Hooke's law is proportional to the ratio of the compression/extension and the natural length of the spring. In this case, the compression of the spring is caused by the mass, and the amount of compression is linearly related to the stiffness of the spring.

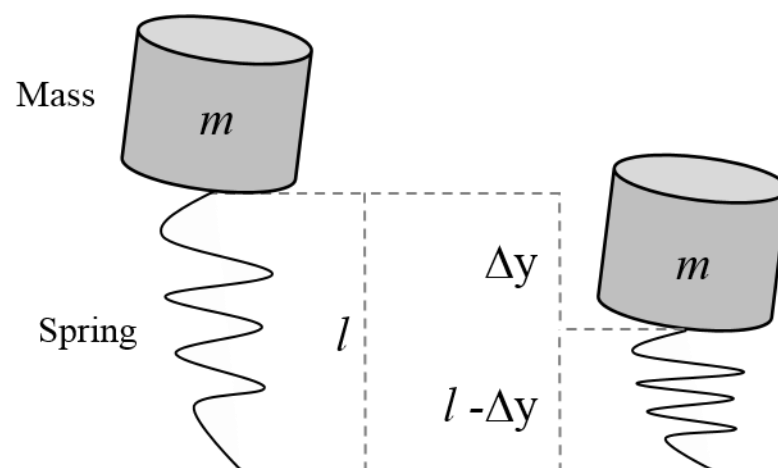


Figure 1.5: Illustration of the simple spring-mass model, where l is the natural length of the spring, Δy is the displacement of the mass (m) and $l - \Delta y$ is the length of the compressed spring.

The GRF acting on the model (GRF_{model}) can therefore be described as in Equation 1.2

$$GRF_{model} = k(l - \Delta y) + mg \quad [\text{Equation 1.2}]$$

Where, k is the spring constants, l is the natural length of the spring when it is under no external load, $(l - \Delta y)$ is the length of the compressed spring, m is the mass and g is the acceleration due to gravity. The linear relationship between GRF_{model} and the displacement of the mass Δy for this spring-mass model is displayed in Figure 1.6. The displacement of the mass is dependent on the mass and the stiffness of the spring (k).

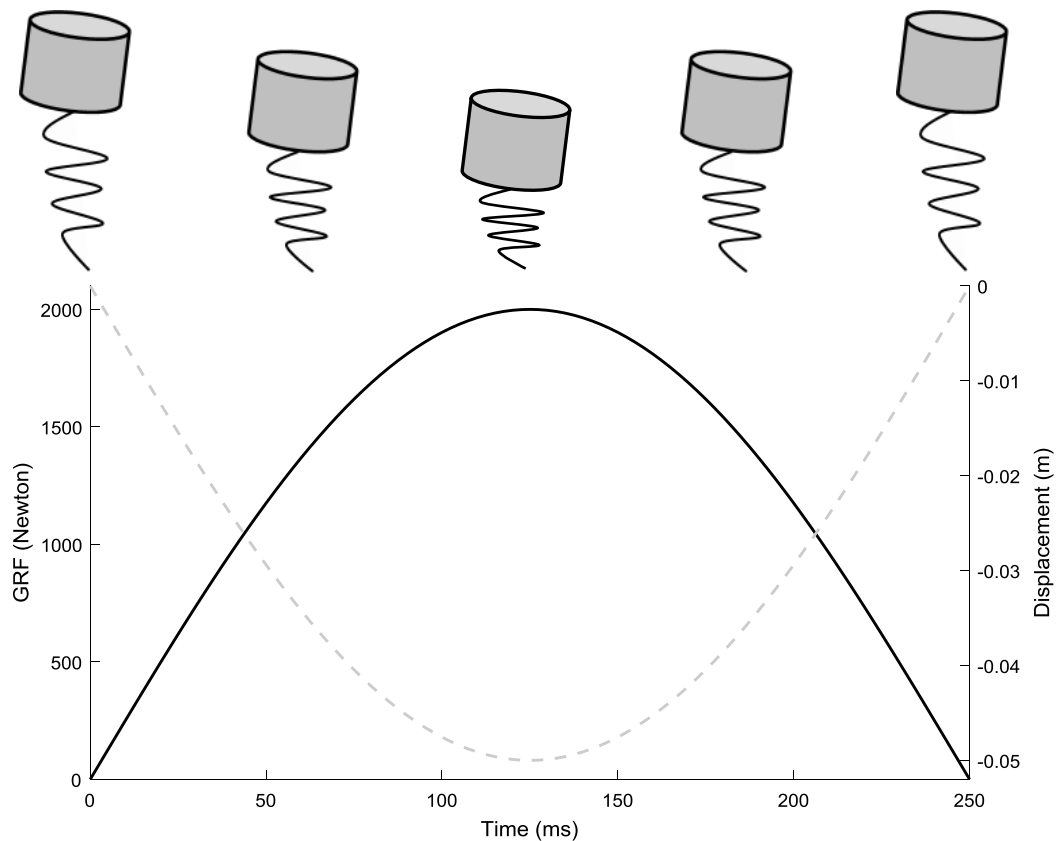


Figure 1.6: Illustration of the linear relationship between displacement of the mass (dashed grey line) and the GRF acting on the spring-mass model (black line).

Vertical and leg stiffness are inarguably the most widely used output variables from the simple spring-mass model. The biggest difference between the two is that the vertical

stiffness (k_{ver}) only represent the 1D vertical stiffness whereas leg stiffness (k_{leg}) is a 2D stiffness representing the stiffness of the leg/spring as the angle between the leg/spring and the ground changes during the contact phase. k_{ver} is calculated from the maximum GRF (GRF_{max}) divided by the maximal CoM displacement (Δy_{max}) and k_{leg} is defined as GRF_{max} divided by the maximal vertical displacement of the leg/spring (ΔL_{max}), see Equation 1.3 and 1.4 (Zadpoor and Nikooyan, 2010).

$$k_{ver} = \frac{GRF_{max}}{\Delta y_{max}} \quad \text{[Equation 1.3]}$$

$$k_{leg} = \frac{GRF_{max}}{\Delta L_{max}} \quad \text{[Equation 1.4]}$$

1.3.3. Current application of spring-mass models

Spring-mass models have been used since the late 1980s to explore how changes in running mechanics relate to energy cost and performance. McMahon et al. (1987) showed that running with increased knee flexion reduced k_{ver} and though this was associated with an attenuation in the impact forces, it increased the oxygen consumption by as much as 50% (McMahon et al., 1987). A number of studies have since explored the change in k_{ver} and/or k_{leg} and fatigue during exhaustive running (Dalleau et al., 1998; Dutto and Smith, 2002; Fourchet et al., 2015; Rabita et al., 2013), middle distance running (Girard et al., 2013) and mountain ultra-marathon races (Degache et al., 2016; Morin et al., 2011). In addition, a number of studies have within recent years explored the relationship between spring stiffness and sprint performance using the spring-mass model approach (Arampatzis et al., 1999; Girard et al., 2016a; Girard et al., 2016b; Girard et al., 2011; Hobara et al., 2010; Morin et al., 2006; Taylor and Beneke, 2012).

The simple spring-mass model has more recently been adopted to team sports, where vertical trunk accelerometry from GPS devices have been used to determine contact time

(t_c) and flight time (t_f) from which k_{ver} is calculated following the spring-mass model approach by Morin et al. (2005). See Equation 1.5 and 1.6, where g is the gravitational acceleration and m the mass of the participant.

$$GRF_{max} = m \cdot g \cdot \frac{\pi}{2} \cdot \left(\frac{t_f}{t_c} + 1\right) \quad [\text{Equation 1.5}]$$

$$\Delta y_{max} = \frac{GRF_{max} \cdot t_c^2}{m \cdot \pi^2} + g \cdot \frac{t_c^2}{8} \quad [\text{Equation 1.6}]$$

This approach has been used to estimate the CoM movement, GRF and k_{ver} when running on different surfaces such as natural grass and sand (Gaudino et al., 2013) and to explore induced lower-limb imbalance during running (Buchheit et al., 2015). One of the studies showed that k_{ver} can be estimated successfully with the trunk accelerometry spring-mass model approach and potentially give insight into monitoring of neuromuscular fatigue in team sports (Buchheit et al., 2015). The same study also explored the lower-limb imbalance between a taped and non-taped ankle. A large effect of taping was seen as t_c , t_f and k_{ver} increased for the taped leg when these were measured on a treadmill with instrumented force transducers. This effect was also observed in the trunk accelerometry data for t_c and k_{ver} , though the increase was not as high and the t_f data was reported as unclear (Buchheit et al., 2015). The latter illustrates that the combination of trunk accelerometry data and spring-mass models potentially can provide useful insight into biomechanical load monitoring and its relationship with injuries.

1.3.4. Limitations of the simple spring-mass model

Though this simplistic modelling of the human body in motion where the GRF is simulated as a half sine-wave, has been applied in a large range of sports and contexts as illustrated in the previous paragraph, it obviously has limitations in estimating the asymmetric GRF patterns, i.e. patterns in which the rising part is not equal to the falling

part of the GRF profile. Though GRF patterns from forefoot running in many cases are similar to the symmetric half sine-wave, it often deviates from the symmetric pattern. In fact, variables such as running speed (Clark et al., 2014; Clark and Weyand, 2014), foot-strike and footwear (Clark et al., 2014; Lieberman et al., 2010) and even the level of the athlete (Clark and Weyand, 2014) have all shown to affect the GRF pattern. The collision between the foot and ground causes a high frequency impact peak in the initial GRF pattern which the simple spring-mass model is not able to estimate (Bobbert et al., 1992), see Figure 1.7.

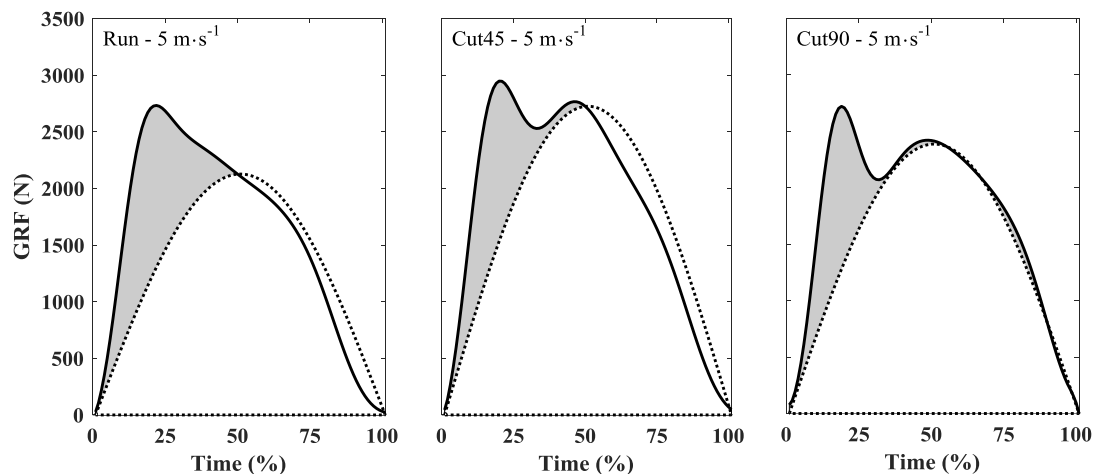


Figure 1.7: Measured GRF (solid black line) and GRF estimated from a simple spring-mass model (dotted black line) for running and change of direction of 45° and 90°. The shared grey area illustrates the differences between the measured and modelled GRF.

Studies have shown that the spring-mass model estimates the active peak (2nd GRF peak) but neglects the impact peak (Bullimore and Burn, 2007). In a recent study it was demonstrated that competitive sprinters deviated (higher impact GRF) significantly more from the simple half sine-wave GRF pattern than non-competitive sprinters for running speeds at 5, 7 m·s⁻¹ and their individual top speed. It was therefore concluded that the simple spring-mass model has limited application in analysis of sprint performance in competitive sprinters (Clark and Weyand, 2014). Similarly, the application of the simple

spring-mass model in a biomechanical loading context is limited because it neglects the GRF impact peak which for instance has been associated with the development of overuse musculoskeletal injuries in long distance runners (Hreljac, 2004; Nigg et al., 1995).

1.3.5. Multi-body models

Multi-body models consisting of two or more masses have been proposed to better estimate the multi-segment dynamics of the human body during running activities (Nikooyan and Zadpoor, 2011). These multi-body models build on the theoretical framework presented by Alexander et al. (1986) which demonstrated that multi-body models were capable of predicting both the impact and active GRF peak observed in running animals (Alexander et al., 1986). This multi-body model consisting of a spring-mass on top of another spring-mass, where the upper spring-mass represents the upper body and the lower spring-mass represents the foot/lower limb. This model has been used to explore the mechanical properties of the human heel pad (Ker et al., 1989) and to estimate GRF during forefoot and rear-foot running at different running velocities (Clark et al., 2014). Alexander et al. (1986) did however demonstrate that the double spring-mass model could go into oscillation due to the impact from the ground. A damper element, which dissipates some of the energy from the impact collision between the lower spring and the ground was therefore connected to the lower spring (see Figure 1.8), to successfully estimate the asymmetric GRF pattern observed in running animals and humans (Alexander et al., 1986; Derrick et al., 2000).

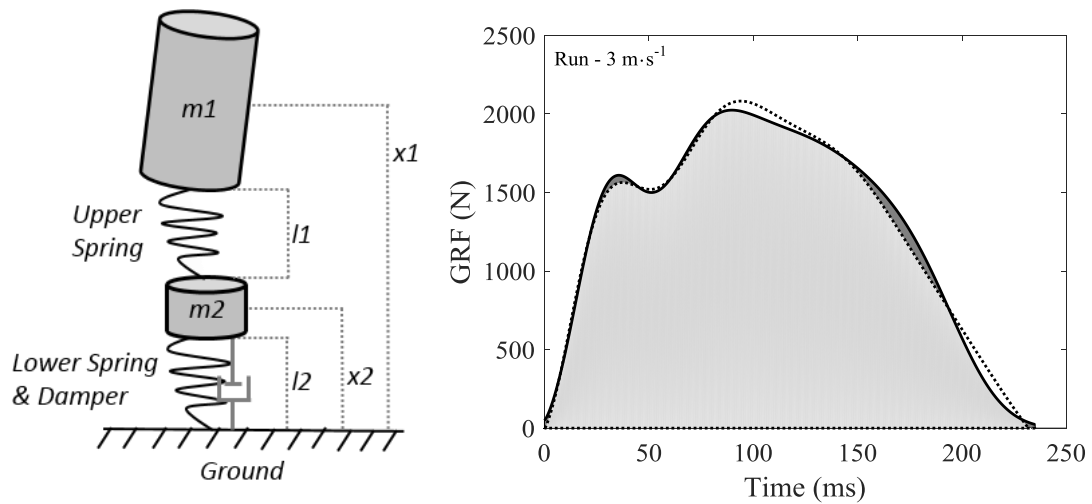


Figure 1.8: Illustration of the MSD-model used by Derrick et al. (2000) to estimate GRF patterns and an example of the simulated GRF from this model (dotted black line) and the measured GRF (solid black line) for running.

The following assumptions are made for the mass-spring-damper model (MSD-model) proposed by Alexander et al. (1986) and Derrick et al. (2000) for running animals/humans:

- The lower mass (m_2) represents the support leg
- The upper mass (m_1) represents the rest of the body
- The horizontal velocity of the model is assumed to be constant
- The model neglects movement in the horizontal direction and consider only the movements and forces in the vertical direction
- The model only consists of passive elements and therefore neglects energy from active elements such as muscles
- The model is limited to analyse the movement of the system during stance phase only

The vertical motion of the upper mass (m_1) and lower mass (m_2) can be described as in Equations 1.7 & 1.8 (Alexander et al., 1986; Derrick et al., 2000).

$$a_1(t) = \frac{-k_1}{m_1}(x_1 - x_2) + \frac{k_1 l_1}{m_1} + g \quad [\text{Equation 1.7}]$$

$$a_2(t) = -\frac{k_1+k_2}{m_1}x_2 + \frac{k_1}{m_2}x_1 - \frac{c}{m_2}v_2(t) + \frac{k_2 l_2 - k_1 l_1}{m_1} + g \quad [\text{Equation 1.8}]$$

Where x_1 , a_1 are the vertical position and acceleration of the upper mass, x_2 , v_2 , a_2 are the vertical position, velocity and acceleration of the lower mass. Example of the displacement, velocity and acceleration of the two masses is displayed in Figure 1.9. k_1 and k_2 are the linear spring constants of the massless upper and lower spring, c is the damping coefficient of the lower spring and g is the acceleration due to gravity ($-9.81 \text{ m}\cdot\text{s}^{-2}$). Finally, l_1 and l_2 are the natural lengths of the upper and lower spring under no external load. The GRF acting on the MSD-model (GRF_{model}) can be estimated when the motion, spring characteristics and damping coefficient of the lower mass is known (Equation 1.9).

$$GRF_{model} = k_2(l_2 - x_2) - cv_2 \quad [\text{Equation 1.9}]$$

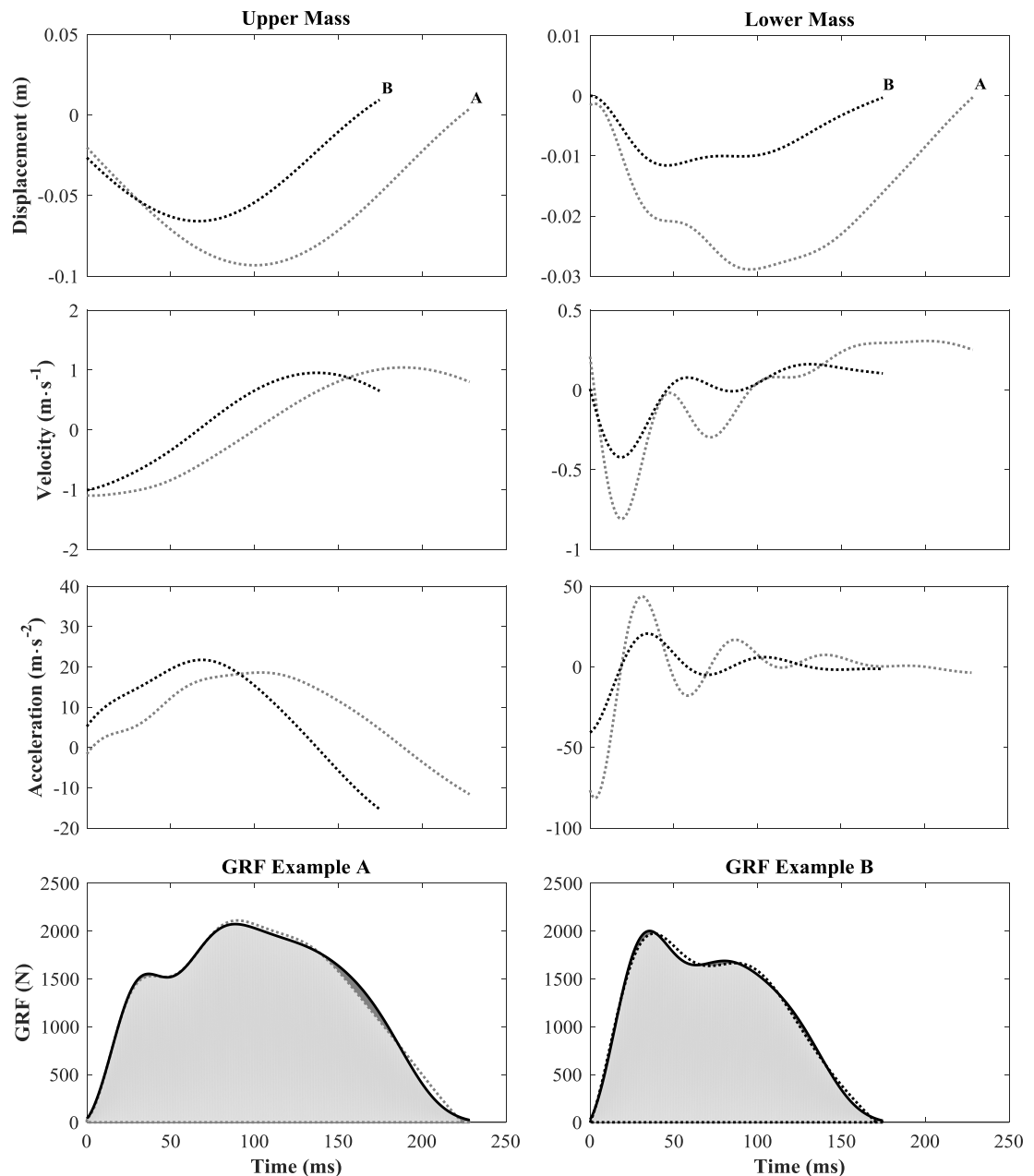


Figure 1.9: The displacement, velocity and acceleration of the upper and lower mass for two running examples (example A: dotted grey line and example B: dotted black line). The bottom row display the measured GRF (solid black line) and simulated MSD-model GRF (dotted grey line) from the two examples.

The MSD-model has until this thesis only been used to replicate GRF patterns from running at $3.83 \text{ m}\cdot\text{s}^{-1} \pm 5\%$ (Derrick et al., 2000). In that study the MSD-model successfully replicated the GRF patterns with an average difference in impulse between the measured and modelled GRF of $6.99 \text{ N}\cdot\text{s}$ (2.5%) and average difference in loading rate of 4.3 N/BW (4.7 %) (Derrick et al., 2000). In addition, a sensitivity analysis of the

individual model parameters' influence on the modelled GRF as well as the effect of stride length on the model's stiffness characteristics (stiffness of the upper and lower springs) were explored in the study by Derrick et al. (2000). The MSD-model's application is currently limited to the study by Derrick et al. (2000) and it is therefore still unknown to what extent the MSD-model can replicate GRF patterns from typical team sports movements.

1.3.6. More complex models

A number of more complex multi-body spring-mass models with additional masses, springs, dampers and active elements to simulate the energy from muscles and shoe cushioning have been introduced in the literature (Nikooyan and Zadpoor, 2011). However, these are not addressed in this literature review, because the MSD-model proposed by Alexander et al. (1986) and Derrick et al. (2000) has demonstrated sufficient ability to mimic the asymmetric GRF patterns and features typically observed for running.

1.4. Summary

The physiological training load and its relationship with performance enhancement and injury risk has been explored extensively in team sports whereas our understanding of biomechanical load, which is associated with the external forces players are exposed to from the player-ground interaction, still remain largely unexplored. The introduction of wearable GPS devices in team sports has made it possible to monitor the external training load on a daily basis (Aughey, 2011; Dellaserra et al., 2014). These devices have typically been used to monitor the kinetic energy demands associated with the players' movements around the pitch, but the integrated accelerometer could potentially provide useful information about the external biomechanical training load.

The direct relationship between the acceleration from trunk-mounted GPS integrated accelerometers and whole-body biomechanical loading (GRF) is however still largely underexplored in the literature (Tran, 2010; Wundersitz et al., 2013). Whole-body biomechanical loading depends on the complex multi-segmental dynamics of the body, a complex system that successfully has been modelled as a MSD-model system in the past (Alexander et al., 1986; Derrick et al., 2000). The generalisability of the MSD-model for team sport movements such as running and change of direction at different intensities is however yet to be established. If a direct relationship does not exist between body-worn accelerometry and whole-body acceleration, the ability to use the acceleration signal measured from the GPS integrated accelerometer to drive a MSD-model should be explored. If the external GRF acting on a player's body can be successfully estimated from a combination of trunk-mounted accelerometry and a MSD-model it might open a new avenue for external biomechanical load monitoring in team sports during training sessions and match-play.

1.5. Aim and objectives

The overall aim of the present thesis was to explore if body-worn accelerometry can be used for whole-body biomechanical load monitoring in team sports.

This will be explored through the fulfilment of the following studies and objectives:

- **Study 1:** To explore the association between whole-body accelerations and body-worn accelerometry during team sports movements.
- **Study 2:** To establish the generalisability of a mass-spring-damper model to simulate ground reaction forces from team sports related movements.
- **Study 3:** Based on a positive outcome of the first two, to introduce a novel approach to estimating ground reaction forces from body-worn accelerometry and a mass-spring-damper model.

The successful completion of the above aim and objectives will potentially enable researchers and practitioners to monitor the external whole-body biomechanical load from body-worn accelerometry in professional team sports.

CHAPTER 2
Estimating whole-body loading from
body-worn accelerometry

This study has been accepted for publication in the International Journal of Sports Physiology and Performance. The aim of this study was to investigate the relationship between whole-body accelerations and body-worn accelerometry during team sports related movements. Though the study demonstrated that body-worn accelerometry correlates to whole-body loading in team sports movements and can reveal useful estimation concerning biomechanical loading, these correlations are not strong.

2.1. Introduction

Team sports players experience high external forces on the body, in particular during the large number of accelerations and decelerations they perform (Bloomfield and O'Donoghue, 2007). As a consequence, soft tissues (bones, cartilage, muscles, tendons and ligaments) are put under considerable biomechanical load. The accumulation of this biomechanical load over time can result in structural adaptations that are beneficial (repair, regeneration, and strengthening of the tissue) and/or detrimental (leading to overuse or acute injury). A subtle balance of biomechanical load that depends on the frequency, duration and intensity of the external forces acting on the body is required to have beneficial adaptation yet avoid soft tissue injury (Kjaer et al., 2009). Quantifying the external forces acting on the body during team sport movements in the field could therefore help researchers and practitioners to better monitor and understand the biomechanical load experienced by players in training and matches.

Accelerometers embedded in Global Positioning Systems (GPS) devices are commonly used in professional team sport to monitor the players' energetic demands, e.g. from the distance players cover and the speed they run at or to estimate the external forces acting on the players' body (Boyd et al., 2011, 2013). The GPS integrated accelerometer devices are worn on the dorsal part of the upper trunk within an elastic vest and allow the

registration of acceleration of the (upper) trunk segment. It has previously been demonstrated that the accelerations registered from these GPS integrated accelerometers overestimate the peak external forces acting on the players' body during running and changes in direction (Wundersitz et al., 2013), or in landing and jumping tasks (Tran, 2010). However, the relationship between trunk acceleration from GPS integrated accelerometers and whole-body biomechanical loading during team sports movements it is still largely unexplored.

The estimation of external forces acting on the body from trunk accelerometry is based on Newton's second law of motion ($F_{whole-body} = m_{whole-body} \cdot a_{whole-body}$) and the assumption that body-worn accelerometers are able to measure whole-body acceleration. However, because the GPS integrated accelerometers measures trunk accelerations the external forces measured are actually the external forces acting on the trunk ($F_{trunk} = m_{trunk} \cdot a_{trunk}$). If however segmental accelerations from the trunk accelerometer are related to the whole-body acceleration it could be feasible to estimate the external forces experienced by players in the field. Whole-body accelerations, biomechanically expressed as Centre of Mass (CoM) accelerations, do however depend on the complex multi-segmental dynamics of the body. Since the position of the CoM relative to individual segments varies depending on the player's movements it remains questionable whether trunk-mounted accelerometers and body-worn accelerometry in general are able to measure the multi-segment dynamics during those movements that are typically performed in team sports.

The relationship between segmental acceleration from body-worn accelerometry and CoM accelerations seems to be affected by the location of the accelerometer. Accelerometers located at the hip have for example demonstrated an acceptable

association with the external forces acting on the whole body, biomechanically expressed as the ground reaction forces (GRF), during daily life activities (Meyer et al., 2015; Rowlands and Stiles, 2012). In addition accelerometers located at the hip and tibia have shown a strong association with GRF in vertical jumping (Elvin et al., 2007; Setuain et al., 2016). Furthermore, higher accumulated accelerometer-based loading values have recently been observed from a GPS integrated accelerometer located at the hip compared to the trunk for a 90 minute football simulation (Barrett et al., 2014; Barrett et al., 2016b) but it remains uncertain which segmental accelerations would better relate to whole-body biomechanical loading during typical team sports movements.

Altogether, the influence of accelerometer location on the relationship between measured accelerations and CoM accelerations during team sports movements such as running and changes in direction is still largely unexplored. The aim of this study was therefore to investigate the association between whole-body biomechanical loading and accelerations measured from an accelerometer that is attached to an individual body segment. This was done by investigating whether accelerations from the body-worn accelerometers are related to variables that represent whole-body loading, and whether peak accelerations are related to specific features of the CoM accelerations during the time when the player is in contact with the ground.

2.2. Methods

Twenty recreational male team sports athletes volunteered to participate in this study (age 22 ± 4 years, height 178 ± 8 cm, mass 76 ± 11 kg). No participants had a history of severe lower limb injuries (e.g. ACL injuries or ankle sprains). The study was approved by the Institutional Ethics Committee and written consent was obtained from all participants.

2.2.1. Protocol

The participants completed four forward running trials (Run), four anticipated 45° (Cut45) and four 90° side cutting trials (Cut90) at approach speeds of 2, 3, 4 and 5 m·s⁻¹ ($\pm 5\%$) in a randomised condition order. Approach speed was measured with photocell timing gates (Brower Timing System, Utah, USA) that were positioned 2 m apart and 2 m from the centre of a force platform. The participants were instructed to hit the force platform with their dominant leg (defined as their preferred kicking leg) during the Run trials and to perform the cutting step with their dominant leg on the force platform. An individual number of practice trials were incorporated in the warm up routine until the participants were familiar with the different tasks and approach speeds (typically around 4 ± 2 practise trials for each conditions).

2.2.2. Acceleration measurements

Segmental acceleration data were collected from four body-mounted accelerometers: 1) a trunk-mounted tri-axial accelerometer (KXP94, Kionex, Inc., Ithaca, NY, USA) embedded within a commercial GPS device (MinimaxX S4, Catapult Innovations, Scoresby, Australia). This accelerometer had a sampling frequency of 100 Hz and an output range of ± 13 g. The GPS device was positioned on the dorsal part of the upper trunk between the scapulae within a small pocket of a tight fitted elastic vest according to the manufactures recommendations; 2) A tri-axial wireless laboratory accelerometer (518, DTS accelerometer, Noraxon Inc., Scottsdale, USA) with an effective sampling frequency of 1000 Hz, an output range of 24 g, a total weight of 5.7 grams and 19 x 14.2 x 6.3 mm in dimension was tightly fixated to the posterior side of the GPS device using double sided tape. Pilot work showed a difference of approximately 0.34 g in peak acceleration between a laboratory accelerometer fixated to the posterior side of the GPS device compared to the anterior side (see detail in Appendix A). The posterior location

was therefore used for all measurements; 3) A tri-axial wireless accelerometer (same specifications as accelerometer 2) was located inside the shorts worn by the participants (level with the 5th lumbar vertebra) during the session with double sided tape. An elastic belt was strapped around the participant's waist and accelerometer to minimise the movement of the accelerometer relative to pelvis; 4) A tri-axial wireless accelerometer (same specifications as accelerometer 2) was fixed to a lightweight fibre glass plate shaped to the shaft of the tibia with double sided tape and with elastic velcro straps tightly strapped to the front of the tibia shaft with which the participant performed the pivot/cutting step. The location of the four body-mounted accelerometers is displayed in Figure 2.1.

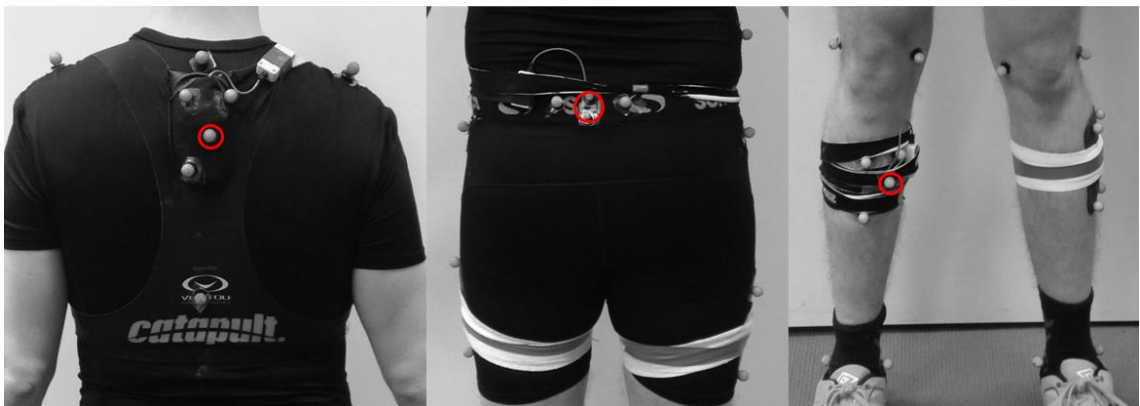


Figure 2.1: Pictures displaying the position of the four body-mounted accelerometers, the red circles display the location of the three laboratory accelerometers (Trunk, Pelvis and Tibia).

The accelerometers' static validity were tested pre and post every test session by rotating the accelerometers through 6 degrees of freedom to detect a $\pm 1g$ acceleration due to gravity (see detail in Appendix B). The average resultant acceleration were calculated over a 10 second time period for each of the sensing axes and the overall averages were calculated from the average values of the sensing axis. A one sample t-test was used to test if the average resultant acceleration obtained from each accelerometer were significant different ($\alpha \leq 0.01$) from 1g pre or post every test session. Neither of the

accelerometers showed a significant difference from 1g pre or post any of the test sessions.

Ground reaction forces (GRF) were collected from a 0.9 x 0.6 m² Kistler force platform (9287C, Kistler Instruments Ltd., Winterthur, Switzerland) embedded in the floor sampling at 3000 Hz. The GRF data were synchronised with the accelerometer data from the three laboratory tri-axial accelerometers through an analogue board and recorded simultaneously in Qualisys Track Manager (Qualisys AB, Gothenburg, Sweden). The Trunk accelerometer was gently tapped three times before each trial creating three clear spikes in the acceleration traces which were used to synchronise the Catapult acceleration data with the other acceleration data (accuracy of ± 10 ms), see detail in Appendix C.

2.2.3. Data processing

All acceleration and GRF data were exported to Matlab (Version R2014a, The MathWorks, Inc., Natick, MA, USA) where the whole-body CoM acceleration was determined by dividing the GRF data by the participants' body mass and subtracting the gravitational acceleration from the vertical GRF data. The GRF data were filtered with a 6th order low-pass filter with a cut-off frequency of 20 Hz, while a similar low-pass filter with a cut-off frequency of 60 Hz, 60 Hz and 90 Hz were applied to the Trunk, Pelvis and Tibia acceleration data, respectively. The accelerometer filtering cut-off frequencies were determined from a sensitivity analysis, see details in Appendix D. The raw Catapult acceleration data were not filtered, as the accelerometer data from the commercial GPS embedded accelerometers according to the authors' knowledge is left unfiltered when used in the field. Resultant accelerations were calculated from the individual axes for the accelerometry and CoM acceleration data. The foot-ground-contacts on the force platform were determined from the vertical GRF, where touch down and take off events

were created when the vertical GRF crossed a 20 N threshold. The following variables were calculated from the accelerometry and CoM acceleration data for each trial: peak resultant acceleration (Peak Acc); the average loading rate (Loading rate) defined as the average gradient of the resultant acceleration data from touch down to Peak Acc within the first 140 ms of the stance phase; the impulse (Impulse) calculated as the integral of the resultant acceleration over time.

2.2.4. Statistical analysis

A linear regression analysis was used to explore the within task relationship between Peak Acc, Loading rate, Impulse of the CoM acceleration and accelerometry from the different accelerometers. In addition, a linear multiple regression using the three laboratory accelerometers was used to explore if accelerometry from multiple accelerometers would improve the relationship with the variables obtained from the CoM acceleration. The linear regression analyses were performed using SPSS (Version 22, SPSS Inc., Chicago, IL, USA).

One-dimensional Statistical Parametric Mapping (SPM) was used to explore the within task relationship between Peak Acc from the different accelerometer locations and CoM acceleration across the entire stance phase for the Run, Cut45 and Cut90 tasks respectively. The SPM analysis is an n-dimensional statistical approach of the traditionally 0-dimensional linear regression and one-sample t test approach performed in SPSS (Pataky, 2012). SPM analysis makes it possible to explore the relationship without having to impose the temporal focus bias (Pataky et al., 2013), that may occur in the 0-dimensional linear regression approach described above, because of the between task variation in the GRF pattern. The SPM analysis will reveal the periods of the stance

phase where Peak Acc from the individual accelerometers is significantly related to the CoM acceleration.

$$CoM\ acc(t) = (\beta_1(t) \times Peak\ Acc) + \alpha_1(t) + \varepsilon(t) \quad [\text{Equation 2.1}]$$

The slopes of the regression line between Peak Acc from the Catapult, Trunk, Pelvis and Tibia accelerometer (β_1 , β_2 , β_3 and β_4 , respectively) and the CoM acceleration were computed at each time node (t) of the stance phase (Equation 2.1) resulting in beta (β) trajectories (third row Figure 2.3). These β trajectories were computed for each participant and were subsequently submitted to a population level one-sample t test, yielding statistical curves (SPM{t}) for each of the four accelerometers describing the strength and slope of the relationship between Peak Acc and CoM acceleration (fourth row Figure 2.3). The significance of each SPM{t} was then determined topologically using random field theory (Adler and Taylor, 2007), with an alpha level at 0.0125, for each of the three tasks Run, Cut45 and Cut90, respectively.

2.3. Results

The segmental acceleration data overestimated the CoM acceleration (Figure 2.2) and whole-body biomechanical loading variables regardless of task (Table 2.1).

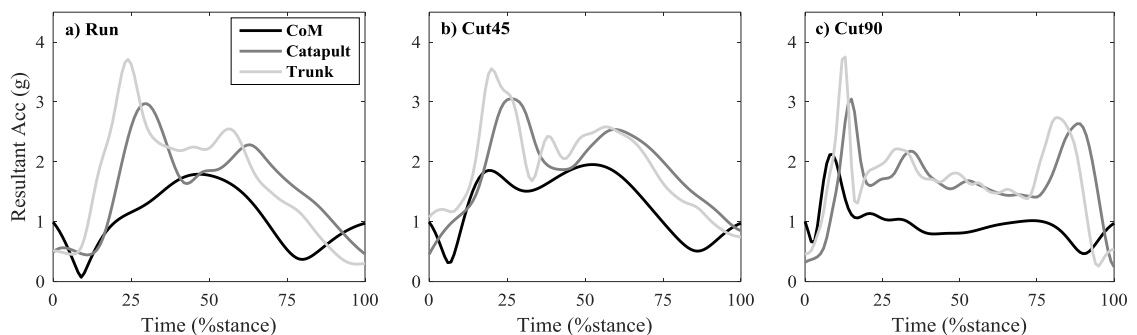


Figure 2.2: Representative examples of the resultant CoM acceleration and resultant acceleration from the Catapult and Trunk accelerometer for the Run, Cut45 and Cut90 at $5\text{ m}\cdot\text{s}^{-1}$. All curves are normalised over the stance phase (%).

Table 2.1: Peak Acc, Loading Rate and Impulse for all tasks (Run, Cut45, Cut90) and approach speeds (2-5 m·s⁻¹) for CoM accelerations and the four body-mounted accelerometers. The values presented are means ± standard deviations and n = 80 trials in total for each task.

	COM M ± SD	Catapult M ± SD	Trunk M ± SD	Pelvis M ± SD	Tibia M ± SD
Peak Acc (g)					
Run 2 m·s ⁻¹	1.32 ± 0.30	2.82 ± 0.60	3.78 ± 1.13	4.56 ± 1.70	8.02 ± 2.77
Run 3 m·s ⁻¹	1.56 ± 0.33	3.33 ± 0.69	4.52 ± 1.22	5.38 ± 1.57	10.47 ± 3.65
Run 4 m·s ⁻¹	1.80 ± 0.30	2.79 ± 0.80	5.09 ± 1.32	6.38 ± 1.72	14.25 ± 3.78
Run 5 m·s ⁻¹	1.85 ± 0.41	2.82 ± 0.89	5.34 ± 1.75	7.39 ± 2.48	20.36 ± 5.39
Cut45 2 m·s ⁻¹	1.40 ± 0.34	2.81 ± 0.63	3.73 ± 1.19	4.90 ± 2.11	8.69 ± 3.54
Cut45 3 m·s ⁻¹	1.72 ± 0.38	3.41 ± 0.79	4.52 ± 1.30	6.06 ± 1.89	11.62 ± 3.86
Cut45 4 m·s ⁻¹	2.04 ± 0.42	2.92 ± 1.09	5.40 ± 1.56	8.62 ± 3.20	16.83 ± 5.19
Cut45 5 m·s ⁻¹	2.25 ± 0.49	3.10 ± 0.95	5.78 ± 1.65	11.36 ± 4.89	18.95 ± 5.99
Cut90 2 m·s ⁻¹	1.49 ± 0.37	3.10 ± 0.82	3.99 ± 1.38	5.52 ± 2.40	9.92 ± 4.15
Cut90 3 m·s ⁻¹	1.90 ± 0.50	3.89 ± 0.96	5.01 ± 1.49	8.73 ± 4.71	14.37 ± 6.27
Cut90 4 m·s ⁻¹	2.08 ± 0.51	2.86 ± 1.03	5.08 ± 1.36	10.33 ± 4.28	16.95 ± 6.26
^a Cut90 5 m·s ⁻¹	2.28 ± 0.51	3.05 ± 1.04	5.35 ± 1.56	12.53 ± 5.45	19.85 ± 5.72
Loading rate (g·s⁻¹)					
Run 2 m·s ⁻¹	18.6 ± 4.6	31.7 ± 9.8	56.2 ± 24.2	83.6 ± 38.2	233.1 ± 111.8
Run 3 m·s ⁻¹	22.7 ± 5.5	38.3 ± 10.9	70.7 ± 27.1	116.9 ± 45.0	318.8 ± 166.8
Run 4 m·s ⁻¹	30.8 ± 11.1	34.6 ± 16.6	83.4 ± 28.6	146.4 ± 52.1	463.6 ± 176.5
Run 5 m·s ⁻¹	44.8 ± 18.4	51.9 ± 16.8	93.1 ± 34.2	191.9 ± 73.7	731.4 ± 249.9
Cut45 2 m·s ⁻¹	15.4 ± 3.8	30.8 ± 10.5	54.9 ± 26.7	87.8 ± 53.3	261.8 ± 141.3
Cut45 3 m·s ⁻¹	19.8 ± 6.5	38.4 ± 12.1	67.3 ± 28.1	126.2 ± 57.9	355.3 ± 128.3
Cut45 4 m·s ⁻¹	36.9 ± 20.2	45.8 ± 18.2	86.2 ± 36.4	202.8 ± 96.8	565.7 ± 234.3
Cut45 5 m·s ⁻¹	52.7 ± 26.2	63.6 ± 19.3	97.1 ± 36.2	266.1 ± 145.7	690.7 ± 315.3
Cut90 2 m·s ⁻¹	18.3 ± 10.7	33.7 ± 13.1	55.0 ± 28.5	92.4 ± 53.6	301.2 ± 180.1
Cut90 3 m·s ⁻¹	32.8 ± 20.9	42.8 ± 17.1	69.5 ± 26.6	154.8 ± 88.6	446.1 ± 224.2
Cut90 4 m·s ⁻¹	44.1 ± 23.6	52.8 ± 13.0	71.9 ± 24.6	199.4 ± 105.6	567.9 ± 268.5
^a Cut90 5 m·s ⁻¹	56.3 ± 21.4	65.3 ± 15.8	76.9 ± 28.6	247.2 ± 126.6	701.0 ± 237.9
Impulse (g·s)					
Run 2 m·s ⁻¹	0.25 ± 0.04	0.42 ± 0.03	0.43 ± 0.04	0.51 ± 0.04	0.75 ± 0.09
Run 3 m·s ⁻¹	0.24 ± 0.04	0.40 ± 0.03	0.41 ± 0.04	0.50 ± 0.05	0.84 ± 0.09
Run 4 m·s ⁻¹	0.24 ± 0.04	0.38 ± 0.04	0.39 ± 0.05	0.51 ± 0.05	1.00 ± 0.11
Run 5 m·s ⁻¹	0.21 ± 0.04	0.33 ± 0.05	0.34 ± 0.05	0.47 ± 0.08	1.14 ± 0.14
Cut45 2 m·s ⁻¹	0.28 ± 0.05	0.47 ± 0.04	0.47 ± 0.04	0.55 ± 0.05	0.81 ± 0.11
Cut45 3 m·s ⁻¹	0.30 ± 0.04	0.46 ± 0.05	0.47 ± 0.05	0.57 ± 0.06	0.93 ± 0.12
Cut45 4 m·s ⁻¹	0.31 ± 0.04	0.46 ± 0.06	0.49 ± 0.07	0.63 ± 0.08	1.12 ± 0.15
Cut45 5 m·s ⁻¹	0.29 ± 0.04	0.41 ± 0.07	0.46 ± 0.07	0.62 ± 0.13	1.25 ± 0.21
Cut90 2 m·s ⁻¹	0.35 ± 0.06	0.55 ± 0.08	0.56 ± 0.08	0.64 ± 0.09	0.92 ± 0.14
Cut90 3 m·s ⁻¹	0.38 ± 0.05	0.58 ± 0.08	0.60 ± 0.09	0.72 ± 0.13	1.09 ± 0.20
Cut90 4 m·s ⁻¹	0.41 ± 0.06	0.58 ± 0.09	0.68 ± 0.10	0.80 ± 0.13	1.28 ± 0.27
^a Cut90 5 m·s ⁻¹	0.38 ± 0.06	0.54 ± 0.09	0.66 ± 0.10	0.81 ± 0.12	1.44 ± 0.25

^a One of the participants was not able to perform the four Cut90 trials with an approach speed at 5 m·s⁻¹ (n = 76 for this task).

In general, the Catapult and Trunk accelerations were the closest to the CoM acceleration, followed by Pelvis and Tibia accelerations regardless of task and variable of interest. The loading variables increased with an increase in approach speed regardless of task and accelerometer location.

Weak to moderate within task relationships were observed between the segmental acceleration data and CoM acceleration data (Table 2.2). The Catapult and Trunk accelerometry data most strongly predicted whole-body Peak Acc and Impulse whereas Pelvis and Tibia accelerometry data were the strongest predictor of Loading Rate regardless of task. The addition of multiple accelerometers only showed minor improvements of the relationship with the CoM acceleration loading variables.

Table 2.2: Within task linear regression values (R^2) for Peak Acc, Loading Rate and Impulse between the CoM acceleration and acceleration data from the individual accelerometers and multiple laboratory accelerometers.

	N	Catapult	Trunk	Pelvis	Tibia	Trunk & Hip	Trunk & Shank	Trunk, Hip & Shank
Peak Acc (g)								
Run	320	0.26	0.20	0.08	0.26	0.21	0.31	0.31
Cut45	320	0.42	0.32	0.35	0.50	0.42	0.52	0.54
Cut90	316 ^a	0.55	0.46	0.48	0.34	0.60	0.53	0.61
Loading rate ($\text{g}\cdot\text{s}^{-1}$)								
Run	320	0.27	0.41	0.29	0.45	0.47	0.56	0.56
Cut45	320	0.38	0.34	0.59	0.45	0.59	0.49	0.62
Cut90	316 ^a	0.36	0.32	0.59	0.43	0.62	0.49	0.64
Impulse (g·s)								
Run	320	0.26	0.25	0.13	0.02	0.26	0.26	0.26
Cut45	320	0.26	0.25	0.17	0.10	0.27	0.29	0.29
Cut90	316 ^a	0.59	0.57	0.44	0.27	0.57	0.57	0.57

^a One of the participants was not able to perform the four Cut90 trials with an approach speed at $5 \text{ m}\cdot\text{s}^{-1}$.

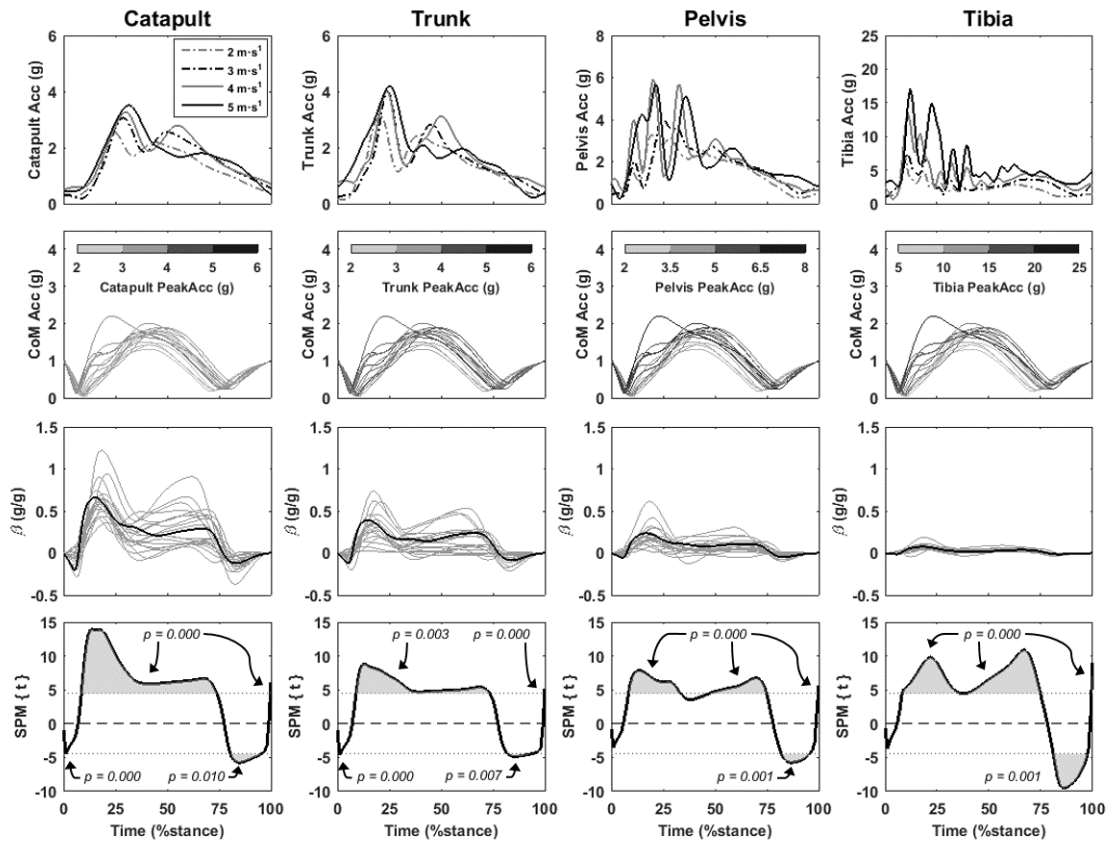


Figure 2.3: SPM1D regression analysis of the Run task for the four body-worn accelerometers, all curves are normalised over the stance phase (%). The top row shows a representative acceleration from the four approach speeds and accelerometer locations for one participant. The second row shows the CoM acceleration, coloured according to the peak acceleration from the same participant for all trials. The third row shows the β curves from all participants. The specific β curve generated from the data in the second row is shown in black. The bottom row shows the statistical relationship (SPM{t}) between Peak Acc and CoM acceleration across the entire stance phase. Shaded areas indicate a significant relationship ($p < 0.0125$) between Peak Acc from the accelerometer and CoM acceleration.

The SPM analysis for the Run and Cut45 task generally showed that peak segmental accelerations, regardless of accelerometer location, were significantly positive related to the CoM accelerations during the 10-75% of the stance phase with the strongest relationship from the 10-50% of the stance phase (Figure 2.3 and 2.4). While a significantly negative relationship were observed for all accelerometers from the 75-95% of the stance phase between peak segmental acceleration and CoM acceleration for the Run task before take off where the CoM acceleration were low (Figure 2.3).

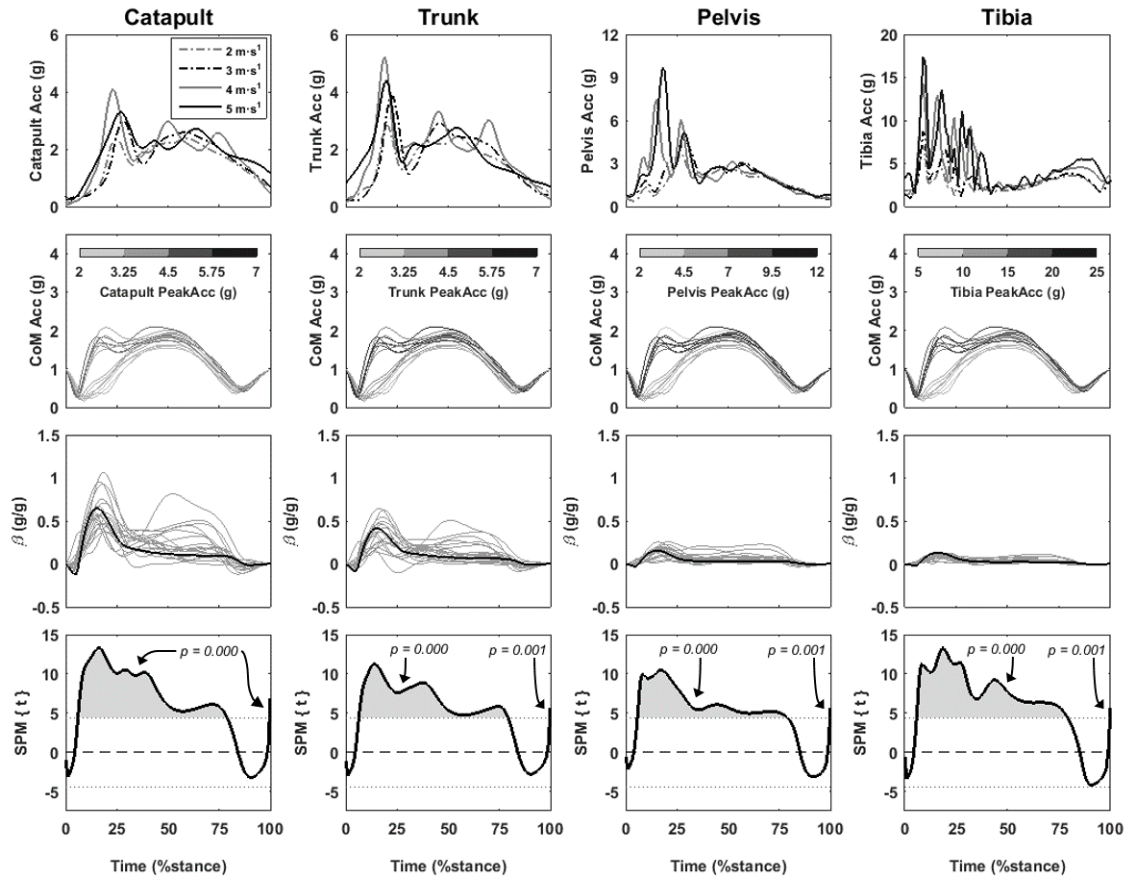


Figure 2.4: SPM1D regression analysis of the Cut45 task for the four body-worn accelerometers, all curves are normalised over the stance phase (%). See Figure 2.3 for a detailed explanation of the data displayed in the individual rows.

For the Cut90 task, Peak Acc and CoM acceleration was in general positive significantly related to the CoM acceleration in the initial part of the weight acceptance phase (10-25% stance phase), apart from the peak Tibia acceleration which also demonstrated a positive significant relationship from 70-80% of the stance phase (Figure 2.5).

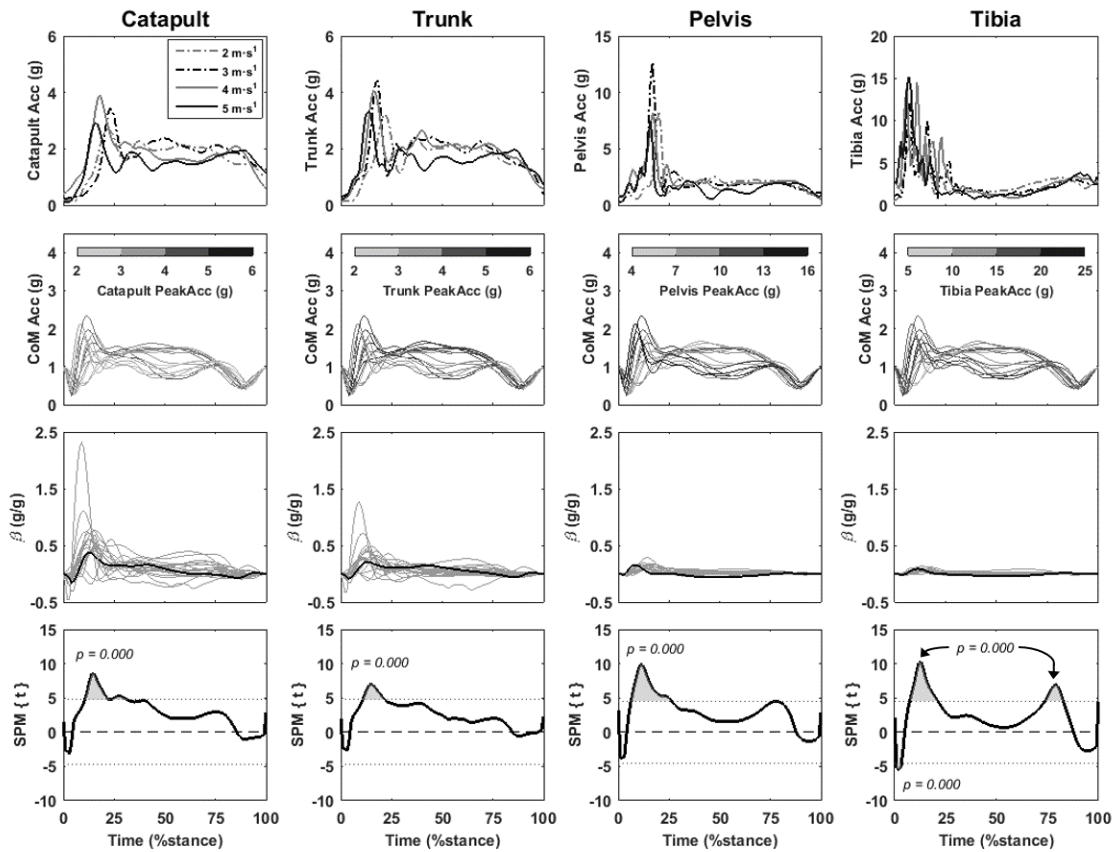


Figure 2.5: SPMID regression analysis of the Cut90 task for the four body-worn accelerometers, all curves are normalised over the stance phase (%). See Figure 2.3 for a detailed explanation of the data displayed in the individual rows.

2.4. Discussion

The aim of the study was to investigate the association between whole-body biomechanical loading and segmental accelerations measured from body-worn accelerometers. The segmental acceleration data consistently overestimated the whole-body biomechanical loading variables investigated in this study regardless of task and a weak relationship was observed between segmental acceleration and CoM acceleration. Furthermore, this study showed that peak segmental acceleration data is primarily related to whole-body biomechanical loading in the 10-50% of foot-ground-contact.

Body-worn accelerometry only measures the acceleration of the segment it is attached to and therefore according to our results it is inadequate to measure the acceleration of the

whole body due to the complex multi-segment motion during team sports movements. Furthermore, this linear relationship has previously been questioned, because the relationship between lower limb segmental acceleration and whole-body loading is influenced by the kinematics of the lower limbs at initial foot-ground-contact (Derrick, 2004). The difference between acceleration of individual segments and the acceleration of the whole body can explain the consistent overestimation of peak whole-body loading from body-worn accelerometers observed in this study. These results are in line with the weak relationship previously observed between peak resultant accelerations from a GPS integrated trunk-mounted accelerometer and resultant peak GRF during running and change of directions at similar intensities (Wundersitz et al., 2013).

The peak segmental accelerations measured with the Catapult and Trunk accelerometers were the closest to the peak CoM acceleration. This may be explained by the attenuation of the acceleration signal as it travels up through the body (Hamill et al., 1995). In addition, the trunk segment represents the largest proportion of the whole-body mass (49.7%) compared to the pelvis (14.2%) and tibia (4.7%) segments (Dempster, 1955) which may explain why the segmental acceleration of the trunk best represented the acceleration of the whole body in the current study. The trunk segment's higher mass may also explain why the two trunk-mounted accelerometers demonstrated a higher relationship with the impulse of the CoM acceleration as the impulse represent the acceleration measured over time. This indicates that the current practice of positioning GPS integrated accelerometers on the trunk may be the best location to represent the accumulated whole-body biomechanical loading to which team sport players are exposed in the field.

The results from this study showed that tibial segmental accelerations were not a good indicator of whole-body biomechanical loading. However, tibial segmental accelerations could potentially provide valuable information about the impact forces the lower extremities are exposed to during initial foot-ground-contact. Studies on overuse injuries in running have for instance showed that runners with previous stress fracture history were exposed to high initial peak ground reaction forces and higher loading rate than runners with no previous stress fracture history (Hreljac, 2004). The potential of using tibia mounted accelerometer to monitor initial loading rate in team sport is supported by the results of this study as the tibia mounted accelerometer demonstrated a higher relationship with whole-body loading rate than the trunk-mounted accelerometer. Consideration should therefore be given to accelerometer location in team sports based on the mechanical variable/s of interest.

The GPS integrated accelerometer (Catapult) consistently measured lower accelerations than the Trunk laboratory accelerometer, and the Peak Acc was slightly delayed in the Catapult data (see Figure 2.2). The difference in sampling frequencies (Catapult: 100 Hz, laboratory accelerometer: 1000 Hz) may explain the systematic difference between the two trunk-mounted accelerometers. The commercial GPS embedded accelerometers' ability to measure peak acceleration during high frequency movements has previously been questioned when compared to laboratory accelerometers with a higher sampling frequency (Kelly et al., 2015; Lake et al., 2014). Increasing the sampling frequency of the commercial GPS integrated accelerometers may improve their ability to represent the true accelerations experienced in team sports.

The Statistical Parametric Mapping analysis enabled us to investigate the relationship between peak segmental accelerations from body-worn accelerometry and CoM

acceleration across the stance phase. This analysis showed that peak segmental accelerations, regardless of accelerometer location, were strongest related to CoM acceleration from the 10-50% of the stance phase. Peak segmental accelerations, which previously have been used to investigate whole-body biomechanical loading in daily life activities (Meyer et al., 2015; Rowlands and Stiles, 2012) or as in this and previously studies to validate whole-body loading from body-worn accelerometry (Tran, 2010; Wundersitz et al., 2013), can therefore describe only part of the biomechanical loading the body's soft tissues is exposed to during foot-ground-contact. Trying to use peak segmental accelerations to understand whole-body biomechanical loading during foot-ground-contact in team sport movements could therefore be misleading. Additional information other than peak segmental accelerations is needed to better represent the whole-body biomechanical loading across the stance phase in dynamic sports movements.

Our results indicated that the relationship between peak segmental acceleration and whole-body loading is task dependent. The difference observed between the two change-in-direction tasks may be explained by the difference in the segmental and CoM acceleration patterns during the stance phase with a clear initial peak after touch down in the Cut90 task (Figure 2.4) compared to the later occurrence of peak CoM acceleration in the Cut45 task (Figure 2.3). Furthermore, the CoM accelerations of the Cut45 task indicated that approach speed changed the shape of CoM acceleration pattern while the accelerometer trace remained consistent (Figure 2.3) and thereby affect the relationship with the peak segmental acceleration.

Limitations within this study include the attachment of the individual accelerometers which may have resulted in errors in the accelerometry signal due to the movement of the

accelerometer relative to the segment. The attachment methods and locations were chosen with a combination of ideal and applied approach in mind for potential use in team sports. Fixing the accelerometer directly to the skin may have improved the accuracy of the accelerometer data but this is currently less feasible in an everyday field context. In addition, lower filtering cut-off frequency of the accelerometry data may have improved the relationship with the CoM accelerations, as previously demonstrated for GPS-embedded accelerometers (Tran, 2010; Wundersitz et al., 2013). However, it was beyond the scope of this study to determine the optimal cut-off frequency as this most likely will be dependent on task and intensity making it difficult to apply optimal filter settings in the field. Importantly though, improving the relationship with specific cut-off frequencies does not change the fundamental issue with the use of body-worn accelerometry to estimate CoM acceleration as it only measures the accelerations of the segment it is attached to and not the accelerations of the whole-body.

The assumption of a simple linear relationship, based on Newton's second law of motion, where segmental accelerations is measured from body-worn accelerometers is not sufficient to determine the linked multi-segment dynamics of the whole body during team sports movements in the field. For instance when this linear assumption is used to investigate the relationship between GPS integrated accelerometry data and risk of soft tissue injuries (Colby et al., 2014; Ehrmann et al., 2016). To better estimate whole-body acceleration, the multibody dynamics of a complex system, such as the human body, must be accounted for. Future studies should not assume that a linear approach is sufficient to estimate the mechanical external force acting on players in the field but investigate the application of multi-segment models for this purpose (Derrick et al., 2000).

Although a linear relationship exists between body-worn accelerometry (e.g. GPS integrated accelerometers) and whole-body accelerations the assumption of a simple linear relationship, based on Newton's second law of motion, should be used with caution. Practitioners should therefore be careful when attempts are made to monitor, summarise and evaluate the biomechanical load the players are exposed to from body-worn accelerometry or associated to soft tissue injury risk. New methods need to be developed to use body-worn accelerometry to more accurately explain whole-body biomechanical loading in dynamic team sports.

2.5. Conclusion

Whilst a weak to moderate correlation was observed between segmental accelerations from body-worn accelerometry and can reveal useful estimations of whole-body biomechanical loading in team sports movements, particularly in the first 10-50% of foot-ground-contact, the linear relationship is weak regardless of accelerometer location and task. Body-worn accelerometry only measures the acceleration of the segment it is attached to and is inadequate to measure the acceleration of the whole body due to the complex multi-segment motion during team sports movements. Practitioners should consider the weak to moderate linear relationship between body-worn accelerometry and whole-body biomechanical loading when interpreting the accelerometry data in this context.

CHAPTER 3

Generalisability of a mass-spring-damper model for team sports movements

The aim of this study was to establish the generalisability of a mass-spring-damper model to simulate ground reaction forces during team sports movements. The study demonstrated that the mass-spring-damper model's generalisability to mimic ground reaction forces from team sports movements was strong, though larger mean differences and limits of agreements were observed for the 90° side cut at high intensities.

3.1. Introduction

Human running is spring-like in nature as the elastic tissues of the support leg absorb and return elastic energy. Simple spring-mass models have therefore been used to explore the mechanics of running (Alexander et al., 1986; Blickhan, 1989; McMahon and Cheng, 1990). The simplest and most widely used spring-mass model consists of a mass-less spring attached to a point mass representing the body's centre of mass (CoM). These models have primarily been used to describe vertical stiffness and leg stiffness during running, calculated as a ratio between the maximal force and maximal leg compression or maximal vertical displacement of the CoM, respectively (Farley and Gonzalez, 1996; McMahon and Cheng, 1990; Morin et al., 2005). The stiffness data obtained from these models has for example been used to explore running economy (Dalleau et al., 1998; McMahon et al., 1987), changes in stiffness at different running velocities (Brughelli and Cronin, 2008), or fatigue effects on performance during long distance running (Degache et al., 2016; Morin et al., 2006; Morin et al., 2011), middle distance running (Girard et al., 2013) and repeated sprints and high intensity running (Girard et al., 2016a; Girard et al., 2016b; Taylor and Beneke, 2012).

The principle of the spring-mass model is that the vertical ground reaction force (GRF) can be estimated as a half-sine wave from the vertical movement of the mass. The spring is compressed in the first half of the stance time as the CoM moves downwards until mid-

stance at which time the CoM reaches its lowest position. In the second half of stance the CoM is accelerated upwards as the stored elastic energy is released generating a half-sine wave GRF with a single peak at mid-stance (Alexander et al., 1986; Blickhan, 1989; McMahon and Cheng, 1990). It is however well-known that GRF patterns deviate from this pattern depending on foot-strike (Lieberman et al., 2010), running speed (Clark et al., 2014; Hamill et al., 1983) and/or level of the athlete (Clark and Weyand, 2014). As the body is exposed to high-frequency impact forces when the foot collides with the ground, an impact peak is often present in the initial phase of stance, particularly in heel-toe running (Bobbert et al., 1991; Nigg et al., 1995) and cutting manoeuvres (Besier et al., 2001). These impact forces are passively absorbed by the soft tissues of the lower limbs (bones, cartilage, ligaments, tendons) (Bobbert et al., 1991), by the position of the joints (Bobbert et al., 1992; Derrick et al., 2002), and actively by the muscles (Christina et al., 2001). The commonly used spring-mass model consisting of a single mass and a single spring does not account for the energy absorbed by the shock absorption of the support leg in the initial stance phase (Alexander et al., 1986; Derrick et al., 2000).

To model the GRF pattern during heel-toe running a modified mass-spring-damper model (MSD-model) with a second mass in series with a spring-damper is needed. Such a model has been successful in estimating both the impact and active vertical peak for straight line running at $3.83 \text{ m}\cdot\text{s}^{-1}$ ($\pm 5\%$) (Derrick et al., 2000). An understanding of this model's generalisability to other running speeds, and to running actions typically seen in team sports (football, hockey, basketball etc.), is largely unexplored. In team sports the majority of playing time is spent in running related utility movements such as jogging, accelerations/decelerations, sprinting and changing direction at different intensities (Di Salvo et al., 2007). As a consequence of these movements the players' soft tissues (bones, cartilage, muscles, tendons and ligaments) are put under biomechanical load and over

time the accumulation of this load will result in strengthening on the one hand, but it can also lead to weakening and subsequently injury, on the other hand (Hreljac, 2004; Kjaer et al., 2009; Nigg et al., 1995). If a MSD-model is capable of estimating GRF patterns from a variety of movements such as running at different intensities and when changing direction, then this could be used to gain a better understanding of whole-body biomechanical load during team sports. The aim of this study was therefore to explore the generalisability of a MSD-model to estimate GRF during running and side cutting at different running speeds.

3.2. Methods

Twenty recreational male team sports athletes (age 22 ± 4 years, height 178 ± 8 cm, mass 76 ± 11 kg) completed four straight line running trials (Run), four anticipated 45° (Cut45) and four 90° side cutting trials (Cut90) at approach speeds of 2, 3, 4 and $5 \text{ m}\cdot\text{s}^{-1}$ ($\pm 5\%$) in a randomised task order. Approach speeds were measured with photocell timing gates (Brower Timing System, Utah, USA) positioned 2 m apart and 2 m from the centre of the force platform as described in Vanrenterghem et al., 2012. No participants had any history of severe lower limb injuries. The study was approved by the institutional ethics committee and written consent was obtained from all participants.

3.2.1. Measured GRF

Ground reaction forces of one ground contact were measured ($\text{GRF}_{\text{measured}}$) with a sampling frequency of 3000 Hz from a Kistler force platform (9287C, Kistler Instruments Ltd., Winterthur, Switzerland). Participants ran over the force platform with their dominant leg during the Run trials. The cutting task was performed at the time that their dominant leg made contact with the force platform during the Cut45 and Cut90 tasks, making an open cut towards the non-dominant side (similar to cutting task as described

in Vanrenterghem et al., 2012). GRF_{measured} were exported to Matlab (Version R2015a, The MathWorks, Inc., Natick, MA, USA) where touch down and take off was defined for each trial based on the vertical GRF crossing a 20 N threshold. GRF_{measured} were filtered with a 4th order Butterworth low-pass filter with a cut-off frequency of 20 Hz.

3.2.2. Mass-spring-damper model

A MSD-model consisting of a lower mass (m_2) on top of a spring-damper combination and an upper mass (m_1) on top of another spring (Figure 3.1) was used in this study (Alexander et al., 1986; Derrick et al., 2000). Eight natural model parameters were determined to describe the motion of the model: the position (p_1) and velocity (v_1) of the upper mass, the position (p_2) and velocity (v_2) of the lower mass, the mass ratio (λ) of the lower mass relative to the participant's total body mass, the natural frequency of the upper (ω_1^2) and lower spring (ω_2^2), and the dampening ratio (ζ) of the damper. The model parameters were defined as described in Appendix E.

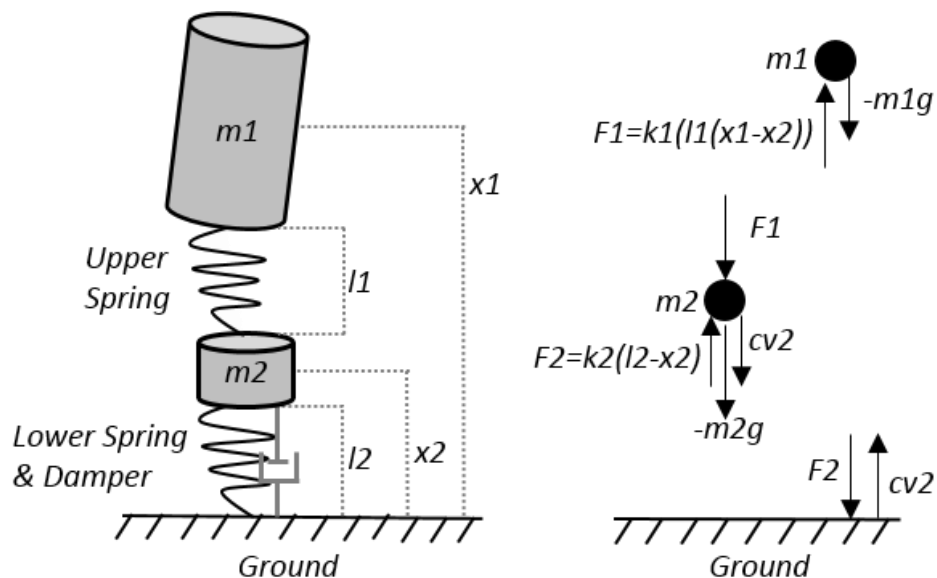


Figure 3.1: Illustration of the MSD-model and a free-body diagram of the model.

The equations of motion of the MSD-model are described in Equations 3.1 and 3.2, where a_1 and a_2 are the acceleration of the upper and lower mass respectively, and g is the acceleration due to gravity ($-9.81 \text{ m}\cdot\text{s}^{-2}$).

$$a_1(t) = -\omega_1^2(p_1 - p_2) + g \quad [\text{Equation 3.1}]$$

$$a_2(t) = -\omega_2^2 p_2 + \omega_1^2 \lambda (p_1 - p_2) - 2\zeta \omega_2 v_2 + g \quad [\text{Equation 3.2}]$$

Finally, the GRF acting on the MSD-model ($\text{GRF}_{\text{model}}$) could be estimated as described in Equations 3.3, where M is the total mass.

$$\text{GRF}_{\text{model}} = \frac{M\omega_2}{1+\lambda} (\omega_2 p_2 + 2\zeta v_2) \quad [\text{Equation 3.3}]$$

3.2.3. Optimisation Routine

The eight model parameters were determined for each trial from a gradient descent optimisation routine in Matlab to estimate $\text{GRF}_{\text{model}}$ (Figure 3.2). The two second order differential equations (Equations 3.1 and 3.2) were transformed to four first order differential equations which were solved numerically using a Runge Kutta 4th order method to determine the eight model parameters. The MSD-model was fitted to the resultant $\text{GRF}_{\text{measured}}$ rather than to individual vector components of GRF because the two cutting tasks (Cut45 and Cut90) clearly involved three-dimensional movements that were not represented along one single primary lab axis (e.g. vertical) or in any primary plane (e.g. sagittal plane). The best fit between $\text{GRF}_{\text{measured}}$ and $\text{GRF}_{\text{model}}$ was determined as the sum of squared errors (SSE) across the contact phase (Equation 3.4).

$$\text{SSE} = \sum \sqrt{(\text{GRF}_{\text{measured}}(t) - \text{GRF}_{\text{model}}(t))^2} \quad [\text{Equation 3.4}]$$

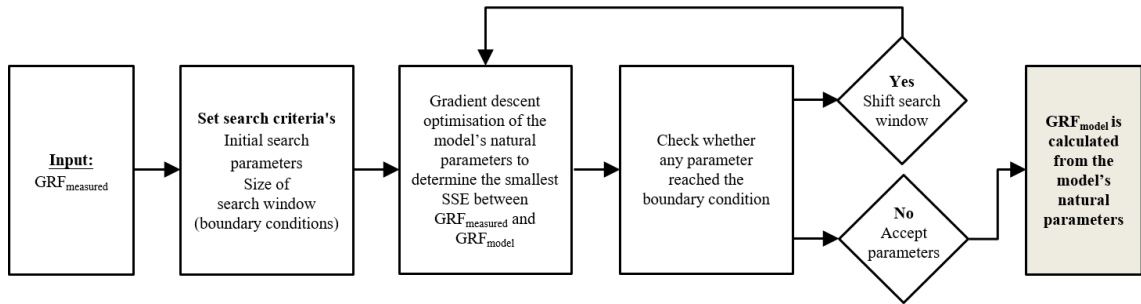


Figure 3.2: Flow-chart of the purpose built gradient descent optimisation routine used to estimate GRF_{model} .

The initial search parameters for the optimisation routine were determined from a two-step process including 1) typical model parameters presented by Derrick et al. (2000) for running and 2) median parameters across tasks and approach speeds from 4 participants (see detail in Appendix F). The initial search parameters of each parameter were split into a range of 5 values creating an 8^5 model parameter solution from which the solution with the smallest SSE was used to determine the search direction for the gradient descent optimisation. Furthermore, the parameter range obtained from the initial search parameters determined the size of the search window (boundary conditions) of the gradient descent optimisation. If any model parameter reached the boundary condition after the gradient descent optimisation, the search window was shifted and the gradient descent optimisation was repeated. The gradient descent optimisation was restricted to progress in a maximum of 500 iterations or until the SSE was less than 0.001. The $GRF_{measured}$ were downsampled to 100 Hz to reduce computation time. Examples of the SSE and model parameter history from the gradient descent optimisation routine along with the associated GRF_{model} is displayed in Figure 3.3.

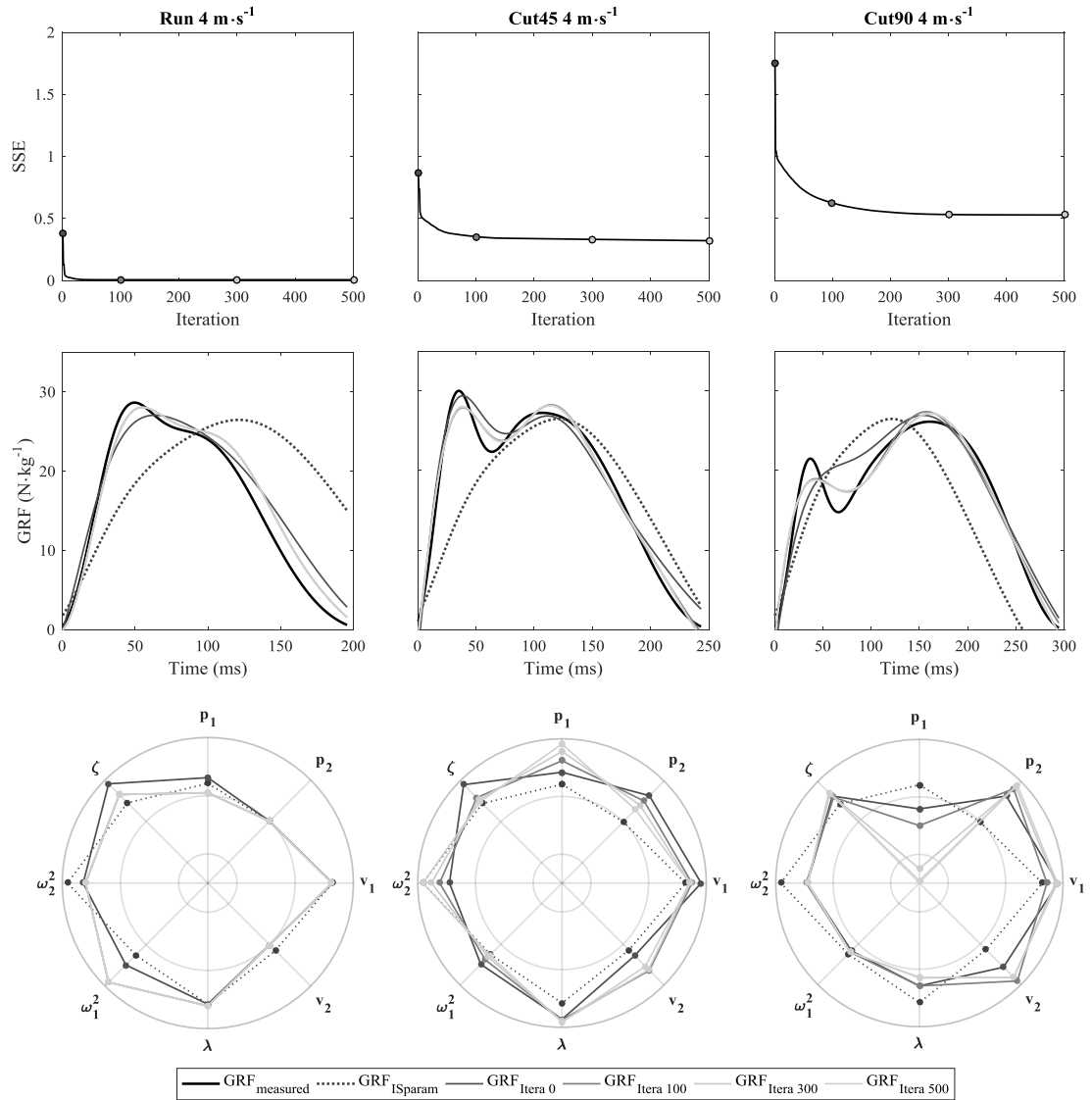


Figure 3.3: The top row display the SSE history from the gradient descent optimisation. The second row display $GRF_{measured}$ and GRF_{model} calculated from the initial search parameters (ISparam) and the model parameters from iteration 0, 100, 300 and 500 (Itera). The polar plots in the bottom row display the model parameter history from the initial search parameters to iteration step 500 (in scaled dimensionless values).

3.2.4. Data processing

The $GRF_{measured}$ and GRF_{model} were normalised to the participants' mass. The SSE was further normalised for the duration of stance time. The ability of the MSD-model to estimate specific GRF loading characteristics was evaluated using the following GRF trajectory characteristics: impulse, calculated as the integral of GRF across the stance time; impact peak, defined as peak GRF within the first 25% of the stance time; time to impact peak, defined as the time from touch down to the impact peak; average loading

rate, defined as the average gradient from touch down to the impact peak; active peak, defined as peak GRF in the last 75% of stance time; and time to active peak, defined as the time from touch down to the active peak. These GRF variables, stance time, SSE, and the eight model parameters, were averaged per condition for each individual participant. One of the participants was not able to complete the Cut90 condition with an approach speed at $5 \text{ m}\cdot\text{s}^{-1}$, and therefore all statistical analyses for this condition only included data from 19 participants.

3.2.5. Statistical analysis

Similarities between $\text{GRF}_{\text{measured}}$ and $\text{GRF}_{\text{model}}$ were interpreted from the magnitude of SSE, being poor ($>75 \text{ N}\cdot\text{kg}^{-1}\cdot\text{ms}^{-1}$), moderate ($25\text{-}75 \text{ N}\cdot\text{kg}^{-1}\cdot\text{ms}^{-1}$), good ($10\text{-}25 \text{ N}\cdot\text{kg}^{-1}\cdot\text{ms}^{-1}$), and very good ($<10 \text{ N}\cdot\text{kg}^{-1}\cdot\text{ms}^{-1}$). A two-way ANOVA analysis was used to evaluate the effect of task and approach speed on the SSE. Pairwise post-hoc analyses, with a Bonferroni corrected alpha level set at 0.0125, were used to test for any significant differences between tasks or approach speeds. Linear regression analyses were used to explore the within condition relationship between the GRF loading variables calculated from the $\text{GRF}_{\text{measured}}$ and $\text{GRF}_{\text{model}}$. The magnitudes of the linear relationships were interpreted as described by (Hopkins et al., 2009). The two-way ANOVA and linear regression analyses were performed using SPSS 22.0 (SPSS Inc. Chicago, IL, USA). Finally, Bland-Altman analyses were used to explore within conditions the mean difference (bias) and the 95% limits of agreement (LoA) between the GRF loading variables calculated from $\text{GRF}_{\text{measured}}$ and $\text{GRF}_{\text{model}}$ (Bland and Altman, 2010).

3.3. Results

The MSD-model was able to mimic the GRF_{measured} with moderate to very good similarity across the different conditions (Figure 3.4). The best and worst similarity were observed for Run (SSE between 2.5 ± 1.6 and $5.8 \pm 2.4 \text{ N}\cdot\text{kg}^{-1}\cdot\text{ms}^{-1}$) and Cut90 (SSE between 9.9 ± 6.3 and $33.8 \pm 16.8 \text{ N}\cdot\text{kg}^{-1}\cdot\text{ms}^{-1}$), respectively, and the SSE generally increased, i.e. showing less similarity, with increasing approach speeds (Table 3.1). The main effect from the two-way ANOVA analysis showed that SSE was significantly affected by both task and approach speed (task: $F_{2,227} = 69.5$, $p = <0.001$; approach speed: $F_{3,227} = 22.2$, $p = <0.001$). Post-hoc analysis revealed that mean SSE was significantly higher for Cut45 compared to Run, and that SSE for Cut90 was significantly higher than both Run and Cut45 (Table 3.1). In addition, SSE for the two fastest approach speeds (4 and $5 \text{ m}\cdot\text{s}^{-1}$) was significantly higher than the two slowest approach speeds (2 and $3 \text{ m}\cdot\text{s}^{-1}$).

Table 3.1: Mean \pm standard deviation for SSE ($\text{N}\cdot\text{kg}^{-1}\cdot\text{ms}^{-1}$) for the individual tasks and approach speeds. Mean difference and 98.75% confidence interval (CI) of the difference in SSE between tasks and approach speeds ($\alpha = 0.0125$) obtained from the two-way ANOVA and post-hoc analysis.

	Run	Cut45	Cut90	
2 m·s⁻¹	2.5 \pm 1.6	3.3 \pm 1.9	9.9 \pm 6.3	
3 m·s⁻¹	3.3 \pm 2.3	5.6 \pm 4.0	18.0 \pm 15.1	
4 m·s⁻¹	4.1 \pm 2.1	13.9 \pm 10.7	29.1 \pm 19.2	
5 m·s⁻¹	5.8 \pm 2.4	17.3 \pm 13.8	33.8 \pm 16.8	
Post-Hoc	Mean Difference	98.75% CI		p - value
		Lower	Upper	
Run vs. Cut45	-6.1	-10.8	-1.4	0.001*
Run vs. Cut90	-18.6	-23.3	-13.9	>0.001*
Cut45 vs. Cut90	-12.5	-17.2	-7.8	>0.001*
2 m·s⁻¹ – 3 m·s⁻¹	-3.7	-9.5	2.1	0.293
2 m·s⁻¹ – 4 m·s⁻¹	-10.5	-16.3	-4.6	>0.001*
2 m·s⁻¹ – 5 m·s⁻¹	-13.5	-19.3	-7.6	>0.001*
3 m·s⁻¹ – 4 m·s⁻¹	-6.8	-12.6	-0.9	0.002*
3 m·s⁻¹ – 5 m·s⁻¹	-9.8	-15.6	-3.9	>0.001*
4 m·s⁻¹ – 5 m·s⁻¹	-3.0	-8.9	2.8	0.652

* Indicates a significant difference between tasks or approach speeds ($\alpha = 0.0125$).

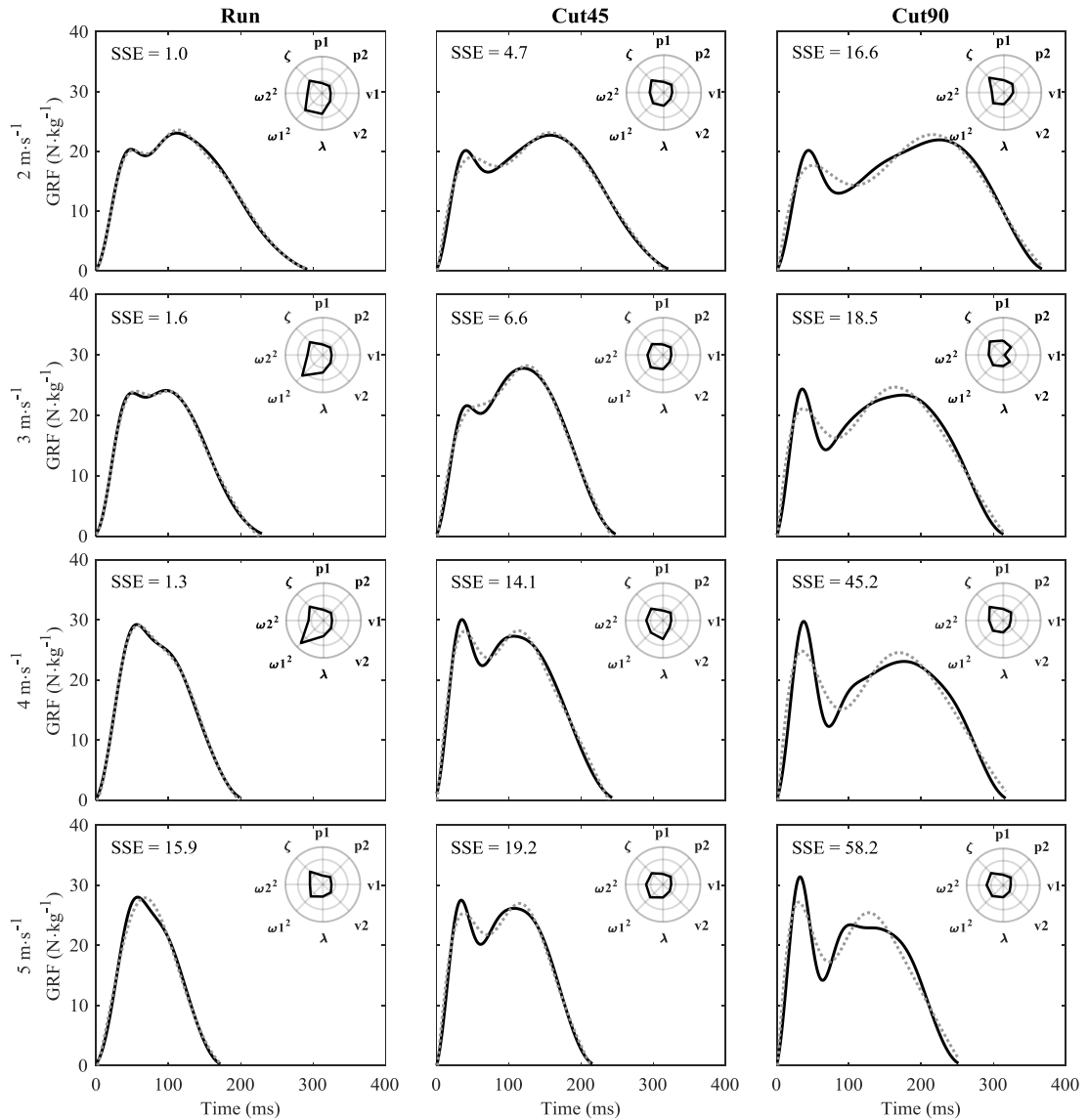


Figure 3.4: Representative example of $GRF_{measured}$ (solid black line) and GRF_{model} (dotted grey line) and the associated SSE for the conditions investigated in this study.

Very strong correlations (R^2 : 0.9 to 1.0) were found for the majority of GRF loading variables calculated from $GRF_{measured}$ and GRF_{model} across the different tasks and approach speeds (Table 3.2). Overall, the GRF loading variables showed smaller bias (GRF_{model} underestimating or overestimating the variables from $GRF_{measured}$) and smaller LoA (within condition variability) for the Run and Cut45 tasks compared to the Cut90 task (Figure 3.5). The Cut45 at the fastest approach speeds (4 and 5 m·s⁻¹) showed larger bias and LoA than the Run for impact peak, loading rate and active peak. Larger bias and

LoA were in particularly observed for the Cut90 task compared to the Run and Cut45 tasks for impact peak, time to impact peak, loading rate and active peak.

Table 3.2: Mean \pm standard deviation and R^2 for the extracted GRF variables from the $GRF_{measured}$ and GRF_{model} for the individual tasks and approach speeds.

	Run			Cut45			Cut90		
	$GRF_{measured}$	GRF_{model}	R^2	$GRF_{measured}$	GRF_{model}	R^2	$GRF_{measured}$	GRF_{model}	R^2
Impulse ($N \cdot s \cdot kg^{-1}$)									
2 $m \cdot s^{-1}$	4.1 \pm 0.2	4.1 \pm 0.2	0.99	4.5 \pm 0.4	4.5 \pm 0.4	0.99	5.2 \pm 0.6	5.3 \pm 0.7	0.98
3 $m \cdot s^{-1}$	4.0 \pm 0.3	4.0 \pm 0.2	1.00	4.5 \pm 0.5	4.5 \pm 0.5	1.00	5.4 \pm 0.8	5.5 \pm 0.8	1.00
4 $m \cdot s^{-1}$	3.8 \pm 0.3	3.8 \pm 0.3	1.00	4.5 \pm 0.5	4.5 \pm 0.5	1.00	5.8 \pm 0.8	5.8 \pm 0.9	1.00
5 $m \cdot s^{-1}$	3.3 \pm 0.4	3.2 \pm 0.4	1.00	4.0 \pm 0.5	4.0 \pm 0.5	1.00	5.3 \pm 0.7	5.3 \pm 0.8	1.00
Impact peak ($N \cdot kg^{-1}$)									
2 $m \cdot s^{-1}$	18.6 \pm 1.8	18.5 \pm 1.9	0.96	18.2 \pm 2.0	18.1 \pm 2.1	0.95	20.4 \pm 3.3	19.6 \pm 2.5	0.94
3 $m \cdot s^{-1}$	20.0 \pm 2.3	20.2 \pm 2.4	0.98	20.6 \pm 2.4	20.4 \pm 2.2	0.96	24.9 \pm 5.2	23.4 \pm 3.9	0.95
4 $m \cdot s^{-1}$	22.9 \pm 2.7	23.1 \pm 2.4	0.99	25.8 \pm 4.3	24.9 \pm 3.4	0.93	27.7 \pm 5.3	25.0 \pm 4.1	0.88
5 $m \cdot s^{-1}$	25.6 \pm 2.8	25.5 \pm 2.6	0.98	28.9 \pm 5.0	27.8 \pm 4.5	0.95	29.4 \pm 4.6	26.7 \pm 4.1	0.96
Time to impact peak (ms)									
2 $m \cdot s^{-1}$	81 \pm 12	82 \pm 11	0.98	79 \pm 15	80 \pm 14	0.98	77 \pm 20	83 \pm 18	0.85
3 $m \cdot s^{-1}$	66 \pm 9	67 \pm 8	0.94	62 \pm 14	66 \pm 11	0.90	59 \pm 16	68 \pm 18	0.82
4 $m \cdot s^{-1}$	54 \pm 7	55 \pm 7	0.90	50 \pm 12	54 \pm 12	0.90	55 \pm 14	63 \pm 19	0.87
5 $m \cdot s^{-1}$	44 \pm 4	47 \pm 5	0.80	44 \pm 8	46 \pm 9	0.93	46 \pm 8	51 \pm 12	0.81
Loading rate ($N \cdot kg^{-1} \cdot s^{-1}$)									
2 $m \cdot s^{-1}$	235 \pm 54	233 \pm 50	0.92	245 \pm 73	237 \pm 66	0.94	307 \pm 126	263 \pm 104	0.91
3 $m \cdot s^{-1}$	310 \pm 74	312 \pm 68	0.92	361 \pm 113	331 \pm 86	0.93	474 \pm 193	405 \pm 171	0.94
4 $m \cdot s^{-1}$	438 \pm 99	434 \pm 86	0.96	559 \pm 178	511 \pm 161	0.97	550 \pm 198	487 \pm 215	0.94
5 $m \cdot s^{-1}$	584 \pm 91	561 \pm 86	0.92	684 \pm 207	645 \pm 186	0.99	659 \pm 165	612 \pm 201	0.97
Active peak ($N \cdot kg^{-1}$)									
2 $m \cdot s^{-1}$	22.5 \pm 2.2	22.5 \pm 2.2	0.96	22.7 \pm 2.8	23.0 \pm 2.7	0.99	22.6 \pm 3.0	22.9 \pm 3.0	0.93
3 $m \cdot s^{-1}$	24.9 \pm 2.0	25.0 \pm 2.0	0.96	25.5 \pm 2.6	25.9 \pm 2.6	0.96	24.5 \pm 2.9	24.9 \pm 3.0	0.91
4 $m \cdot s^{-1}$	27.0 \pm 1.7	27.1 \pm 1.6	0.98	27.3 \pm 2.6	27.9 \pm 2.6	0.93	23.8 \pm 2.7	25.1 \pm 2.9	0.94
5 $m \cdot s^{-1}$	27.1 \pm 2.5	27.4 \pm 2.4	0.98	28.3 \pm 3.0	28.9 \pm 3.0	0.94	24.5 \pm 3.5	25.6 \pm 3.5	0.94
Time to active peak (ms)									
2 $m \cdot s^{-1}$	125 \pm 14	126 \pm 16	0.83	143 \pm 25	144 \pm 26	0.88	169 \pm 49	167 \pm 44	0.96
3 $m \cdot s^{-1}$	109 \pm 14	109 \pm 15	0.89	125 \pm 23	124 \pm 23	0.90	137 \pm 32	139 \pm 33	0.74
4 $m \cdot s^{-1}$	92 \pm 14	93 \pm 14	0.92	108 \pm 22	106 \pm 24	0.75	126 \pm 33	131 \pm 40	0.88
5 $m \cdot s^{-1}$	68 \pm 17	65 \pm 16	0.84	84 \pm 23	85 \pm 25	0.93	122 \pm 26	123 \pm 28	0.76
Stance time (ms) – from $GRF_{measured}$									
2 $m \cdot s^{-1}$	331 \pm 38			332 \pm 43			368 \pm 63		
3 $m \cdot s^{-1}$	274 \pm 27			284 \pm 32			334 \pm 51		
4 $m \cdot s^{-1}$	231 \pm 21			256 \pm 32			351 \pm 61		
5 $m \cdot s^{-1}$	195 \pm 19			218 \pm 29			316 \pm 58		

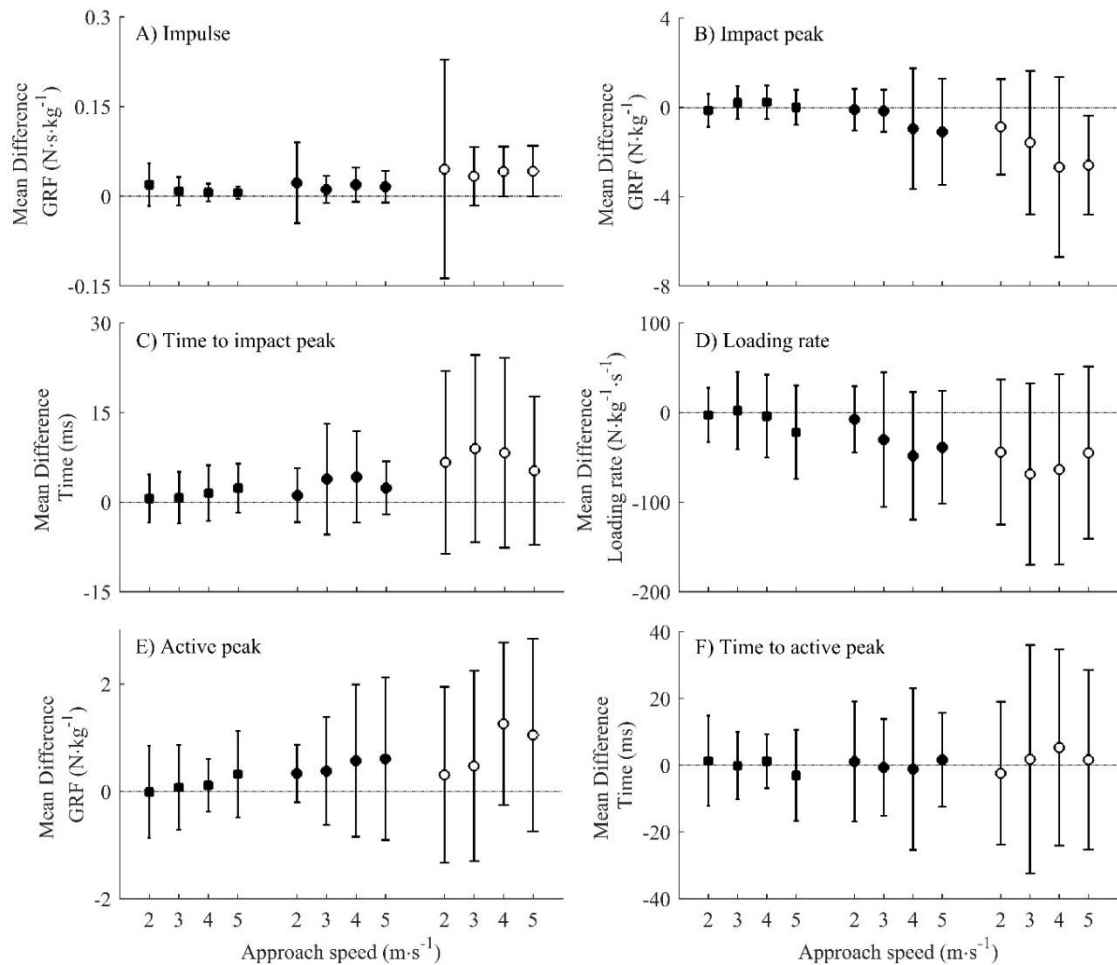


Figure 3.5: Results from the Bland-Altman analysis, showing the mean difference (marker) and 95% limits of agreements (error bar) for the Run (solid square), Cut45 (solid circle) and Cut90 (open circle) across the different tasks and approach speeds.

The average model parameters, apart from p_2 , saw limited change within tasks or approach speeds, similarly did p_2 vary the most within tasks (Figure 3.6). The illustrative polar plots of the eight model parameters displayed in Figures 3.4 and 3.7 showed that λ , ω_1^2 , ω_2^2 and ζ varied the most across the different GRF patterns observed in this study. Generally higher values of ω_1^2 (the natural frequency of the upper spring) were for example observed for the Run task compared to the two cutting tasks, whereas the smallest values of ω_2^2 (the natural frequency of the lower spring) were observed for the Cut90 task (Table 3.3).

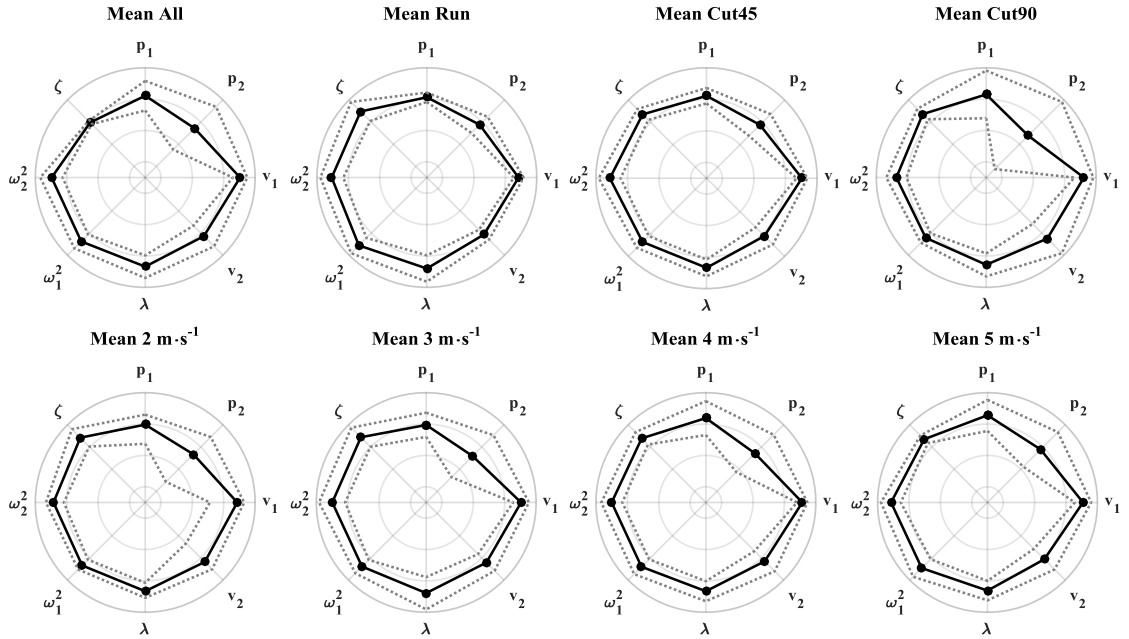


Figure 3.6: Polar plots displaying the mean (black line and circles) and standard deviations (dotted grey line) of the model parameters (in scaled dimensionless values) across all conditions and for the individual tasks and approach speeds.

Table 3.3: Mean \pm standard deviation of the eight model parameters for the individual tasks and approach speeds.

	p_1 (m)	p_2 (m)	v_1 (m·s ⁻¹)	v_2 (m·s ⁻¹)	λ (au)	ω_1^2 (N·m ⁻¹ ·kg ⁻¹)	ω_2^2 (N·m ⁻¹ ·kg ⁻¹)	ζ (au)
Run 2 m·s⁻¹	0.00 ± 0.03	0.01 ± 0.01	-1.00 ± 0.54	0.19 ± 0.33	4.42 ± 2.70	616 ± 339	2771 ± 1905	0.53 ± 0.53
Run 3 m·s⁻¹	0.00 ± 0.01	0.00 ± 0.01	-1.16 ± 0.57	-0.14 ± 0.24	6.43 ± 8.49	765 ± 448	3989 ± 3496	0.53 ± 0.52
Run 4 m·s⁻¹	-0.01 ± 0.01	0.00 ± 0.01	-1.26 ± 0.27	-0.09 ± 0.40	3.80 ± 2.41	810 ± 465	3973 ± 2288	0.41 ± 0.36
Run 5 m·s⁻¹	-0.02 ± 0.02	0.00 ± 0.00	-1.11 ± 0.20	-0.05 ± 0.23	2.97 ± 1.64	878 ± 542	4804 ± 2364	0.33 ± 0.10
Cut45 2 m·s⁻¹	0.00 ± 0.02	0.00 ± 0.01	-1.10 ± 0.40	-0.22 ± 0.37	3.98 ± 3.19	400 ± 345	4063 ± 2688	0.31 ± 0.20
Cut45 3 m·s⁻¹	-0.01 ± 0.03	0.00 ± 0.01	-1.33 ± 0.37	-0.22 ± 0.31	3.94 ± 2.61	400 ± 216	4719 ± 2928	0.32 ± 0.37
Cut45 4 m·s⁻¹	-0.02 ± 0.03	0.00 ± 0.01	-1.65 ± 0.45	-0.22 ± 0.48	3.20 ± 2.62	443 ± 287	4083 ± 2559	0.34 ± 0.19
Cut45 5 m·s⁻¹	-0.03 ± 0.03	0.00 ± 0.01	-1.47 ± 0.40	-0.02 ± 0.67	3.32 ± 2.33	638 ± 465	4164 ± 2075	0.31 ± 0.13
Cut90 2 m·s⁻¹	0.01 ± 0.06	0.01 ± 0.02	-1.41 ± 0.74	-0.41 ± 0.68	2.53 ± 2.63	307 ± 239	2481 ± 2374	0.31 ± 0.21
Cut90 3 m·s⁻¹	0.02 ± 0.08	0.02 ± 0.03	-1.74 ± 0.88	-0.57 ± 0.83	2.51 ± 3.09	344 ± 309	2296 ± 2172	0.35 ± 0.17
Cut90 4 m·s⁻¹	-0.06 ± 0.12	0.01 ± 0.03	-1.68 ± 0.48	-0.34 ± 1.00	3.82 ± 4.89	277 ± 336	2963 ± 2455	0.31 ± 0.16
Cut90 5 m·s⁻¹	-0.07 ± 0.10	0.01 ± 0.03	-1.82 ± 1.01	-0.18 ± 0.97	3.88 ± 5.08	244 ± 234	3808 ± 2434	0.31 ± 0.21

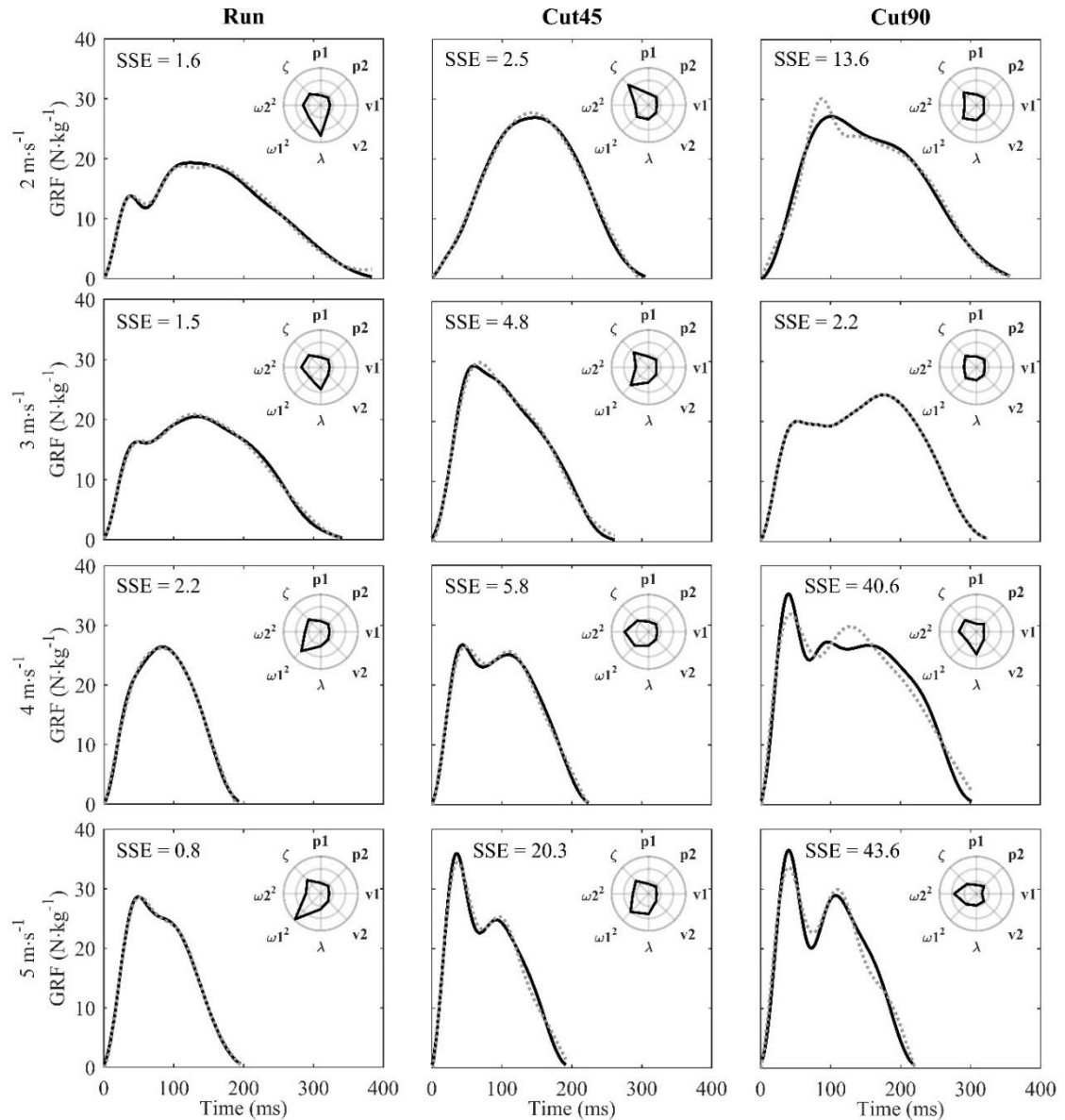


Figure 3.7: Examples of the MSD-models ability to estimate the range of different GRF patterns ($GRF_{measured}$ is the solid black line and GRF_{model} is the dotted grey line) observed in this study between participants, tasks and approach speeds. The SSE ($N \cdot kg^{-1} \cdot ms^{-1}$) and polar plots displaying the model parameters (in scaled dimensionless values) for the individual trials.

3.4. Discussion

The aim of this study was to explore the generalisability of a mass-spring-damper model to estimate GRF in running and changing direction at different running speeds. The MSD-model was able to mimic GRF patterns observed in this study with moderate to very good accuracy. Less similarity between modelled and measured GRF was observed in both side cutting tasks. In addition, significantly better similarity was observed for the two slowest

approach speeds (2 to 3 m·s⁻¹) compared to the fastest approach speeds (4 to 5 m·s⁻¹). The biomechanically most relevant features of the GRF trajectories could be represented through the model as strong (R^2 : 0.7 to 0.9) to very strong (R^2 : 0.9 to 1.0) correlations were found between the GRF loading variables calculated from GRF_{measured} and GRF_{model} for all conditions, despite larger bias and LoA observed in Cut90.

The moderate to very good similarity between GRF_{measured} and GRF_{model} across tasks and approach speeds, and small mean difference in the impulse, illustrated that a simple MSD-model can mimic GRF patterns and its biomechanically relevant features for utility movements at different intensities. In fact, the differences in impulse between GRF_{measured} and GRF_{model} observed across tasks and approach speeds in this study were smaller than what was previously observed by Derrick et al. (2000) for running at 3.83 m·s⁻¹ (19.9 N·s \approx 0.26 N·s·kg⁻¹). In comparison the mean difference in impulse observed in this study was 0.01 N·s·kg⁻¹ for running at 4 m·s⁻¹, which is similar to the difference in impulse (-1.3 N·s \approx -0.02 N·s·kg⁻¹) observed by Derrick et al. (2000) after their 10% adjustment of GRF_{model} . Derrick et al. (2000) only included the spring constants of the upper and lower spring (k_1 and k_2) and the position of the lower mass (p_2) in their optimisation routine. The damping ratio was for example kept constant ($\zeta = 0.35$), whereas it was included in the optimisation routine in the present study. Damping ratios between 0.31 and 0.53 were observed between conditions in the present study, which is within the range previously reported for running (Cavagna, 1970; McMahon and Greene, 1979). The additional model parameters included in our optimisation routine may explain the fact that better agreement for parameters such as impulse was found in this study compared to the study by Derrick et al. (2000).

Team sport players spend the majority of playing time performing running related utility movements at different intensities, amongst which changes in direction are in general characterised by a large deceleration of the body followed by an acceleration to push off in a new direction (Jones et al., 2016; Jones et al., 2015). These movements can to some extent fail to follow spring-like behaviour, particularly when the energy absorbed during the deceleration is larger than that which the body is able to generate when (re-)accelerating the body in a new direction. The CoM velocity at the end of foot-ground-contact would then be lower than the CoM velocity at the beginning of foot-ground-contact, and the return of energy is then likely postponed to the following steps when the body is already moving into the new direction. This was confirmed through full-body kinematics, as the average resultant CoM velocity decreased by $0.24 \pm 0.19 \text{ m}\cdot\text{s}^{-1}$ for Cut90, compared to 0.13 ± 0.12 and $0.16 \pm 0.04 \text{ m}\cdot\text{s}^{-1}$ for Cut45 and Run, respectively. This energy absorption therefore likely explained why the MSD-model's accuracy for representing GRF was lowest for the Cut90 task.

Strong to very strong correlations were observed for the GRF loading variables investigated in this study demonstrating that the model estimates follow measured variations closely. Though the accuracy of the GRF loading variables estimated from the model decreased for Cut90 task, we believe these under- and overestimations are still within an acceptable range for this simple model approach to estimate GRF characteristics acting on the human body. GRF loading variables are largely unexplored in team sports, but the simple MSD-model approach might help researchers explore if accumulation of high impact forces, impulse, or loading rates are associated with increased risk of overuse injuries in team sports, something which has already been demonstrated in long distance runners (Hreljac, 2004).

The MSD-model showed to be the least accurate for GRF patterns characterised by a high impact peak, loading rate and long stance times, such as the examples of the Cut90 at 4 and 5 m·s⁻¹ displayed in Figures 3.4 and 3.7. The model especially underestimated the impact peak when the stance time increased. Derrick et al. (2000) demonstrated that the MSD-model, due to its spring-like behaviour, increases the stance time by decreasing the natural frequencies of the two springs (ω_1^2 and ω_2^2). This is similar to the results observed in this study where the change in direction tasks had the longest stance time (Table 3.2) and the lowest natural frequencies of the two springs (ω_1^2 and ω_2^2) (Table 3.3). The impact peak was however systematically underestimated as a consequence of the decreased spring stiffness. The natural “springs” in our body are the soft tissues of the lower extremities which can absorb and return elastic energy. It might very well be the case that for shorter contact times the body is increasingly able to utilize the stiffness of its tendons (e.g. the Achilles tendon), something which was suggested to be the case when jumping towards different heights (Vanrenterghem et al., 2004).

There are a number of limitations to this study. One limitation is the fact that the approach speeds and tasks included in this study do not cover all of the agility movements team sports player perform. For instance, the model’s generalisability to simulate GRF from running velocities higher than 5 m·s⁻¹ remains unknown, though it might be expected that the model can mimic these GRF trajectories because GRF patterns previously presented for sprinting (Clark and Weyand, 2014) are largely similar to those predicted in this study. Another limitation is that the simplified MSD-model does not account for the energy generated by the body’s “active” structures (muscles). Whilst a more complex model could account for these it is questionable if the addition of “active” elements actually would improve the simulation of GRF trajectories. A third limitation is that the gradient descent optimisation routine used in this study may find local minima and not the true

global minimum. A number of local minima (model parameter solutions) might exist close to the global minimum due to the number of model parameter solutions which exist close to the global minimum. The gradient descent optimisation was however believed to be sufficient for this study.

The eight model parameters, required to estimate GRF from the MSD-model, are currently obtained from GRF measured by a force platform, which to some extent limits the application of the MSD-model in team sports. For wider applicability, researchers should investigate if the model parameters can be established from other methods. For example, professional team sport players currently wear trunk-mounted accelerometers during training (Akenhead and Nassis, 2016; Cummins et al., 2013). Although these accelerometers only measure the accelerations of the trunk (Nedergaard et al., 2016; Wundersitz et al., 2013), future studies should explore if trunk accelerometry can be used to establish the eight model parameters. If that is the case, then one could start estimating GRF from MSD-models using model parameters obtained from trunk accelerometry.

3.5. Conclusion

In conclusion, this study demonstrated that a mass-spring-damper model is generalisable for estimating GRF patterns and related loading variables observed during a broad range of movements in team sports. The MSD-model approach may well become a useful approach for researchers to estimate whole-body biomechanical loading in team sports, which could be invaluable for linking biomechanical load to injury risk.

CHAPTER 4

A new approach to predict biomechanical loading from trunk-mounted accelerometry

This study was presented at the 2nd ASPIRE Sport Science Conference “Monitoring Athlete Training Loads – The Hows and Whys” in Doha, Qatar 2016. The aim of this study was to introduce a novel mass-spring-damper model approach to estimate ground reaction forces from trunk-mounted accelerometry in team sports related movements. The mass-spring-damper model’s upper mass acceleration was able to simulate the measured trunk accelerometry data. Though poor ground reaction forces were predicted from the direct approach a sensitivity analysis of the eight model parameters revealed promising improvements of the ground reaction force predictions.

4.1. Introduction

Team sports players generate forces against the ground to move their body around the pitch e.g. during tasks such as walking, sprinting, accelerating, decelerating and changing direction. This comes at a cost because equal and opposite ground reaction forces (GRF), from the interaction with the ground, are acting on their body imposing the player’s soft tissues under biomechanical stress (bones, cartilage, muscles, tendons and ligaments) (Dye, 2005; Kibler et al., 1992; Nigg et al., 1995). Over time the accumulation of biomechanical load can result in beneficial structural adaptations e.g. repair, regeneration, and strengthening of the player’s soft tissues or negative adaptations leading to overuse or acute injuries depending on the volume, frequency, duration and intensity of the load and recovery period (Dye, 2005; Kibler et al., 1992; Nigg et al., 1995). Overuse injuries are per definition a result of the cumulative tissue damage over time (Clarsen et al., 2015; Finch and Cook, 2014) and monitoring of the biomechanical load may therefore help researchers and practitioners to better understand the relationship between whole-body biomechanical load and soft tissue overuse injuries in team sports.

Measurement of GRF, a surrogate for whole-body biomechanical load, is currently restricted to laboratory environments where force platforms inbuilt to the ground are considered as the gold standard to measure the GRF acting on the body (Winter, 2005). This makes it difficult to monitor the biomechanical loads to which a player is exposed from the external GRF during training sessions or match-play. Researchers and practitioners have therefore focused on the relationship between the exposure to physiological load measurements (e.g. total distance covered or distance covered at high intensity running, session duration dependent rating of perceived exertion) and overuse injuries in the current literature (Ehrmann et al., 2016; Gabbett, 2010; Gabbett and Ullah, 2012). More recently it has been suggested that the accelerometer integrated in the commercial GPS devices, which are used on a daily basis in professional team sports (Akenhead and Nassis, 2016; Cummins et al., 2013), can be used to estimate the GRF acting on the player's body (Boyd et al., 2011). However, the GPS integrated accelerometer is known to overestimate GRF during team sports movements (Nedergaard et al., 2016; Wundersitz et al., 2013).

The challenge with trunk-mounted accelerometry is that it does not measure the body's centre of mass (CoM), but only the accelerations of the segment it is attached to (Nedergaard et al., 2016). This is therefore not sufficient to determine the multi-segment dynamics of the body during dynamic movements. Due to the spring-like behaviour of the human body during running, where the elastic tissues of the support leg absorb and return the elastic energy, simple spring-mass models have been used to estimate the CoM displacement and running mechanics of the human body (Alexander et al., 1986; Blickhan, 1989; McMahon and Cheng, 1990). The vertical GRF can be estimated as a half sinusoidal wave from the vertical movement of the model's mass (the system's centre of mass) but this simple spring-mass model approach is insufficient to estimate the initial

impact forces when the foot collides with the ground (Alexander et al., 1986; Bobbert et al., 1992; Clark and Weyand, 2014). A modified mass-spring-damper model (MSD-model) with a second mass in series with a spring-damper, representing the support leg at initial impact, has been successful in overcoming this issue, and allows one to replicate the GRF pattern of humans during running (Derrick et al., 2000) and change in direction at different intensities (Chapter 3). It is however still unknown if the eight model parameters required to estimate GRF from the MSD-model can be established from trunk accelerometry data (e.g. from a GPS integrated accelerometer). The aim of this study was therefore to explore the opportunity to generate the eight MSD-model parameters from measured trunk accelerometry and thereby predict the GRF during team sports related movements.

4.2. Methods

Twenty recreational male team sports athletes volunteered to participate in this study (age 22 ± 4 years, height 178 ± 8 cm, mass 76 ± 11 kg). No participants had a history of severe lower limb injuries (e.g. ACL injuries or ankle sprains). The study was approved by the institutional ethics committee and written consent was obtained from all participants.

4.2.1. Protocol

The participants completed four forward straight line running trials (Run) and four anticipated 45° (Cut45) and four 90° (Cut90) open side-cutting manoeuvres at approach speeds of 2, 3, 4 and $5 \text{ m}\cdot\text{s}^{-1}$ ($\pm 5\%$) in a randomised condition order. Participants ran over the force platform with their dominant leg during the Run trials and performed the Cut45 and Cut90 when their dominant leg made contact with the force platform (turning in the direction of their non-dominant leg). Approach speeds were measured with photocell

timing gates (Brower Timing System, Utah, USA) positioned 2 m apart and 2 m before the centre of the force platform.

4.2.2. Measurements

Resultant trunk accelerations ($\text{TrunkAcc}_{\text{measured}}$) were collected at 100 Hz using a tri-axial accelerometer embedded within a commercial GPS device (MinimaxX S4, Catapult Innovations, Scoresby, Australia). The GPS device was positioned on the dorsal part of the upper trunk between the scapulae within a small pocket of a tight fitted elastic vest according to the manufacturer's recommendations (Boyd et al., 2011). Resultant ground reaction forces were measured ($\text{GRF}_{\text{measured}}$) with a sampling frequency of 3000 Hz from a Kistler force platform (9287C, Kistler Instruments Ltd., Winterthur, Switzerland). $\text{TrunkAcc}_{\text{measured}}$ and $\text{GRF}_{\text{measured}}$ were exported to Matlab (version R2016a, The MathWorks, Inc., Natick, MA, USA) where a 4th order recursive Butterworth low-pass filter with a cut-off frequency of 20 Hz was applied to the $\text{GRF}_{\text{measured}}$ and $\text{TrunkAcc}_{\text{measured}}$ data. In contrast to Chapter 2, $\text{TrunkAcc}_{\text{measured}}$ was filtered in this study to remove the high frequency content of the signal before it was used as model input, as this was expected to improve the models ability to replicate the trunk accelerometer signal. $\text{TrunkAcc}_{\text{measured}}$ and $\text{GRF}_{\text{measured}}$ were synchronised as described in Nedergaard *et al.* (2016) (see details in Appendix C) and touch down and take off on the force platform were defined for each trial when the vertical GRF crossed a 20 N threshold.

4.2.3. Accelerometry MSD-model

The multi-dynamics of the human body was modelled as a mass-spring-damper model (MSD-model) consisting of a lower mass (m_2) on top of a spring-damper combination representing generally the support leg at initial impact and an upper mass (m_1) on top of another spring representing generally the rest of the body (Alexander et al., 1986; Derrick

et al., 2000). The GRF acting on the MSD-model (GRF_{model}) can mathematically be calculated (Equation 4.3) from the equation of motion of the two masses (Equations 4.1 and 4.2) when eight initial model parameters are known: the position (p_1) and velocity (v_1) of the upper mass, the position (p_2) and velocity (v_2) of the lower mass, the mass ratio (λ) of the lower mass relative to the participant's total body mass, the natural frequency of the upper (ω_1^2) and lower spring (ω_2^2), and the dampening ratio (ζ) of the damper (Derrick et al., 2000).

$$a_1(t) = -\omega_1^2(p_1 - p_2) + g \quad [\text{Equation 4.1}]$$

$$a_2(t) = -\omega_2^2 p_2 + \omega_1^2 \lambda (p_1 - p_2) - 2\zeta \omega_2 v_2 + g \quad [\text{Equation 4.2}]$$

$$GRF_{model} = \frac{M\omega_2}{1+\lambda} (\omega_2 p_2 + 2\zeta v_2) \quad [\text{Equation 4.3}]$$

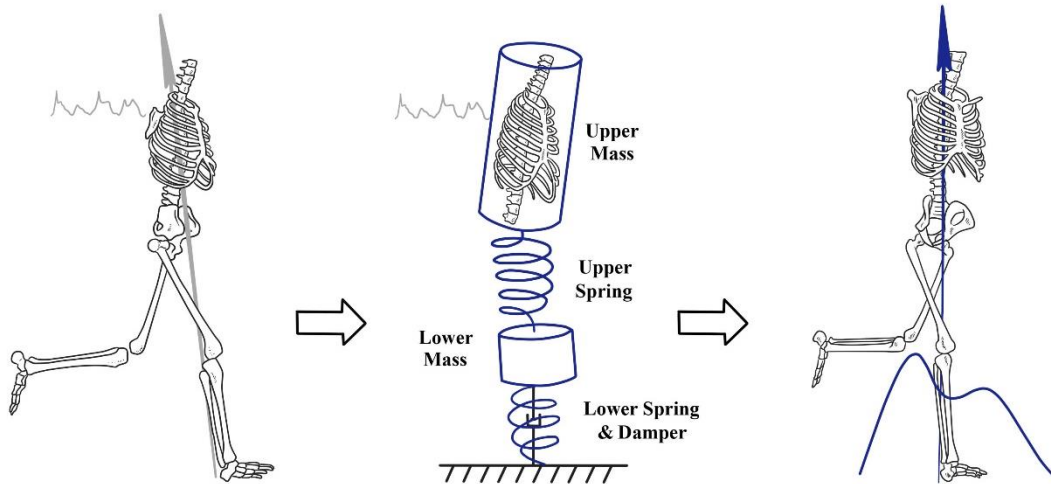


Figure 4.1: Illustration of the accelerometer/MSD-model, where $TrunkAcc_{measured}$ is used to simulate the acceleration of the upper mass from which the eight natural model parameters are obtained required to predict GRF_{model} .

The eight model parameters were determined from a purpose built gradient descent optimisation routine in Matlab where the acceleration of the upper mass (a_1) was simulated using the gravity corrected $TrunkAcc_{measured}$ (Figure 4.1). Assuming that the upper mass is representative of the trunk, the sum of squared errors between the

TrunkAcc_{measured} and a_1 (SSE_{trunk}) was used to determine the eight model parameters from which the model best simulated the TrunkAcc_{measured} (Equation 4.4). The structure of the gradient descent optimisation routine (Figure 4.2) was similar to the structure previously described in Chapter 3, where GRF_{measured} were used to determine the eight model parameters. The initial search parameters for the optimisation routine were defined following the same two-step pilot study approach described in Chapter 3 where the mean model parameter values from Chapter 3 were used as initial search parameters on the data from 4 participants (see details in Appendix F). The two second order differential equations (Equations 4.1 and 4.2) were transformed to four first order differential equations which were solved numerically using a 4th order Runge Kutta method to calculate GRF_{model} and a_1 from the eight model parameters.

$$SSE = \sum \sqrt{(TrunkAcc_{measured}(t) - a_2(t))^2} \quad [\text{Equation 4.4}]$$

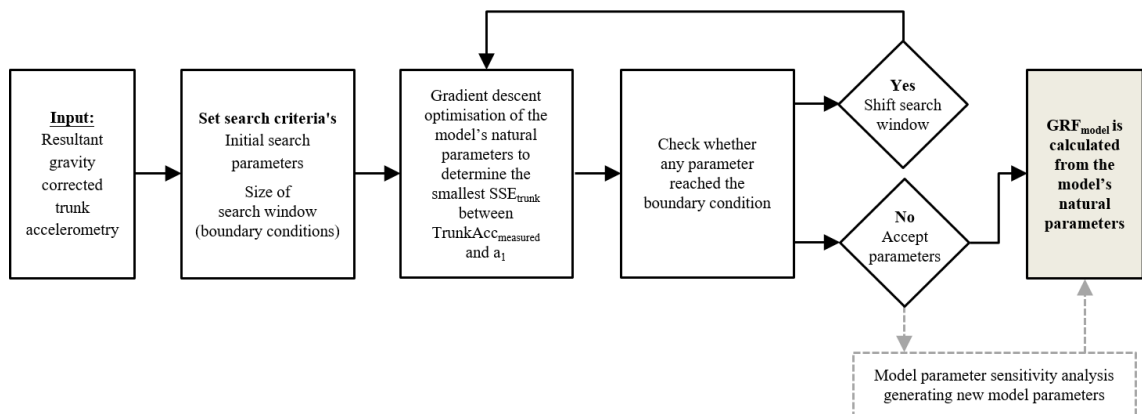


Figure 4.2: Flow-chart of the gradient descent optimisation routine from which the eight model parameters were generated when TrunkAcc_{measured} was used as model input. The model parameter sensitivity analysis is displayed with grey dashed lines.

4.2.4. Model parameter sensitivity analysis

A sensitivity analysis of TrunkAcc_{measured} model parameters on the predicted GRF_{model} and SSE_{GRF} was performed where GRF_{model} was re-calculated with new model parameters

($GRF_{modelNP}$) using the 4th order Runge Kutta method. The combination of the new model parameters was defined from the results of 1) a comparison between the average $TrunkAcc_{measured}$ and $GRF_{measured}$ (data from Chapter 3) model parameters and 2) a linear regression between the $TrunkAcc_{measured}$ and $GRF_{measured}$ model parameters. In case a linear relationship existed, the $TrunkAcc_{measured}$ model parameters were re-calculated based on the slope of the linear regression to generate new model parameters.

4.2.5. Data processing

$GRF_{measured}$ was down-sampled to 100Hz and the sum of squared errors between $GRF_{measured}$ and GRF_{model} were calculated to determine the accuracy of the predicted GRF_{model} . In addition, both SSE_{trunk} and SSE_{GRF} were normalised to stance time to compare between conditions. The $GRF_{measured}$ and GRF_{model} were normalised to the participant's mass. The ability of the MSD-model to estimate specific GRF loading characteristics was evaluated using the following GRF trajectory characteristics: Impulse; Impact peak; Time to impact peak; Loading rate; Active peak and Time to active peak, all defined as previously described in Chapter 3. The eight model parameters, SSE_{trunk} , SSE_{GRF} and the GRF variables were averaged per condition for each individual participant. One of the participants was not able to complete the Cut90 condition with an approach speed at $5 \text{ m}\cdot\text{s}^{-1}$, and therefore all statistical analyses for this condition only included data from 19 participants.

4.2.6. Statistical analysis

Similarities between $TrunkAcc_{measured}$ and a_1 were interpreted from the magnitude of SSE_{trunk} , being poor ($>0.5 \text{ g/frames}$), moderate ($0.2-0.5 \text{ g/frames}$), good ($0.1-0.2 \text{ g/frames}$), and very good ($<0.1 \text{ g/frames}$). The similarities between $GRF_{measured}$ and GRF_{model} were interpreted from the magnitude of SSE_{GRF} , being poor ($>25 \text{ N/kg/frames}$),

moderate (10-25 N/kg/frames), good (1-10 N/kg/frames), and very good (<1 N/kg/frames). A one-way ANOVA analysis was used to evaluate the effect of task and approach speed respectively on the SSE_{trunk} and SSE_{GRF} . Pairwise post-hoc analyses, with a Bonferroni corrected alpha level set at 0.0125, were used to test for any significant differences between tasks or approach speeds. Linear regression analyses were used to explore the within condition relationship between the GRF loading variables calculated from the GRF_{measured} and GRF_{model} . The magnitudes of the linear relationships were interpreted as described by (Hopkins et al., 2009). The one-way ANOVA and linear regression analyses were performed using SPSS 22.0 (SPSS Inc. Chicago, IL, USA). Finally, Bland-Altman analyses were used to explore within conditions mean difference (bias) and the 95% limits of agreement (LoA) between the GRF loading variables calculated from GRF_{measured} and GRF_{model} (Bland and Altman, 2010).

4.3. Results

4.3.1. Simulation of upper mass acceleration

The optimisation routine found a solution in 938 out of 956 trials (Run: 316:320; Cut45: 319:320; 303:316 trials) when a_1 of the MSD-model was fitted to $\text{TrunkAcc}_{\text{measured}}$. The MSD-model was able to simulate the acceleration patterns of the $\text{TrunkAcc}_{\text{measured}}$ with good to very good accuracy across tasks and intensities (Table 4.1), though a_1 generally underestimated the magnitude of the first peak in the acceleration signal during the stance time (Figure 4.3, 4.4 and 4.5).

Table 4.1: Mean \pm standard deviation for SSE_{Trunk} (g/frames) and SSE_{GRF} (N/kg/frames) for the individual tasks and approach speeds. Trials with SSE_{GRF} above 5000 were removed before mean and standard deviations was calculated for SSE_{GRF} , a total of 82 trials were removed (Run: 19 trials; Cut45: 30 trials; Cut90: 33 trials).

Approach speed	Run		Cut45		Cut90	
	SSE_{Trunk}	SSE_{GRF}	SSE_{Trunk}	SSE_{GRF}	SSE_{Trunk}	SSE_{GRF}
$2 \text{ m}\cdot\text{s}^{-1}$	0.04	269	0.04	544	0.08	387
	± 0.03	± 357	± 0.03	± 812	± 0.07	± 361
$3 \text{ m}\cdot\text{s}^{-1}$	0.06	375	0.07	500	0.13	374
	± 0.04	± 432	± 0.05	± 612	± 0.08	± 446
$4 \text{ m}\cdot\text{s}^{-1}$	0.07	463	0.12	362	0.14	427
	± 0.06	± 555	± 0.13	± 419	± 0.11	± 577
$5 \text{ m}\cdot\text{s}^{-1}$	0.07	385	0.09	561	0.13	226
	± 0.06	± 509	± 0.09	± 644	± 0.11	± 306

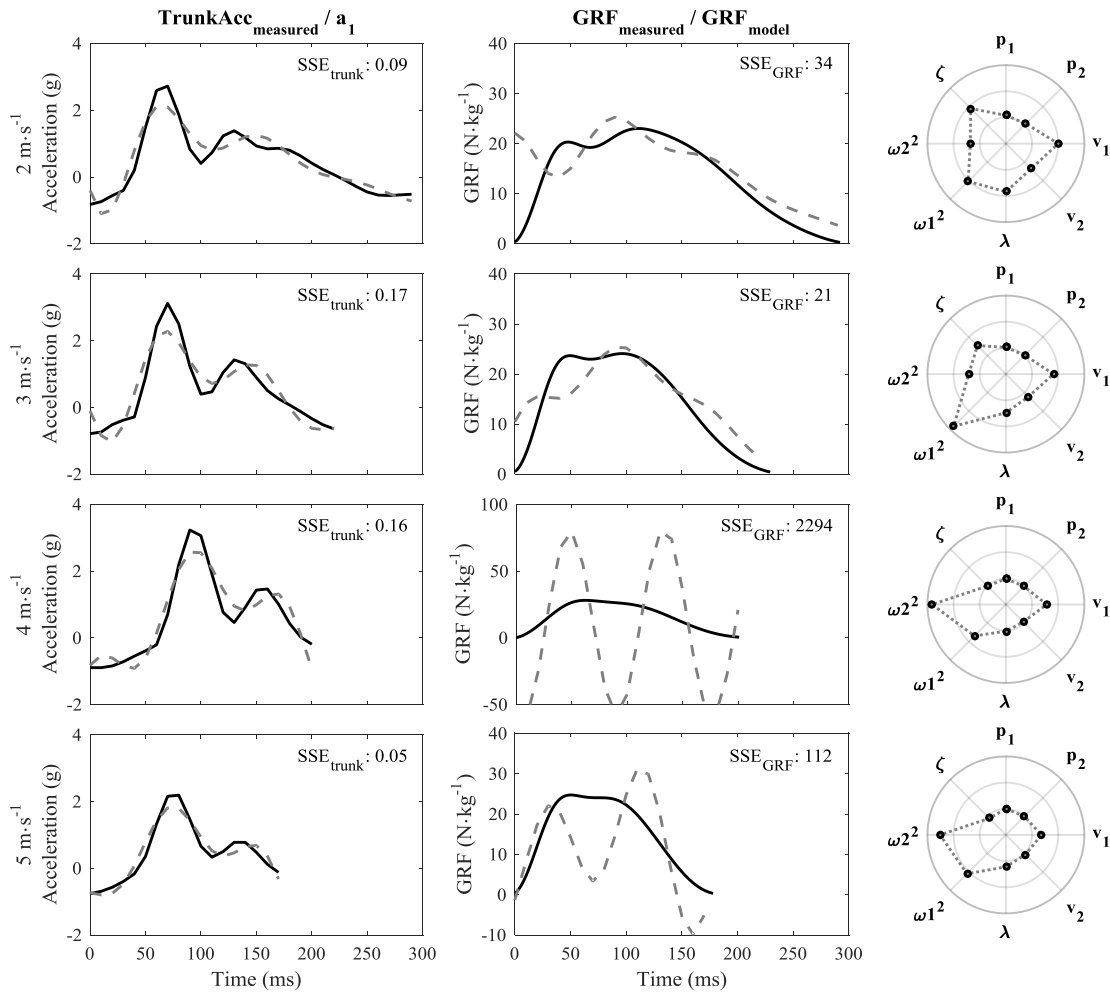


Figure 4.3: Example of $TrunkAcc_{measured}$ (black line), a_1 (dashed grey line), $GRF_{measured}$ (black line) and GRF_{model} (dashed grey line) for the Run from a representative participant. The polar plots display the model parameters (in scaled dimensionless values) for the individual trials.

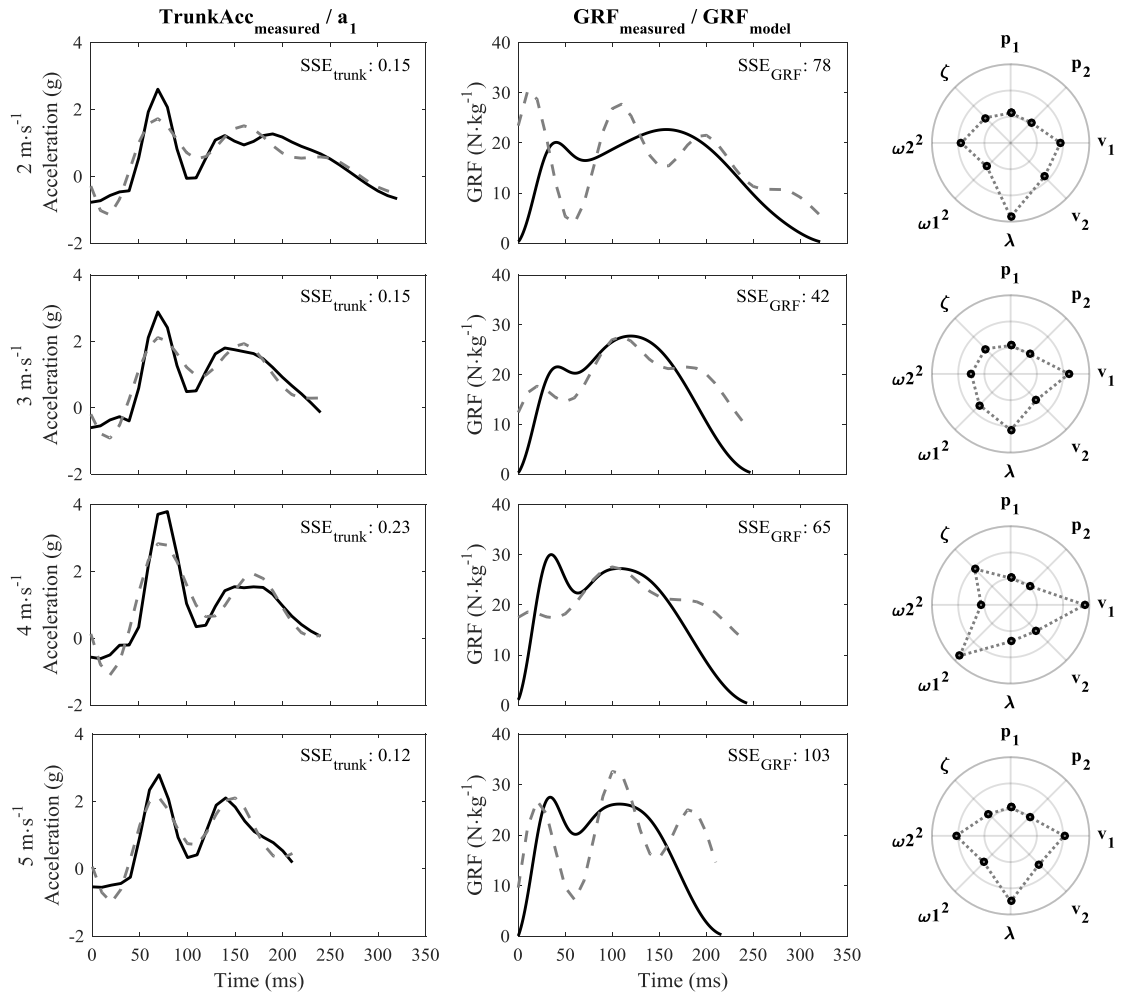


Figure 4.4: Example of $TrunkAcc_{measured}$ (black line), a_1 (dashed grey line), $GRF_{measured}$ (black line) and GRF_{model} (dashed grey line) for the Cut45 from a representative participant. The polar plots display the model parameters (in scaled dimensionless values) for the individual trials.

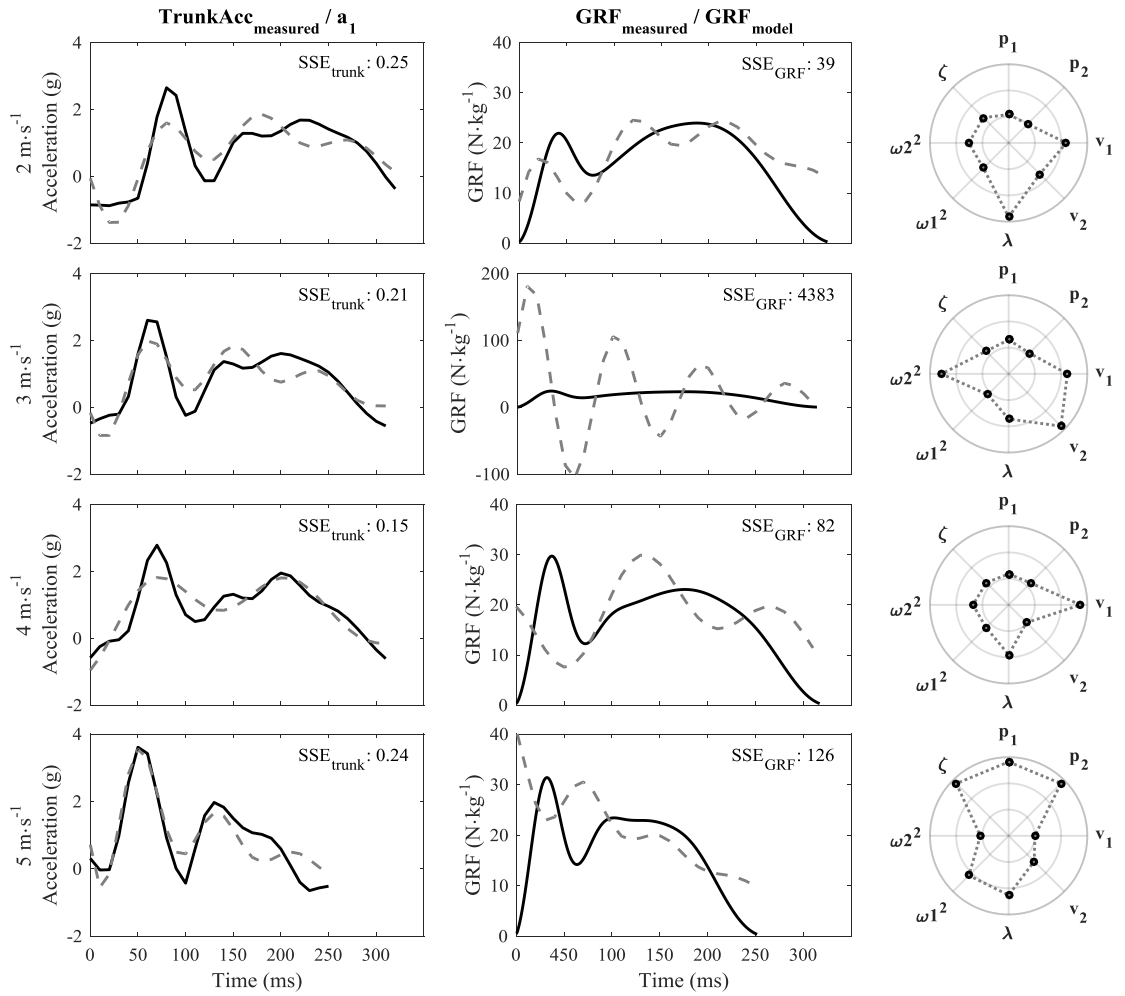


Figure 4.5: Example of $\text{TrunkAcc}_{\text{measured}}$ (black line), a_1 (dashed grey line), $\text{GRF}_{\text{measured}}$ (black line) and $\text{GRF}_{\text{model}}$ (dashed grey line) for the Cut90 from a representative participant. The polar plots display the model parameters (in scaled dimensionless values) for the individual trials.

The smallest SSE_{trunk} was observed for the Run (SSE_{trunk} between 0.04 ± 0.03 and 0.07 ± 0.06 g/frames) compared to the two change in direction tasks (SSE_{trunk} between 0.04 ± 0.03 and 0.14 ± 0.09 g/frames). In addition, the main effect from the one-way ANOVA analysis showed that SSE_{trunk} was significantly affected by both task ($F_{2,227} = 11.8$, $p = < 0.001$) and approach speed ($F_{3,227} = 5.8$, $p = 0.001$). The post-hoc analysis revealed that mean SSE_{trunk} from the Cut90 was significantly higher than the Run and Cut45, and that the mean SSE_{trunk} at 4 and 5 $\text{m}\cdot\text{s}^{-1}$ was significantly higher than the SSE_{trunk} at 2 $\text{m}\cdot\text{s}^{-1}$ (Table 4.2).

Table 4.2: Mean difference and 98.75% confidence interval (CI) of the difference in SSE_{Trunk} (g/frames) between tasks and approach speeds ($\alpha = 0.0125$) obtained from the one-way ANOVA post-hoc analysis.

	Mean	98.75% CI		<i>p</i> - value
	Difference	Lower	Upper	
Run vs. Cut45	-0.02	-0.06	0.02	0.263
Run vs. Cut90	-0.06	-0.10	-0.02	<0.001
Cut45 vs. Cut90	-0.04	-0.08	0.00	0.007
2 $\text{m}\cdot\text{s}^{-1}$ vs. 3 $\text{m}\cdot\text{s}^{-1}$	-0.03	-0.08	0.01	0.173
2 $\text{m}\cdot\text{s}^{-1}$ vs. 4 $\text{m}\cdot\text{s}^{-1}$	-0.59	-0.11	-0.01	0.001
2 $\text{m}\cdot\text{s}^{-1}$ vs. 5 $\text{m}\cdot\text{s}^{-1}$	-0.46	-0.09	0.00	0.015
3 $\text{m}\cdot\text{s}^{-1}$ vs. 4 $\text{m}\cdot\text{s}^{-1}$	-0.03	-0.07	0.02	0.466
3 $\text{m}\cdot\text{s}^{-1}$ vs. 5 $\text{m}\cdot\text{s}^{-1}$	-0.01	-0.06	0.03	1.000
4 $\text{m}\cdot\text{s}^{-1}$ vs. 5 $\text{m}\cdot\text{s}^{-1}$	0.01	-0.03	0.06	1.000

Despite the good to very good match between a_1 and $\text{TrunkAcc}_{\text{measured}}$, poor SSE_{GRF} were observed regardless of task and approach speed for the accelerometer/MSD-model (Table 4.1). The lowest average p_1 , p_2 , v_1 , v_2 values were generally observed for the two cutting tasks compared to the Run (Table 4.3). The lowest ω_1^2 and ω_2^2 values were observed for the Cut90 (ω_1^2 : between 314 ± 401 and $478 \pm 450 \text{ N}\cdot\text{kg}^{-1}\cdot\text{ms}^{-1}$; ω_2^2 : between 1446 ± 1296 and $2511 \pm 1471 \text{ N}\cdot\text{kg}^{-1}\cdot\text{ms}^{-1}$) compared to the Cut45 and Run (ω_1^2 : between 388 ± 433 and $755 \pm 671 \text{ N}\cdot\text{kg}^{-1}\cdot\text{ms}^{-1}$; ω_2^2 : between 2571 ± 1427 and $3404 \pm 1427 \text{ N}\cdot\text{kg}^{-1}\cdot\text{ms}^{-1}$).

Table 4.3: Mean \pm standard deviation of the eight model parameters from the accelerometer/MSD-model for the individual tasks and approach speeds.

	p_1 (m)	p_2 (m)	v_1 (m·s ⁻¹)	v_2 (m·s ⁻¹)	λ (au)	ω_1^2 (N·kg ⁻¹ ·ms ⁻¹)	ω_2^2 (N·kg ⁻¹ ·ms ⁻¹)	ζ (au)
Run 2 m·s⁻¹	-0.03 ±0.03	-0.01 ±0.03	-0.60 ±0.19	-2.22 ±1.32	3.42 ±2.69	542 ±504	2571 ±1427	0.29 ±0.18
Run 3 m·s⁻¹	-0.02 ±0.05	-0.01 ±0.04	-0.71 ±0.17	-2.04 ±1.77	3.00 ±3.00	755 ±671	2885 ±1851	0.25 ±0.13
Run 4 m·s⁻¹	-0.03 ±0.05	-0.02 ±0.04	-0.72 ±0.17	-2.32 ±1.81	3.11 ±2.88	740 ±581	3246 ±1930	0.23 ±0.14
Run 5 m·s⁻¹	-0.05 ±0.06	-0.03 ±0.05	-0.59 ±0.23	-2.38 ±2.95	2.55 ±2.14	745 ±605	3404 ±2047	0.22 ±0.18
Cut45 m·s⁻¹	-0.04 ±0.05	-0.02 ±0.05	-0.71 ±0.18	-2.59 ±2.07	3.42 ±4.34	385 ±433	3044 ±1466	0.22 ±0.17
Cut45 3 m·s⁻¹	-0.04 ±0.05	-0.01 ±0.05	-0.89 ±0.23	-3.03 ±2.54	3.51 ±3.52	452 ±519	3317 ±1702	0.18 0.14
Cut45 4 m·s⁻¹	-0.06 ±0.07	-0.03 ±0.06	-1.03 ±0.34	-3.36 ±3.17	3.48 ±3.64	541 ±519	3002 ±1984	0.22 ±0.18
Cut45 5 m·s⁻¹	-0.06 ±0.06	-0.03 ±0.05	-0.98 ±0.34	-3.13 ±3.17	3.85 ±3.09	620 ±589	3143 ±1817	0.20 ±0.21
Cut90 2 m·s⁻¹	-0.06 ±0.05	-0.02 ±0.05	-0.94 ±0.31	-4.28 ±3.65	2.86 ±3.80	314 ±401	2511 ±1471	0.24 ±0.19
Cut90 3 m·s⁻¹	-0.09 ±0.13	-0.04 ±0.10	-1.24 ±0.49	-4.74 ±5.29	4.79 ±6.44	414 ±549	2305 ±1637	0.24 ±0.26
Cut90 4 m·s⁻¹	-0.11 ±0.11	-0.06 ±0.08	-1.60 ±0.58	-3.72 ±3.89	4.46 ±4.39	413 ±449	1446 ±1296	0.35 ±0.34
Cut90 5 m·s⁻¹	-0.11 ±0.12	-0.06 ±0.09	-1.55 ±0.61	-4.58 ±5.36	4.31 ±3.94	478 ±450	1730 ±1672	0.36 ±0.41

4.3.2. Model parameter sensitivity analysis

The average model parameter values for v_1 , λ and ω_1^2 were similar to the values obtained from the GRF fitting (Chapter 3), whereas p_1 , p_2 , v_2 deviated the most from the $\text{GRF}_{\text{measured}}$ model parameters, especially for the Cut90 task (Figure 4.6).

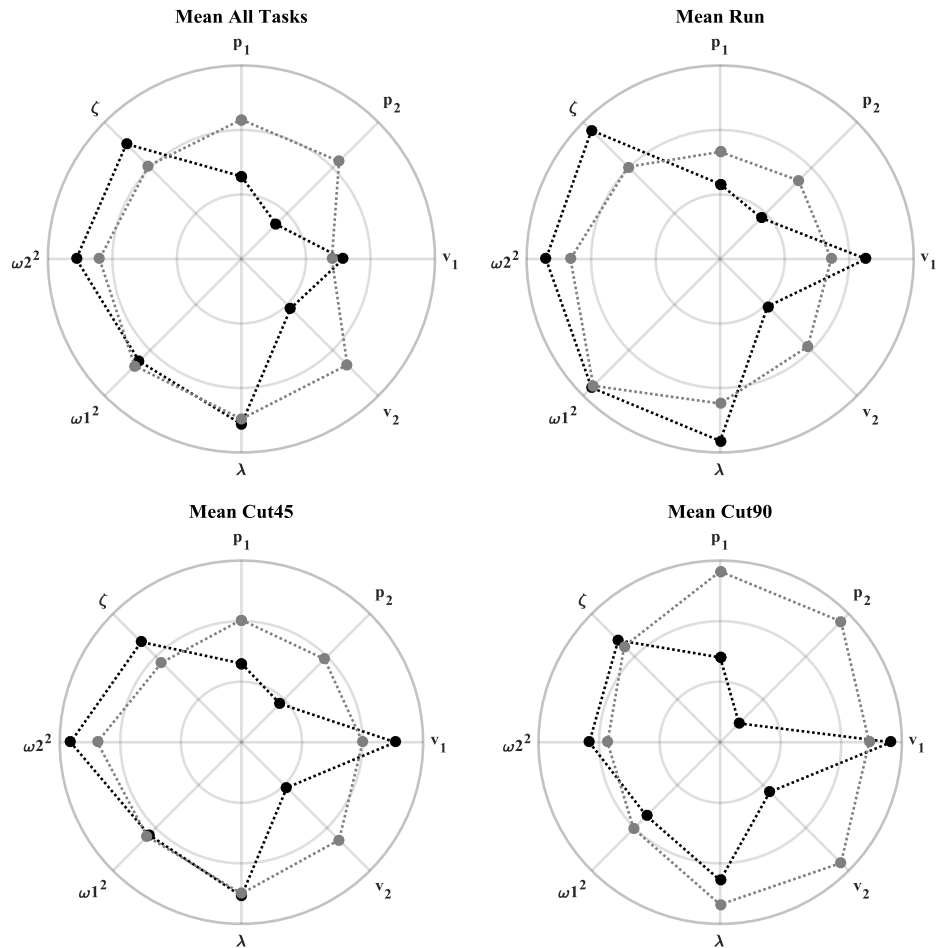


Figure 4.6: Polar plots displaying the mean model parameters (in scaled dimensionless values) across all tasks and for the individual tasks. The grey circles display the average model parameters for $\text{TrunkAcc}_{\text{measured}}$ and the black circles display average model parameters for $\text{GRF}_{\text{measured}}$ (Chapter 3).

A relationship (Figure 4.7), though it was weak to moderate (R^2 between 0.01 and 0.61), was observed for p_2 (R^2 : 0.17), v_1 (R^2 : 0.61), ω_1^2 (R^2 : 0.60) and ω_2^2 (R^2 : 0.36) between average model parameters from $\text{TrunkAcc}_{\text{measured}}$ and $\text{GRF}_{\text{measured}}$ (Chapter 3).

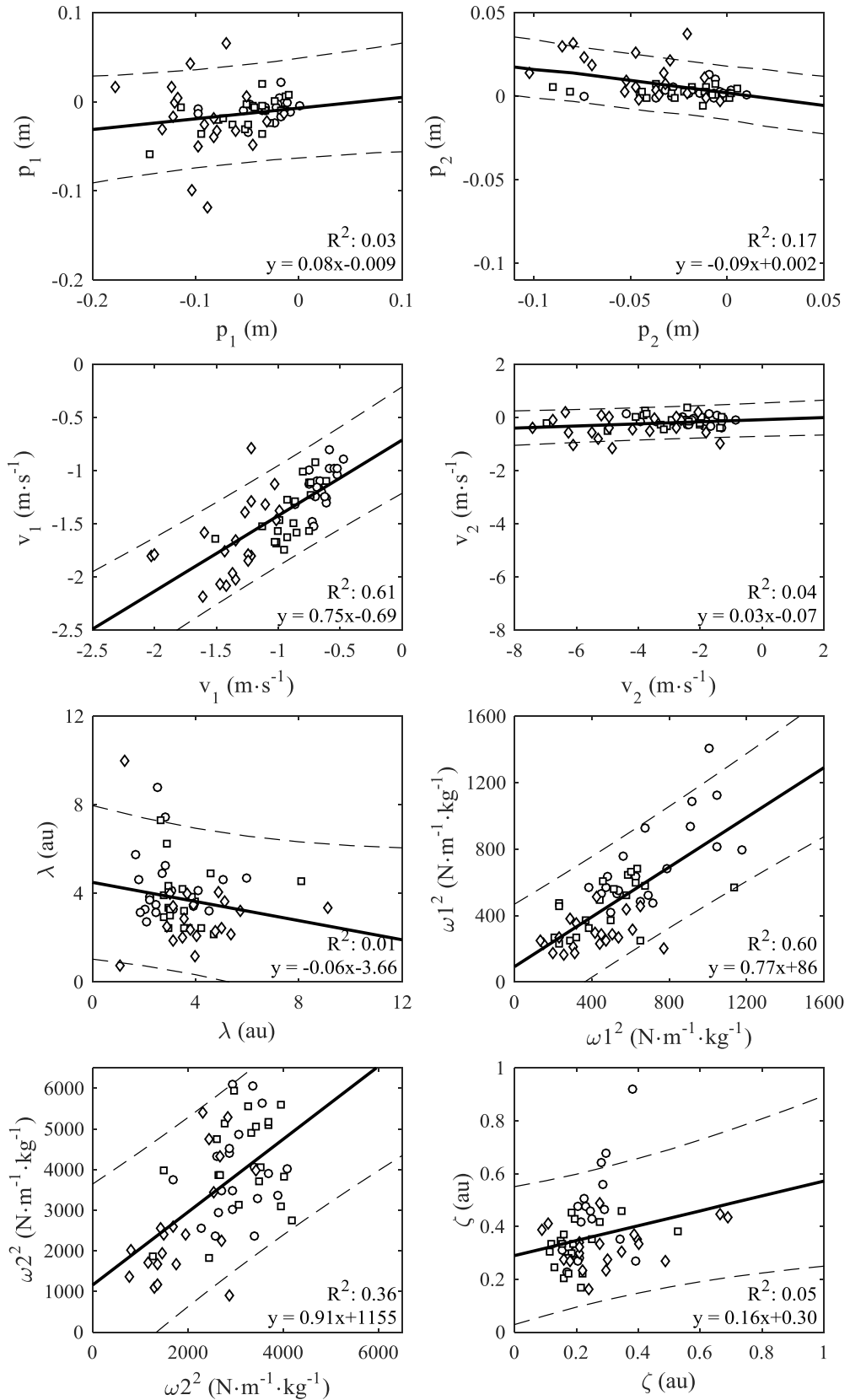


Figure 4.7: Linear regression between TrunkAcc_{measured} (horizontal axis) and GRF_{measured} (vertical axis) model parameters. Each circle represents the participants mean within task parameters (Run: circle; Cut45: square and Cut90: diamond). Mean within task parameters outside the 95% prediction interval (dashed line) were not included in the regression analysis.

GRF_{modelNP} was calculated from five new model parameter combinations to explore if this would improve the predicted GRF_{model} . The new model parameters were created using the $TrunkAcc_{\text{measured}}$ model parameters from the optimisation routine and/or the parameters were kept constant based on the average model parameter values found in Chapter 3, and/or the $TrunkAcc_{\text{measured}}$ model parameters were recalculated from the slope of the linear regression where a relationship existed. The specific new model parameter combinations and representative examples of GRF_{modelNP} from Run, Cut45, and Cut90 at an approach speed of $4 \text{ m}\cdot\text{s}^{-1}$ are displayed in Figure 4.8.

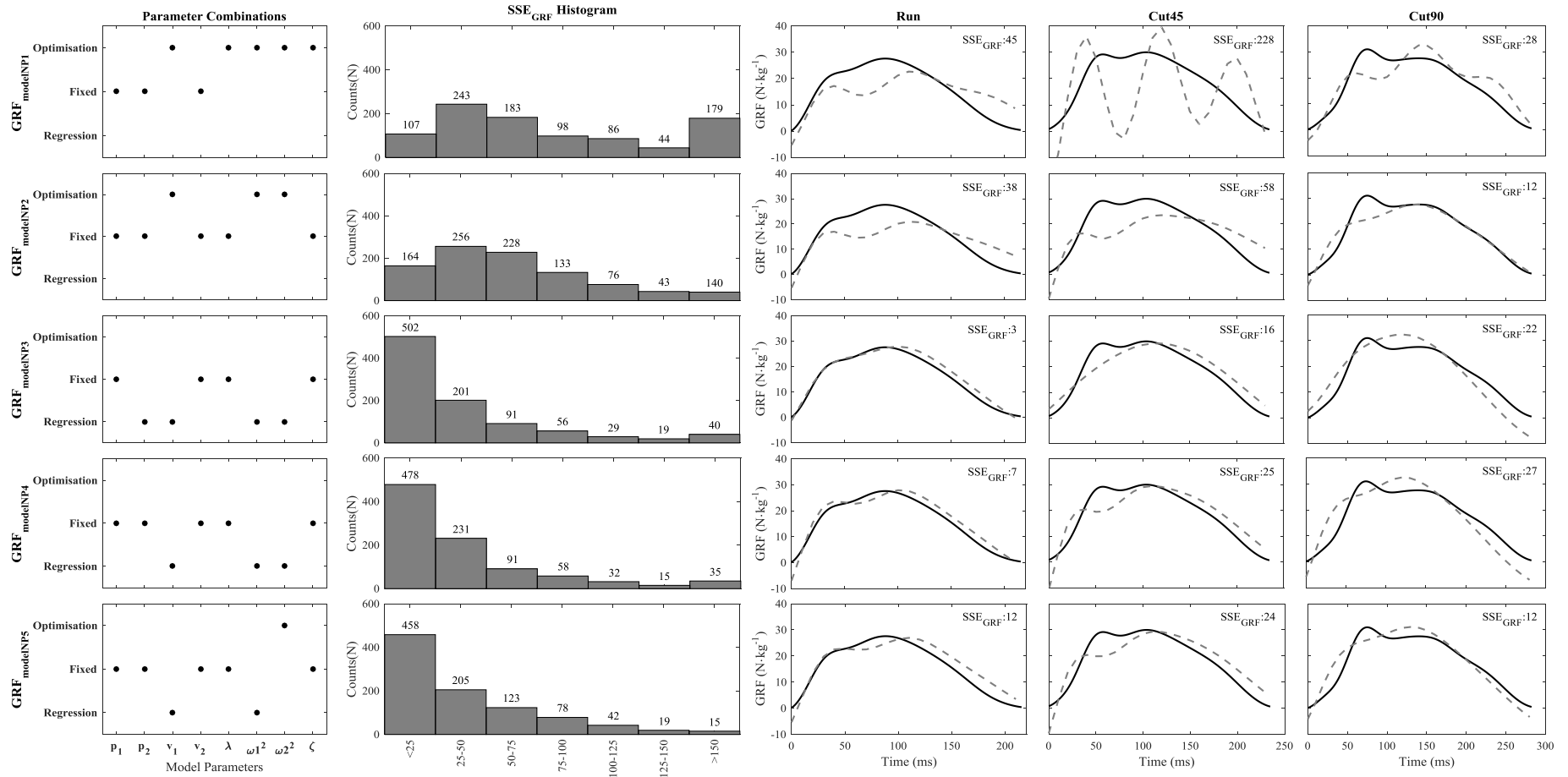


Figure 4.8: Displaying the five new model parameter combinations ($GRF_{modelNP1-5}$) and histograms of the SSE_{GRF} distribution for the different model parameter combinations. Representative examples of $GRF_{measured}$ (black line) and $GRF_{modelNP1-5}$ (dashed grey line) for the Run, Cut45 and Cut90 at an approach speed of $4 \text{ m}\cdot\text{s}^{-1}$.

Table 4.4: Mean \pm standard deviation for SSE_{GRF} (N/kg/frames) for $GRF_{modelNP3}$, $GRF_{modelNP4}$ and $GRF_{modelNP5}$ across the individual tasks and approach speeds. Trials with SSE_{GRF} above 100 were removed before mean and standard deviations were calculated, the number of trials removed are indicated in brackets.

	$GRF_{modelNP3}$ (88)			$GRF_{modelNP4}$ (82)			$GRF_{modelNP5}$ (76)					
	Run (11)	Cut45 (9)	Cut90 (68)	Run (11)	Cut45 (13)	Cut90 (58)	Run (16)	Cut45 (30)	Cut90 (30)			
2 m·s⁻¹	18 \pm 10	17 \pm 10	23 \pm 15	19 \pm 10	18 \pm 9	22 \pm 29	16 \pm 11	14 \pm 8	14 \pm 7			
3 m·s⁻¹	19 \pm 8	19 \pm 14	28 \pm 12	20 \pm 8	20 \pm 12	29 \pm 13	24 \pm 17	21 \pm 15	29 \pm 19			
4 m·s⁻¹	20 \pm 10	29 \pm 16	45 \pm 18	23 \pm 9	31 \pm 16	43 \pm 21	35 \pm 16	44 \pm 24	42 \pm 21			
5 m·s⁻¹	35 \pm 19	46 \pm 20	55 \pm 21	38 \pm 17	46 \pm 18	47 \pm 18	52 \pm 18	51 \pm 16	51 \pm 22			
Post-Hoc	Mean	98.75% CI		<i>p</i> - value	Mean	98.75% CI		<i>p</i> - value	Mean	98.75% CI		<i>p</i> - value
	Difference	Lower	Upper		Difference	Lower	Upper		Difference	Lower	Upper	
Run vs Cut45	-5	-13	4	0.287	-4	-12	4	0.447	-1	-11	9	1.000
Run vs Cut90	-14	-23	-6	<0.001*	-10	-18	-2	0.001*	-2	-12	8	1.000
Cut45 vs Cut90	-9	-18	-1	0.006*	-6	-14	2	0.061	-1	-11	9	1.000
2 m·s⁻¹ vs 3 m·s⁻¹	-3	-12	6	1.000	-4	-12	5	1.000	-10	-19	0	0.010*
2 m·s⁻¹ vs 4 m·s⁻¹	-11	-21	-2	<0.001*	-13	-21	-4	<0.001*	-25	-35	-16	<0.001*
2 m·s⁻¹ vs 5 m·s⁻¹	-26	-35	-17	<0.001*	-24	-32	-15	<0.001*	-37	-46	-27	<0.001*
3 m·s⁻¹ vs 4 m·s⁻¹	-8	-18	1	0.034	-9	-18	-1	0.006*	-16	-25	-6	<0.001*
3 m·s⁻¹ vs 5 m·s⁻¹	-23	-33	-14	<0.001*	-20	-29	-12	<0.001*	-27	-37	-17	<0.001*
4 m·s⁻¹ vs 5 m·s⁻¹	-15	-24	-5	<0.001*	-11	-20	-2	0.001*	-11	-21	-2	0.002*

* Indicates a significant difference between tasks or approach speeds ($\alpha = 0.0125$).

The new model parameters used for $\text{GRF}_{\text{modelNP3}}$, $\text{GRF}_{\text{modelNP4}}$ and $\text{GRF}_{\text{modelNP5}}$ had the highest number of trials with a SSE_{GRF} below 25 N/kg/frames and similarly these model parameter combinations were able to reduce the number of trials with an SSE_{GRF} above 150 N/kg/frames compared to $\text{GRF}_{\text{modelNP1}}$ and $\text{GRF}_{\text{modelNP2}}$ (Figure 4.8). Poor to good SSE_{GRF} (between 14 ± 7 and 52 ± 18 N/kg/frames) was observed across tasks and approach speeds for $\text{GRF}_{\text{modelNP3}}$, $\text{GRF}_{\text{modelNP4}}$ and $\text{GRF}_{\text{modelNP5}}$ (Table 4.4). The lowest SSE_{GRF} were observed for the two slowest approach speeds (between 14 ± 7 and 29 ± 19 N/kg/frames) compared to the two fastest approach speeds (between 20 ± 10 and 52 ± 18 N/kg/frames) and the main effect from the one-way ANOVA analysis showed that SSE_{GRF} was significantly affected by approach speed ($\text{GRF}_{\text{modelNP3}}$: $F_{3,227} = 30.3$, $p < 0.001$; $\text{GRF}_{\text{modelNP4}}$: $F_{3,227} = 30.0$, $p < 0.001$; $\text{GRF}_{\text{modelNP5}}$: $F_{3,227} = 54.8$, $p < 0.001$). In contrast, the SSE_{GRF} was only significantly affected by task for $\text{GRF}_{\text{modelNP3}}$ ($F_{2,227} = 11.7$, $p < 0.001$) and $\text{GRF}_{\text{modelNP4}}$ ($F_{2,227} = 7.2$, $p = 0.001$), but not for $\text{GRF}_{\text{modelNP5}}$ ($F_{2,227} = 0.2$, $p = 0.826$).

The post-hoc analysis revealed that mean $\text{SSE}_{\text{trunk}}$ from the $5 \text{ m}\cdot\text{s}^{-1}$ approach speed was significantly higher than the other approach speeds for $\text{GRF}_{\text{modelNP3}}$, $\text{GRF}_{\text{modelNP4}}$ and $\text{GRF}_{\text{modelNP5}}$. In addition, the post-hoc analysis showed that mean $\text{SSE}_{\text{trunk}}$ from the Cut90 was significantly higher than both the Run and Cut45 for $\text{GRF}_{\text{modelNP3}}$, but only significantly higher than the Run for the $\text{GRF}_{\text{modelNP4}}$ (Table 4.4). Representative examples of $\text{GRF}_{\text{modelNP3}}$ and $\text{GRF}_{\text{modelNP5}}$ for the different tasks and approach speeds are displayed in Figure 4.9.

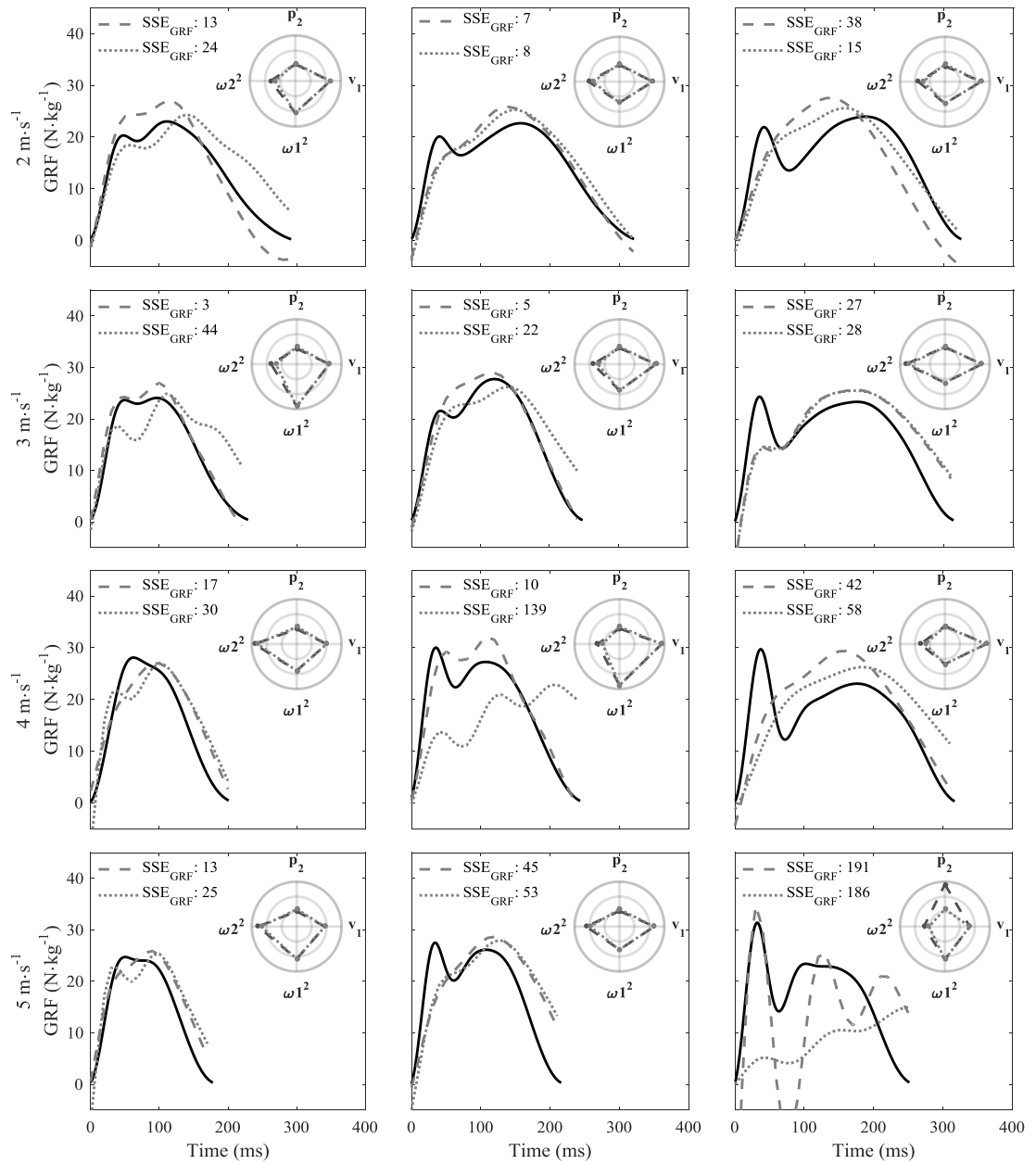


Figure 4.9: Examples of the $GRF_{measured}$ (black line), $GRF_{modelNP3}$ (dashed grey line), $GRF_{modelNP5}$ (dotted grey line) for the difference tasks and approach speeds from a representative participants. The SSE_{GRF} (N/kg/frames) and polar plots displaying the model parameters of the four model parameters that was not kept constant.

4.3.3. GRF loading variables

GRF loading variables were not calculated for GRF_{model} because of the high SSE_{GRF} observed, or for GRF_{modelNP4} due to the similarities in SSE_{GRF} between GRF_{modelNP3} and GRF_{modelNP4} (Table 4.4). Therefore, the GRF loading variables were only calculated for GRF_{modelNP3} and GRF_{modelNP5} . Trials with SSE_{GRF} above 100 were removed before the GRF loading variables were calculated, as such a total number of 88 and 76 trials were removed from GRF_{modelNP3} (Run: 11 trials; Cut45: 9 trials; Cut90: 68 trials) and GRF_{modelNP5} (Run: 16 trials; Cut45: 30 trials; Cut90: 30 trials), respectively.

Table 4.5: Correlation (R^2) values from the linear regression analysis between the GRF variables from GRF_{measured} and GRF_{NP3} and GRF_{NP5} respectively.

	Run		Cut45		Cut90	
	GRF_{modelNP3}	GRF_{modelNP5}	GRF_{modelNP3}	GRF_{modelNP5}	GRF_{modelNP3}	GRF_{modelNP5}
Impulse						
2 m·s ⁻¹	0.49	0.20	0.62	0.69	0.56	0.73
3 m·s ⁻¹	0.41	0.67	0.64	0.79	0.78	0.86
4 m·s ⁻¹	0.80	0.84	0.64	0.75	0.71	0.81
5 m·s ⁻¹	0.84	0.86	0.69	0.67	0.40	0.81
Impact peak						
2 m·s ⁻¹	0.25	0.14	0.31	0.18	0.04	0.40
3 m·s ⁻¹	0.21	0.08	0.32	0.12	0.42	0.02
4 m·s ⁻¹	0.11	0.00	0.54	0.01	0.00	0.19
5 m·s ⁻¹	0.51	0.15	0.20	0.11	0.29	0.42
Time to impact peak						
2 m·s ⁻¹	0.80	0.46	0.22	0.54	0.34	0.54
3 m·s ⁻¹	0.68	0.59	0.52	0.34	0.19	0.26
4 m·s ⁻¹	0.31	0.23	0.47	0.04	0.41	0.39
5 m·s ⁻¹	0.42	0.49	0.23	0.16	0.41	0.19
Loading rate						
2 m·s ⁻¹	0.62	0.43	0.06	0.22	0.07	0.13
3 m·s ⁻¹	0.39	0.52	0.30	0.33	0.08	0.22
4 m·s ⁻¹	0.08	0.07	0.44	0.41	0.09	0.13
5 m·s ⁻¹	0.57	0.32	0.29	0.21	0.43	0.03
Active peak						
2 m·s ⁻¹	0.29	0.34	0.69	0.57	0.48	0.56
3 m·s ⁻¹	0.71	0.44	0.71	0.51	0.61	0.42
4 m·s ⁻¹	0.48	0.42	0.30	0.38	0.47	0.64
5 m·s ⁻¹	0.70	0.58	0.16	0.37	0.51	0.30
Time to active peak						
2 m·s ⁻¹	0.37	0.01	0.75	0.62	0.38	0.27
3 m·s ⁻¹	0.36	0.22	0.68	0.24	0.39	0.09
4 m·s ⁻¹	0.01	0.00	0.50	0.25	0.16	0.27
5 m·s ⁻¹	0.16	0.23	0.44	0.52	0.52	0.07

Impulse showed the strongest correlations with moderate (R^2 : 0.3-0.5) to very strong (R^2 : 0.7-0.9) correlations across tasks and approach speed (Table 4.5), with mean within condition Impulse for $GRF_{modelNP3}$ (between 3.6 ± 0.3 and 5.6 ± 0.6 N·s/kg) and $GRF_{modelNP5}$ (between 3.5 ± 0.3 and 5.9 ± 0.7 N·s/kg) close to the Impulse observed for $GRF_{measured}$ (between 3.3 ± 0.4 and 5.8 ± 0.8 N·s/kg). Small (R^2 : 0.1-0.3) to very strong correlations were observed for Active peak, with mean Active peak overestimations between 0.1 and 5.2 N·kg⁻¹ for $GRF_{modelNP3}$ and between 0.1 and 1.8 N·kg⁻¹ for $GRF_{modelNP5}$ (Table 4.6). Trivial (R^2 : <0.1) to strong (R^2 : 0.5-0.7) correlations were observed for Impact peak, with mean Impact peak overestimations between 0.9 and 7.6 N·kg⁻¹ for $GRF_{modelNP3}$ and between 1.2 and 11.1 N·kg⁻¹ for $GRF_{modelNP5}$.

Table 4.6: Mean \pm standard deviation for the GRF loading variables from $GRF_{measured}$ (bold font), GRF_{NP3} and GRF_{NP5} for the individual tasks and approach speeds.

	Run			Cut45			Cut90		
	$GRF_{measured}$	$GRF_{modelNP3}$	$GRF_{modelNP5}$	$GRF_{measured}$	$GRF_{modelNP3}$	$GRF_{modelNP5}$	$GRF_{measured}$	$GRF_{modelNP3}$	$GRF_{modelNP5}$
Impulse ($N \cdot s \cdot kg^{-1}$)									
2 $m \cdot s^{-1}$	4.1 \pm 0.2	4.2 \pm 0.2	4.5 \pm 0.2	4.5 \pm 0.4	4.6 \pm 0.4	4.8 \pm 0.3	5.2 \pm 0.6	5.1 \pm 0.4	5.4 \pm 0.4
3 $m \cdot s^{-1}$	4.0 \pm 0.3	4.1 \pm 0.3	4.3 \pm 0.3	4.5 \pm 0.5	4.6 \pm 0.4	4.7 \pm 0.3	5.4 \pm 0.8	5.3 \pm 0.5	5.5 \pm 0.5
4 $m \cdot s^{-1}$	3.8 \pm 0.3	3.9 \pm 0.3	4.0 \pm 0.3	4.5 \pm 0.5	4.5 \pm 0.3	4.6 \pm 0.4	5.8 \pm 0.8	5.4 \pm 0.5	5.9 \pm 0.7
5 $m \cdot s^{-1}$	3.3 \pm 0.4	3.6 \pm 0.3	3.5 \pm 0.3	4.0 \pm 0.5	4.2 \pm 0.4	4.3 \pm 0.5	5.3 \pm 0.7	5.6 \pm 0.6	5.6 \pm 0.6
Impact peak ($N \cdot kg^{-1}$)									
2 $m \cdot s^{-1}$	18.6 \pm 1.8	19.5 \pm 1.8	16.8 \pm 1.5	18.2 \pm 2.0	18.9 \pm 2.3	17.0 \pm 1.7	20.3 \pm 3.5	18.7 \pm 2.3	17.0 \pm 1.5
3 $m \cdot s^{-1}$	20.0 \pm 2.3	20.9 \pm 2.5	18.2 \pm 1.8	20.6 \pm 2.4	19.9 \pm 2.9	18.4 \pm 2.3	24.6 \pm 4.7	20.2 \pm 2.5	17.3 \pm 2.7
4 $m \cdot s^{-1}$	22.9 \pm 2.7	21.0 \pm 2.4	19.4 \pm 2.1	25.8 \pm 4.3	21.5 \pm 4.1	18.4 \pm 2.1	27.0 \pm 4.9	21.9 \pm 3.5	17.2 \pm 3.2
5 $m \cdot s^{-1}$	25.7 \pm 3.6	20.1 \pm 2.3	19.9 \pm 2.6	28.8 \pm 5.0	21.2 \pm 4.0	20.6 \pm 3.1	29.2 \pm 4.5	23.9 \pm 4.7	18.1 \pm 3.3
Time to impact peak (ms)									
2 $m \cdot s^{-1}$	81 \pm 12	79 \pm 11	69 \pm 13	79 \pm 15	77 \pm 12	74 \pm 16	77 \pm 21	87 \pm 13	85 \pm 15
3 $m \cdot s^{-1}$	66 \pm 9	63 \pm 7	56 \pm 7	62 \pm 14	66 \pm 9	61 \pm 12	59 \pm 16	76 \pm 13	75 \pm 15
4 $m \cdot s^{-1}$	53 \pm 7	54 \pm 6	52 \pm 5	50 \pm 12	59 \pm 8	57 \pm 9	55 \pm 14	77 \pm 12	80 \pm 16
5 $m \cdot s^{-1}$	44 \pm 4	46 \pm 5	44 \pm 4	44 \pm 8	51 \pm 7	50 \pm 7	46 \pm 8	70 \pm 12	72 \pm 12
Loading rate ($N \cdot s^{-1} \cdot kg^{-1}$)									
2 $m \cdot s^{-1}$	235 \pm 54	305 \pm 42	300 \pm 44	245 \pm 73	319 \pm 117	294 \pm 73	305 \pm 129	282 \pm 74	264 \pm 78
3 $m \cdot s^{-1}$	310 \pm 74	415 \pm 95	348 \pm 64	362 \pm 113	386 \pm 146	400 \pm 129	470 \pm 193	381 \pm 209	334 \pm 136
4 $m \cdot s^{-1}$	441 \pm 105	495 \pm 124	535 \pm 107	560 \pm 179	486 \pm 149	559 \pm 166	529 \pm 183	398 \pm 95	575 \pm 216
5 $m \cdot s^{-1}$	594 \pm 118	584 \pm 136	759 \pm 143	678 \pm 206	552 \pm 102	751 \pm 156	654 \pm 163	451 \pm 153	742 \pm 236
Active peak ($N \cdot kg^{-1}$)									
2 $m \cdot s^{-1}$	22.5 \pm 2.2	24.8 \pm 1.2	23.6 \pm 1.2	22.7 \pm 2.8	25.2 \pm 1.7	24.3 \pm 1.7	22.7 \pm 2.9	25.5 \pm 1.8	24.5 \pm 1.7
3 $m \cdot s^{-1}$	24.9 \pm 2.0	26.2 \pm 1.4	24.8 \pm 1.2	25.5 \pm 2.6	27.0 \pm 1.9	25.9 \pm 1.6	24.4 \pm 2.9	27.2 \pm 2.0	25.4 \pm 2.3
4 $m \cdot s^{-1}$	27.0 \pm 1.6	27.1 \pm 1.4	25.8 \pm 1.5	27.4 \pm 2.6	28.2 \pm 2.6	26.2 \pm 1.6	23.7 \pm 2.7	28.6 \pm 2.2	25.1 \pm 2.6
5 $m \cdot s^{-1}$	27.2 \pm 2.8	26.8 \pm 1.3	25.7 \pm 1.6	28.2 \pm 3.1	29.3 \pm 2.5	27.9 \pm 1.7	24.5 \pm 3.5	29.8 \pm 2.6	26.0 \pm 2.4
Time to active peak (ms)									
2 $m \cdot s^{-1}$	125 \pm 14	143 \pm 10	159 \pm 15	143 \pm 25	154 \pm 16	163 \pm 16	168 \pm 42	173 \pm 20	183 \pm 18
3 $m \cdot s^{-1}$	109 \pm 14	134 \pm 15	146 \pm 13	125 \pm 23	146 \pm 17	156 \pm 17	137 \pm 32	165 \pm 20	193 \pm 38
4 $m \cdot s^{-1}$	92 \pm 14	129 \pm 11	138 \pm 13	107 \pm 22	141 \pm 16	154 \pm 19	131 \pm 40	167 \pm 21	219 \pm 57
5 $m \cdot s^{-1}$	68 \pm 17	124 \pm 13	133 \pm 24	83 \pm 26	131 \pm 20	142 \pm 17	121 \pm 27	157 \pm 23	204 \pm 50

The smallest within condition bias and LoA were generally observed for the Run whereas the largest within condition bias and LoA were observed for the Cut90, and both bias and LoA generally increased with approach speed (Figure 4.10). In general, similar within condition bias and LoA were observed for the $GRF_{modelNP3}$ and $GRF_{modelNP5}$, though smaller Impulse and Impact peak (especially for the Cut90 task) bias and LoA were observed for the $GRF_{modelNP3}$ compared to $GRF_{modelNP5}$. In contrast, the smallest Active peak bias and LoA observed for the $GRF_{modelNP5}$ compared to the $GRF_{modelNP3}$, especially for the Cut90 task.

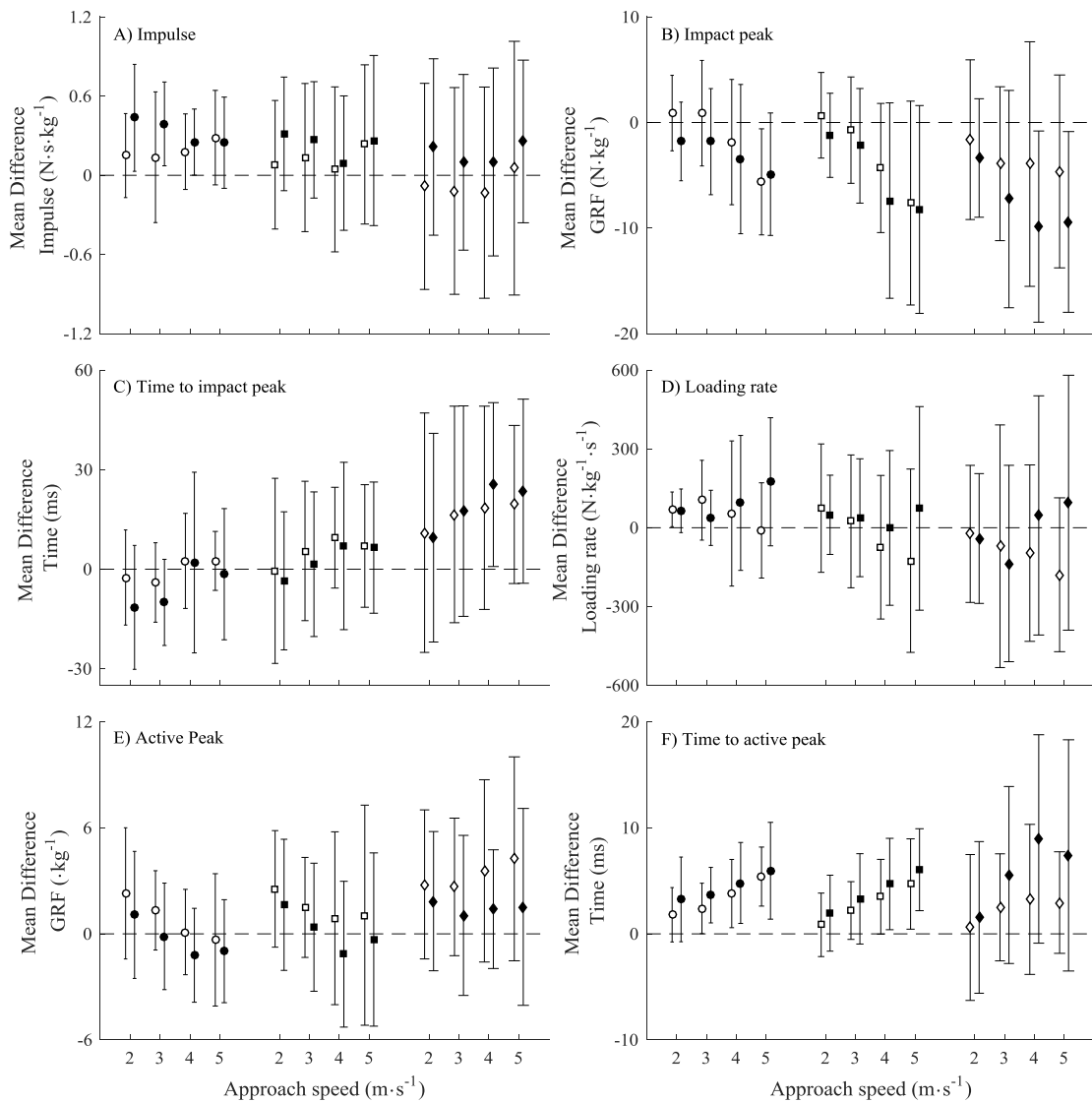


Figure 4.10: Results from the Bland-Altman analysis, showing the mean difference (marker) and 95% limits of agreements (error bar) for the Run (Circle), Cut45 (square) and Cut90 (diamond) across the different tasks and approach speeds calculated from $GRF_{modelNP3}$ (open marker) and $GRF_{modelNP5}$ (filled marker).

4.4. Discussion

The aim of this study was to explore the ability to generate the eight natural MSD-model parameters from measured trunk accelerometry with the purpose of predicting GRF from trunk accelerometry during team sports related movements. The MSD-models upper mass acceleration was able to simulate the measured trunk accelerometer and generate the eight natural model parameters. Despite the good to very good match between the measured trunk accelerometry and the model's upper mass acceleration poor GRF predictions were observed across the different tasks and approach speeds when the trunk accelerometry derived model parameters were used to predict GRF. A sensitivity analysis of the $\text{TrunkAcc}_{\text{measured}}$ model parameter did however reveal that the GRF pattern could be predicted with moderate accuracy for running and side-cutting at low running speeds, when the initial model parameters were kept constant (p_1, v_2, λ, ζ) or recalculated ($p_2, v_1, \omega_1^2, \omega_2^2$) based on the linear relationship observed between $\text{TrunkAcc}_{\text{measured}}$ and $\text{GRF}_{\text{measured}}$ model parameters.

The new accelerometer/MSD-model introduced in this study builds on the assumption that the accelerometer positioned on the upper trunk measures the acceleration of the trunk segment (Nedergaard et al., 2016) and that the model's upper mass primarily represents the mass and motion of the upper body (Alexander et al., 1986; Derrick et al., 2000). One would therefore expect that the trunk accelerometer data would be able to generate the model parameters representing the motion and stiffness of the upper mass and spring (p_1, v_1, ω_1^2) with high accuracy. This was to some extent confirmed by similarities in mean parameter values and high correlations observed for v_1 and ω_1^2 between the $\text{TrunkAcc}_{\text{measured}}$ model parameters and the traditional $\text{GRF}_{\text{measured}}$ model parameters (Figure 4.6 and 4.7). However, the accelerometer/MSD-model overestimated the position of the model's upper mass (p_1) and there was no relationship with the

GRF_{measured} p_1 values. The complexity of MSD-model made it difficult to interpret why the accelerometer/MSD-model only could provide useful model parameters for v_1 and ω_1^2 and not for p_1 . Also, the trunk accelerometry was not able to generate accurate model parameters related to the motion of the lower mass (p_2 and v_2) though a relationship existed between the natural frequency of the lower spring (ω_2^2) obtained from TrunkAcc_{measured} and GRF_{measured}. It is well known that the impact accelerations experienced at the lower limbs, due to the collision between the foot and the ground, are attenuated by the body's soft tissue as it travels through the body (Hamill et al., 1995; Lafortune et al., 1996) and is influenced by the joint angle (e.g. knee joint angle) at touch down (Derrick, 2004; Lafortune et al., 1996). This may explain why the trunk accelerometry data allowed to determine the stiffness of the MSD-model's lower spring (ω_2^2).

Despite the good to very good match between the measured trunk accelerometry and the MSD-model's upper mass acceleration observed in this study, poor GRF predictions were observed from the eight model parameters obtained from the optimisation routine. This naturally raises the question of whether poor GRF predictions observed from the GPS integrated accelerometer signal is because the accelerometer does not measure the acceleration of the trunk well enough. Previous studies have shown that the GPS integrated accelerometer is capable of accurately measuring peak trunk accelerations during team sports movements, when filtered at a cut-off frequency of 10-12 Hz (Wundersitz et al., 2015a; Wundersitz et al., 2015b). The GPS integrated accelerometer data were filtered with a low-pass filter at a cut-off frequency of 20 Hz in this study and applying a filter with a cut-off frequency of 15, 10 or 5 Hz did not improve the GRF predictions obtained from the accelerometer/MSD-model (see detail in Appendix G). Similarly, a previous study has shown that the trunk accelerometer signal is dependent on

the accelerometer's sampling frequency (Nedergaard et al., 2016). Nevertheless, the use of a wireless laboratory accelerometer, with a sampling frequency of 1000 Hz, as model input for the accelerometer/MSD-model had no or minor influence on the optimised model parameters, the linear relationship with the $GRF_{measured}$ model parameters, or the SSE_{GRF} (see details in Appendix H).

Using vertical acceleration data from trunk kinematics as MSD-model input, measured with a three-dimensional motion capture system, did have a positive influence on the mean model parameter values for p_1 , λ and ζ , and stronger correlations were generally observed (R^2 between 0.19 and 0.61) apart from v_2 (R^2 : 0.04). Nevertheless, poor to moderate GRF predictions were observed and the GRF predictions only got worse when new model parameters were recalculated (see details in Appendix I). Comparisons between the accelerometry data and vertical acceleration from trunk kinematics demonstrated that there were deviations in the acceleration signal, and that the accelerometer especially overestimated the acceleration of the trunk in the first 25% of the stance phase. Nevertheless, this raises the question regarding the accelerometer/MSD-model, in particular the assumption that the model's upper mass acceleration represents the acceleration of the trunk. According to the original MSD-model literature, the upper mass in the MSD-model represent the mass and motion of the entire body apart from the support leg (Alexander et al., 1986; Derrick et al., 2000). This may help explain the poor GRF predictions observed from the accelerometer/MSD-model. This may be improved by the construction of a much more complex MSD-model, defeating the overall translational purpose of our work.

The sensitivity analysis showed that the SSE_{GRF} decreased when the model parameters were kept constant (p_1 , v_2 , λ , ζ) or recalculated (p_2 , v_1 , ω_1^2 , ω_2^2) based on the slope of the

linear relationship observed between $\text{TrunkAcc}_{\text{measured}}$ and $\text{GRF}_{\text{measured}}$ model parameters. Similar SSE_{GRF} were observed for $\text{GRF}_{\text{modelNP3}}$ and $\text{GRF}_{\text{modelNP4}}$ indicating that p_2 only had little influence on the predicted GRF because the only difference between the two model parameter combinations was that p_2 was recalculated in the former but kept constant in the latter. Derrick et al. (2000) previously demonstrated that changes in p_2 influenced both magnitude and timing of the impact peak of $\text{GRF}_{\text{model}}$ at touch down. If the fixed or recalculated p_2 value for instance are higher than the optimal p_2 value for a given foot-ground-contact, $\text{GRF}_{\text{model}}$ becomes negative at touch down, which could be the case in the examples displayed in Figure 4.9 for $\text{GRF}_{\text{modelNP3}}$ and $\text{GRF}_{\text{modelNP4}}$ where p_2 was kept constant. The fact that p_2 was recalculated for $\text{GRF}_{\text{modelNP3}}$ rather than kept constant may explain why the smallest mean differences in the predicted and measured Impact peak were observed for $\text{GRF}_{\text{modelNP3}}$. Furthermore, p_2 is included in the calculation of $\text{GRF}_{\text{model}}$ (Equation 4.3) and the large variation observed between tasks in this study (Figure 4.6) and in Chapter 3, indicates that the re-calculation of p_2 , despite the weak correlation (R^2 : 0.17), can help improve the GRF predictions when the accelerometer/MSD-model is used for a variety of utility movements.

The SSE_{GRF} were significantly influenced by both tasks ($\text{GRF}_{\text{modelNP3}}$, $\text{GRF}_{\text{modelNP4}}$) and approach speeds ($\text{GRF}_{\text{modelNP3}}$, $\text{GRF}_{\text{modelNP4}}$, and $\text{GRF}_{\text{modelNP5}}$). The variation in model parameters between tasks and approach speeds observed in Chapter 3 may have an influence on the model parameters which were kept constant (p_1 , v_2 , λ , ζ) and thereby the SSE_{GRF} . Nevertheless, a sensitive analysis of the fixed model parameters, where (p_1 , v_2 , λ , ζ) were kept constant at the mean condition values presented in Chapter 3, only had a minor influence on the mean SSE_{GRF} for the Run and Cut45 tasks, and actually increased the mean SSE_{GRF} for the Cut90 task for $\text{GRF}_{\text{modelNP3}}$ and $\text{GRF}_{\text{modelNP4}}$ (see details in Appendix J). In fact, keeping four of the model parameters constant was expected to

impair the accelerometer/MSD-model's ability to predict different GRF patterns, especially λ and ζ which is included in the calculation of $\text{GRF}_{\text{model}}$ (Equation 4.3) and vary more between different GRF pattern than p_1 and v_2 (Chapter 3).

Though the SSE_{GRF} decreased when the model parameters were kept constant (p_1, v_2, λ, ζ) or recalculated ($p_2, v_1, \omega_1^2, \omega_2^2$), adjusting the $\text{TrunkAcc}_{\text{measured}}$ model parameters from the optimisation routine to improve the predicted GRF is like solving a puzzle with pieces from another puzzle. In other words, the optimisation routine generates the eight model parameters that best replicate the measured trunk accelerometry data for the given stance time, and are therefore dependent on each other. When the model parameters are kept constant or recalculated, the relationship between the model parameters is broken. This might solve one problem, e.g. decreasing v_1 and ω_2^2 to decrease the magnitude of the Active peak (Derrick et al., 2000), but at the same time it causes a new problem because the decreased velocity and spring stiffness will increase the model's stances time and thereby the Impulse. Furthermore, a sensitivity analysis following the approach by Derrick et al. (2000), where the model parameter data from Chapter 3 was used, showed that the effect of changing the individual model parameters was highly dependent on the stance time and the individual GRF pattern (see details in Appendix K).

The predicted GRF from the new model parameter combinations ($\text{GRF}_{\text{modelNP3}}$ and $\text{GRF}_{\text{modelNP5}}$) typically underestimated the Impact peak but overestimated the Active peak. Nevertheless, the mean difference and correlations of the GRF loading variables were similar to those presented in the literature where GRF were estimated from MSD-models or trunk accelerometry. The mean difference in Impulse between $\text{GRF}_{\text{measured}}$ and $\text{GRF}_{\text{modelNP3}}$ ranged from 0.08 to 0.29 $\text{N}\cdot\text{s}\cdot\text{kg}^{-1}$ across tasks and approach speeds in this study. This is similar to the differences in Impulse previously observed by Derrick et al.

(2000) for running at $3.83 \text{ m}\cdot\text{s}^{-1}$ ($19.9 \text{ N}\cdot\text{s} \approx 0.26 \text{ N}\cdot\text{s}\cdot\text{kg}^{-1}$) using the traditional MSD-model. In comparison, the mean differences in Impulse for the Run at $4 \text{ m}\cdot\text{s}^{-1}$ observed in this study were 0.18 and 0.25 $\text{N}\cdot\text{s}/\text{kg}$ for the $\text{GRF}_{\text{modelNP3}}$ and $\text{GRF}_{\text{modelNP5}}$, respectively. Furthermore, the correlations for Impulse, Impact peak, Active peak and Loading rate observed in this study were similar too, and for some conditions/variables better than the correlations previously observed between trunk accelerations from a commercial GPS integrated accelerometer and CoM acceleration (Nedergaard et al., 2016) or GRF data (Wundersitz et al., 2013). The large within task variation in the correlations observed in this study does however still limit the application of the current accelerometer/MSD-model for whole-body biomechanical loading in field settings. Nevertheless, the results from this study indicate that the accelerometer/MSD-model has the potential to provide better predictions of typical whole-body biomechanical loading variables than the raw trunk accelerometry data.

4.5. Conclusion

In conclusion, the novel accelerometer/MSD-model introduced in this study showed promising results in predicting GRF when four of the eight natural (p_1, v_2, λ, ζ) model parameters derived from the accelerometer/MSD-model was kept constant, and the other four model parameters ($p_2, v_1, \omega_1^2, \omega_2^2$) were re-calculated based on the linear relationship observed between trunk accelerometry and $\text{GRF}_{\text{measured}}$ model parameters. Future work should aim at reducing the model's sensitivity to variations in tasks and approach speeds to more accurately reproduce GRF patterns across tasks and approach speeds. Ultimately, this will give researchers and practitioners in team sports a biomechanically sound foundation to explore the internal musculoskeletal structural stresses and consequent adaptations due to external whole-body biomechanical load from player-ground interaction.

CHAPTER 5
General Discussion

The aim of this chapter is to interpret and reflect on the potential application of the main findings obtained within this thesis with respect to whole-body biomechanical loading in team sports and in general. To better achieve this, after in-depth interpretations of detailed findings in the individual chapters, a birds-eye view will be assumed. Finally, recommendations for future research on whole-body biomechanical loading are suggested based on the findings from this thesis.

5.1. Summary

The overall aim of the present thesis was to explore if body-worn accelerometry could be used to estimate whole-body biomechanical loading during team sports movements. The findings from this thesis showed that; 1) although a linear relationship exists between body-worn accelerometry (e.g. GPS integrated accelerometers) and whole-body accelerations the assumption of a simple linear relationship, based on Newton's second law of motion, should be used with caution for whole-body biomechanical load monitoring; 2) the complex multi-segment dynamics of the body and associated GRF during team sports movements, to a large extent, can be estimated with a MSD-model. However, the MSD-model's accuracy slightly decreases for sharp changes of direction at high intensities, when absorption of energy and generation of energy are decoupled; 3) trunk accelerometry data has the potential to generate the eight MSD-model parameters required to estimate GRF from a MSD-model, though further work is required in particular towards improving the model's sensitivity to estimate GRF. A combination of keeping model parameters constant and re-calculating model parameters based on the relationship between GRF and trunk accelerometry model parameters showed promising results. The novel accelerometer/MSD-model approach introduced in this thesis has the potential to give practitioners in team sports the opportunity to perform biomechanical

field observation of whole-body biomechanical load due to player-ground interaction, a necessity if they wish to predict the consequent musculoskeletal structural adaptations.

5.2. The challenges associated with the use of wearable sensor

technology

The advancements in micro sensor technology within recent years have led to a hype around wearable micro sensor technology and its applications for training load monitoring in professional sports and even in amateur athletes. However, this thesis highlighted one of the biggest challenges with the current use of the commercial wearable micro sensor, namely that the true value of the measurements obtained from these devices only are revealed through carefully evaluating its reliability and validity, as in Chapter 2.

Due to the time taken to conduct and publish such studies, the various micro sensor technologies are often used in the applied settings before independent information on the measurement's precision and limitations are known. This can lead to misinterpretation of the data. This is particularly the case for the GPS devices that are used on a daily basis in professional team sports (Akenhead and Nassis, 2016). The misinterpretation is exemplified by the fact that both practitioners and researchers predominantly use the accelerometer data as an additional measurement of the physiological load (Barrett et al., 2014; Cormack et al., 2013), rather than a tool to monitor biomechanical load as suggested in this thesis (Chapter 1). Similarly, applied research is emerging where the relationship between GPS integrated accelerometer data and overuse injury risk are explored (Bowen et al., 2016; Colby et al., 2014; Ehrmann et al., 2016), despite the findings from Chapter 2 and previous studies (Nedergaard et al., 2016; Tran, 2010; Wundersitz et al., 2013) demonstrating that the raw trunk GPS integrated accelerometer data overestimates GRF during team sports movements, and therefore should be used with caution to monitor

whole-body biomechanical loading. Applied sports scientists working in professional team sports settings are of course restricted by time and their daily obligations within the club. Therefore, they do not have time to rigorously test their measurement methods before application. Instead, they should seek to undertake pilot studies in their search to better understand the GPS integrated accelerometer data (Coutts, 2016). Only if researchers and practitioners together continue to explore the accelerometer's reliability and validity in a biomechanical loading context one is hopeful to obtain a good understanding of its value in the field.

The novel approach introduced in Chapter 4 of the thesis, where accelerometry from a GPS device was used to drive a simple model describing the complex multi-body dynamics of the human body, demonstrated how researchers could explore biomechanical approaches to transform the raw signal from wearable sensors into meaningful biomechanical measures such as GRF. Only through such approach practitioners will become able to relate their data back to basic biomechanical knowledge on tissue loading and the structural adaptations associated with the load. Whilst the biggest strength of wearable sensor technology is undoubtedly the ability to easily collect large non-invasive datasets from patients, athletes etc. in their natural environments (Aughey, 2011; Yang and Hsu, 2010), overly simplified outcome variables can often become difficult to interpret and lead to confusion. To make the sensor data attractive to their clients, commercial companies behind the wearable sensor technology typically develop algorithms and matrices that help reduce the data considerably, which enables practitioners to handle a single variable, e.g. the accumulated accelerometer vector magnitude variables currently provided by the commercial GPS device companies (PlayerLoadTM, BodyLoad etc.). This is undoubtedly an effective way to summarize large datasets on a daily basis, but it makes it difficult to relate the observed changes in such

variable to whole-body biomechanical loading without the knowledge of how it has been constructed. Nevertheless, if we can develop simple but valid biomechanical approaches, to transform raw signals from the wearable sensors into biomechanically meaningful outcome variables, as in Chapter 4, then this will enable researchers and practitioners to better explore the true value of the large datasets collected from athletes and/or patients in their natural environment.

5.3. Application of biomechanical load monitoring in team sports

This thesis has focused on the ability to use GPS integrated accelerometry for whole-body biomechanical load monitoring in team sports. Making considerations of the biomechanical load is not new in professional sports as coaches and physiotherapist already make daily attempts to control the biomechanical stress the players are exposed to. For instance, it is common practice to differentiate the physiological and biomechanical load in rehabilitation of lower limb injuries through aqua jogging exercises (Haupenthal et al., 2010; Prins and Cutner, 1999) and running on lower-body positive-pressure treadmills, also referred to as anti-gravity treadmills (Jensen et al., 2016; Raffalt et al., 2013). The benefit of these methods is that the GRF can be reduced by as much as 20% during walking or running locomotion but the cardiovascular and neuromuscular stimulus that is relevant to team sports is maintained (Haupenthal et al., 2010; Raffalt et al., 2013). Nevertheless, the findings from this thesis may form a starting point to also differentiate between physiological and biomechanical loads from the data collected with the GPS integrated accelerometer during field training sessions, and even match-play. The accelerometer/MSD-model introduced in Chapter 4 could potentially enable practitioners to monitor the impulse of the GRF to which players are exposed, as a measure of the whole-body biomechanical loading from a training session in the same way as heart rate, sRPE or total distance covered are used to monitor the physiological

load. Similarly, the impact peak, loading rate and active peak of the accelerometer/MSD-model predicted GRF could be used to describe the intensity of the biomechanical load to which players are exposed, in the same way as the distance covered in different running velocity zones or number of accelerations and decelerations are used to describe the intensity of the physiological load in professional team sports. This will enable practitioners to monitor, prescribe and adjust the volume and intensity of the biomechanical load across a season, for different individuals in the same way as the physiological load is currently monitored. The results from Chapter 4 do however illustrate that further work on the accelerometer/MSD-model's sensitivity to accurately predict the GRF pattern and in particular the GRF loading variables related to the intensity of the biomechanical load (impact peak and loading rate) is needed before it can be successfully applied. Nevertheless, the following paragraphs include examples of the potential application of the accelerometer/MSD-model to monitor the variation in whole-body biomechanical load.

5.3.1. Example of two players performing the same standardised running task

Trunk accelerometry data was taken from two participants/players (player A: 71 kg and player B 75 kg), performing the straight line running tasks previously described in this thesis at $4 \text{ m}\cdot\text{s}^{-1}$. The trunk accelerometry data included both the acceleration phase, the steady state phase where players were running at $4 \text{ m}\cdot\text{s}^{-1}$, and the deceleration phase where players were decelerating to jogging or walking. A threshold of -0.55 g was used to identify foot-ground-contact in the trunk accelerometry signal (see detail in Appendix L). The accelerometer/MSD-model (new model parameter combination 3) was applied to the trunk accelerometry from the individual foot-ground-contacts, apart from the first step in the acceleration phase and the last step in the deceleration phase, to predict the GRF ($\text{GRF}_{\text{model}}$) from the individual foot-ground-contacts (Figure 5.1). Finally, Impulse,

Impact peak and Active peak were determined for every foot-ground-contact from the GRF_{model} data for player A and B respectively.

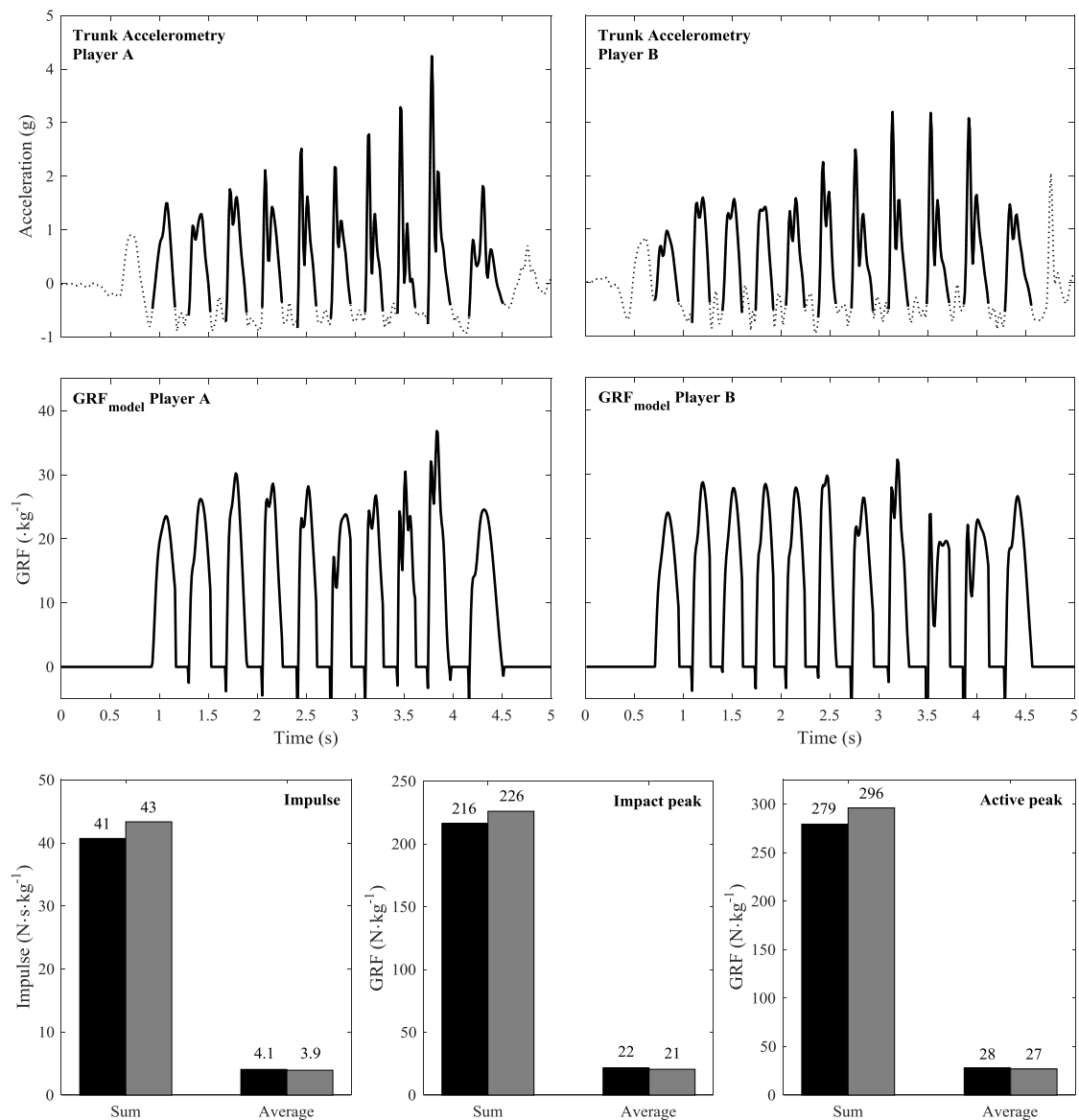


Figure 5.1: Resultant gravity corrected trunk acceleration measured from a trunk-mounted accelerometer is displayed in top row, in which the solid black line indicate the individual foot-ground-contacts. The second row display the GRF_{model} predicted from the accelerometer/MSD-model and the bar plots in the bottom row display the sum and average values from player A (black) and B (grey) respectively for Impulse, Impact peak and Active peak.

It is well known that the magnitude of GRF is sensitive to a person's running kinematics such as footfall (Lieberman et al., 2010) and knee joint angle (Derrick, 2004). As a result, the biomechanical load to which players are exposed will most likely vary when covering the same distance. The example above illustrates that monitoring of the GRF, e.g. from

the accelerometer/MSD-model introduced in this thesis, has the ability to reveal differences in biomechanical load due to the players running style, which typically is ignored when the training duration, running speed, or distance covered is used to estimate the biomechanical load.

5.3.2. Application in the traditional physiological test-batteries

A recent study on the current practise and perception of training load monitoring in high-level football was conducted, and identified that manpower is ranked as the highest perceived barrier for effective monitoring of training load (Akenhead and Nassis, 2016). With this in mind, and the extra data processing currently required to estimate GRF from the accelerometer/MSD-model, as the optimisation routine is required for every foot-ground-contact, it would still be difficult for the biomechanical load to be estimated for every player on a daily basis in a professional club. The work in this thesis has demonstrated that computerisation of GRF estimates based on an accelerometer/MSD-model are still a distant thought, particularly considering the great variety in activities that dictate performance and load in team sports. Nonetheless, it may well be feasible in the near future to apply the accelerometer/MSD-model to the sub-maximal / non-exhaustive performance tests commonly used in professional team sports on a quarterly or even weekly basis (Akenhead and Nassis, 2016). These tests are typically standardised submaximal shuttle runs where the majority of time is spent at straight line running during which the accelerometer/MSD-model can estimate GRF with reasonable accuracy. This could enable practitioners to differentiate the physiological and biomechanical loads from a standardised drill which may help them to better estimate the biomechanical load during small sided games and match-play based on the observed changes in load. The relationship between the biomechanical load observed from the standardised performance tests and the differential session RPE focussing on the perceived “leg” exertion (McLaren

et al., 2016a; McLaren et al., 2016b; Weston et al., 2015) may also provide additional information about the dose-response relationship of the biomechanical load.

5.3.3. Application in return to sport scenarios

The accelerometer/MSD-model introduced in Chapter 4 may enable physiotherapists and sports scientists to more closely monitor the load progression in their injured players during rehabilitation and more importantly during the return to sport period. When a player/athlete gets injured, the first question that is raised is when he/she will be able to return to competition again (Arden et al., 2016; Drust et al., 2014). The decision of releasing a player back to full training/match-play therefore is made over time by gradually releasing the player back into training/match-play. Part of this process is to progressively manage the player's biomechanical load making sure that the damaged tissues respond positively to the load by strengthening the tissue rather than re-injuring it (Arden et al., 2016; Blanch and Gabbett, 2016). Monitoring of the biomechanical load using the accelerometer/MSD-model introduced in this thesis (Chapter 4) may provide practitioners with valuable objective information on the overall external tissue stresses and the level of biomechanical stress players should be able to tolerate to fully return to training/match-play. Rather than monitoring and prescribing the training load solely from physiological measures such as training duration, total distance covered, or high speed running, the biomechanical loading approach introduced in this thesis enables practitioners to prescribe the return to play training load on biomechanical periodization principles (e.g. through the exposure to GRF features such as impulse and impact peak).

5.4. Potential application in other load related studies

The ability to monitor GRF outside the laboratory from the accelerometer/MSD-model introduced in this thesis also has the potential to be applied in other fields, such as when exploring the consequences of training periodization. The results from Chapter 3 illustrated that the MSD-model can estimate the multi-body dynamics of the human body during straight line running at submaximal speeds ($4-5 \text{ m}\cdot\text{s}^{-1}$) with high accuracy. Similarly, better GRF predictions were observed for straight line running tasks compared to the change in direction tasks when the trunk accelerometer data were used to predict GRF (Chapter 4). These results illustrate that the accelerometer/MSD-model has the potential to estimate whole-body biomechanical load with high accuracy during activities such as long-distance running. In fact, this might be the best application for the current accelerometer/MSD-model, as it can enable researchers to monitor exposure to whole-body biomechanical load, rather than the exposure to measurements of the physiological load, when the relationship between running and chronic injuries such as patella femoral pain, Achilles tendon injuries, stress fractures is explored (Hreljac, 2004; Nielsen et al., 2012; Nielsen et al., 2013). Also, as highlighted in Chapter 2, an accelerometer measures the acceleration of the segment it is attached to, and therefore trunk-mounted accelerometry could be complemented with accelerometry data from a tibial mounted accelerometer to provide comprehensive insights if the aim is to monitor/measure the biomechanical stress on the tibial bone during running (Hreljac, 2004).

The ability to monitor the external whole-body biomechanical load via GRF from the accelerometer/MSD-model introduced in this thesis may as well help us to better understand how the longitudinal exposure and periodization of GRF are associated with the internal joint contact forces. The relationship between knee joint contact forces from physical activity and the development of knee osteoarthritis has been explored

extensively in the current literature, but with contrasting results (Miller et al., 2014). Monitoring of the GRF that runners are exposed to could potentially be used to estimate the internal contact forces and help us to better understand the relationship between the development of knee osteoarthritis and the external whole-body biomechanical load experienced during running.

Body-worn accelerometers are commonly used in physical activity monitoring to estimate the energy expenditure, for classification of movement/posture, and to identify individuals at increased risk of falling during daily life activities (Mathie et al., 2004; Yang and Hsu, 2010). Though the biomechanical load is largely unexplored in physical activity monitoring the accelerometer/MSD-model could be useful, even if it should be used with caution for daily life activities. The key limitation is that the current MSD-model builds on the assumption that the human body follows a spring-like behaviour (Chapter 3), which is violated during walking, standing and sitting. This limits the application of the accelerometer/MSD-model in physical activity monitoring. Researchers seeking to explore the whole-body biomechanical load could instead use the assumption that during daily life activities a linear relationship exists between body-worn accelerometry and whole-body acceleration, as previous studies have showed that such a linear relationship exists for low intensity daily life activities such as walking (Meyer et al., 2015; Rowlands and Stiles, 2012).

5.5. The relationship between external and internal biomechanical load

The accelerometer/MSD-model introduced in this thesis (Chapter 4) has the potential to improve our ability to monitor the external whole-body biomechanical load in the field. Monitoring of GRF is interesting from a biomechanical point of view as the positive and negative adaptations of the body's soft tissues such as cartilage (Eggli et al., 1988;

Slowman and Brandt, 1986; Swann and Seedhom, 1993), bone (Forwood and Parker, 1991; Frost, 1997) and tendons (Dye, 2005; Kjaer et al., 2009; Maganaris et al., 2004) depends on the mechanical stresses to which the body is exposed (Dye, 2005; Nigg et al., 1995). However, the GRF does not directly provide information about the internal forces without additional information and complex inverse dynamic calculations (Damsgaard et al., 2006; Delp et al., 2007). The relationship between biomechanical loading and tissue adaptations is complex, and the optimal biomechanical loading distribution and positive tissue adaptations still remains unclear in terms of the variation in response rate and how the response rate is influenced by factors such as age, gender, fitness or fatigue. The ability to monitor the external biomechanical load is nevertheless a first step to estimate the internal responses leading to tissue regeneration or damage in sports. Furthermore, if we can establish the internal tissue response to GRF, the accelerometer/MSD-model introduced in this study will ultimately give scope for better monitoring of overuse injuries in sports as these per definition are a result of the cumulative tissue damage over time (Clarsen et al., 2015; Finch and Cook, 2014).

5.6. Recommendations for future research

In this thesis a novel approach to monitor whole-body biomechanical loading from trunk-mounted accelerometry has been introduced, ultimately with an attempt to differentiate between the physiological and biomechanical load. Based on the studies conducted in this thesis some recommendations for future research on biomechanical load monitoring have been formulated.

5.6.1. Model sensitivity

Future research on the accelerometer/MSD-model's validity, reliability, generalisability and sensitivity is essential if this approach is ever to be used to monitor the biomechanical

load in team sports. Additional sensitivity studies will enable us to better understand the strengths and limitations of this approach and as a result the potential application of this approach. Model improvements may as well emerge which can improve the accelerometer/MSD-model's ability to monitor athletes' GRF in their natural environment. In the short term, studies are needed that explore the interaction between model parameters, or that explore the influence of only including the four model parameters that have shown a relationship with the GRF derived model parameters (p_2 , v_1 , ω_1^2 , ω_2^2) in the trunk accelerometer optimisation routine. Or studies that explore the opportunity to apply boundary conditions to the individual model parameters so that model parameter solutions with unrealistic model parameters can be better avoided. In the long term, researchers could explore the opportunity to including extra elements in the model that can account for the loss of energy during less-elastic movements such as the Cut90. This could for instance be in the form of the inclusion of an extra damper in series with the upper spring to allow energy to dissipate, or even the addition of an actuator that can add energy to the system.

5.6.2. Biomechanical load monitoring with wearable technologies

Future research could explore how the continuous development of wearable technologies can contribute to the biomechanical load monitoring in team sports. Team sports could seek inspiration from clinical gait analysis where development of full-body inertial measurement unit technologies to measure full-body kinematics is emerging (Ferrari et al., 2010). Kinematic analysis of a player's movement pattern, e.g. joint angles, enables us to better understand how a player's movement pattern and external forces acting on their body increase the risk of overuse injuries. Furthermore, smart clothes with wearable sensor technologies such as integrated electromyography (EMG) electrodes are emerging enabling researchers and practitioners to monitor the player's muscle activity during

training/match-play (Düking et al., 2016; Finni et al., 2007). However, the validity and reliability of these technologies and generalisability to team sports should be established before it is deployed in team sports. The introduction of additional technologies will furthermore increase the data processing time and it is therefore important to identify if and how these measurements can be turned into knowledge about the biomechanical load that is easily accessible and meaningful for the practitioner.

5.6.3. Consideration of the biomechanical load in future studies on training load

This thesis has made a first attempt to not only distinguish between the physiological and biomechanical load from collisions with opponents (Gabbett, 2013; Gastin et al., 2014) but also to distinguish between the physiological and biomechanical load associated with the players' movements around the pitch. Future studies on training load should therefore recognise that there is a difference between physiological and biomechanical load and explore the opportunity to monitor this separately. For instance, through the use of accelerometer/MSD-model introduced in this thesis or similar methods that can estimate whole-body biomechanical loading from the player-ground interaction in the field, future studies may provide objective data supporting that there is a difference between physiological and biomechanical load which until now has only been described theoretically (Vanrenterghem et al., Under Review).

5.6.4. Establishment of the biomechanical dose-response relationship

Whereas the accelerometer/MSD-model improves our ability to better monitor the external biomechanical load, it still does not provide direct information about the internal biomechanical load. Future research should therefore explore how volume, frequency and intensity of the external biomechanical load each lead to positive or negative tissue adaptations and how these adaptations are influenced by fatigue, recovery time and the

individual's response level. In a field context, researchers and practitioners will need to explore if GRF exposure from the accelerometer/MSD-model is a stronger indicator of tissue damage than existing estimates of load, and consequently if it is, for example, a better predictor of muscle soreness (McLellan et al., 2011; McNamara et al., 2013) or "leg exertion" (McLaren et al., 2016a; McLaren et al., 2016b; Weston et al., 2015) in team sports. In a clinical context, future intervention studies should explore the relationship between the longitudinal GRF exposure from physical activity and changes in tendon properties (e.g. stiffness and hypertrophy) or bone adaptations (e.g. mass and calcium content) (Kibler et al., 1992; Nigg et al., 1995).

5.6.5. Establish the relationship between biomechanical load and overuse injury risk

Based on the findings of the present work, future research may have the possibility to explore if the estimated biomechanical load from the accelerometer/MSD-model is a better predictor of overuse injuries than other estimates such as the accumulated vector magnitude currently obtained from the GPS integrated accelerometer (Bowen et al., 2016; Colby et al., 2014; Ehrmann et al., 2016). A unique asset of the accelerometer/MSD-model is that it allows to investigate the relationship between specific GRF loading features and specific overuse injuries, and that in a field context. Lab studies have, for example, already suggested such relationship between increased loading rate and risk of tibial stress fractures in long distance runners (Hreljac, 2004), yet field-based observations would allow more in depth understanding of such relationship in terms of the specific roles of factors such as intensity, volume, or frequency.

5.7. General conclusion

This thesis has made a first attempt to distinguish between the physiological and biomechanical load associated with team sports players' movements around the pitch during training sessions and match-play. GPS integrated accelerometers are commonly used in professional team sports and are therefore a strong candidate for whole-body biomechanical monitoring in the field. Nevertheless, findings from this thesis have shown that body-worn accelerometry overestimates whole-body biomechanical loading. Practitioners should therefore exercise some caution when GPS integrated accelerometers are used to estimate the whole-body biomechanical load players are exposed to from the interaction between the player and the ground (e.g. through the accumulated vector magnitudes). The novel accelerometer/MSD-model approach introduced in this thesis showed promising results in the ability to estimate the multi-segment dynamics of the human body and the associated ground reaction forces from trunk-mounted accelerometry, though future work is needed to reduce the accelerometer/MSD-model's sensitivity to variations in tasks for it to more accurately reproduce GRF patterns from various team sports movements. Ultimately, this will give researchers and practitioners in team sports a biomechanically sound foundation to external whole-body biomechanical load monitoring due to player-ground interaction and potentially provide useful information which may enable us to predict the musculoskeletal structural adaptations of training sessions and match-play in team sports.

REFERENCES

- Adler, R.J., Taylor, J.E., 2007. Random Fields and Geometry. 1st edn. Springer-Verlag New York.
- Akenhead, R., French, D., Thompson, K.G., Hayes, P.R., 2014. The acceleration dependent validity and reliability of 10 Hz GPS. *Journal of Science and Medicine in Sport* 17, 562-566.
- Akenhead, R., Nassis, G.P., 2016. Training Load and Player Monitoring in High-Level Football: Current Practice and Perceptions. *International Journal of Sports Physiology and Performance* 11, 587-593.
- Akubat, I., Barrett, S., Abt, G., 2014. Integrating the internal and external training loads in soccer. *International Journal of Sports Physiology and Performance* 9, 457-462.
- Alexander, J.P., Hopkinson, T., Wundersitz, D., Serpell, B.G., Mara, J., Ball, N.B., 2016. Validity of a wearable accelerometer device to measure average acceleration values during high speed running. *Journal of Strength and Conditioning Research*. (Epub ahead of print)
- Alexander, R.M., 1984. Elastic Energy Stores in Running Vertebrates. *American Zoologist* 24, 85-94.
- Alexander, R.M., Bennett, M.B., Ker, R.F., 1986. Mechanical properties and function of the paw pads of some mammals. *Journal of Zoology* 209, 405-419.
- Arampatzis, A., Bruggemann, G.P., Metzler, V., 1999. The effect of speed on leg stiffness and joint kinetics in human running. *Journal of Biomechanics* 32, 1349-1353.
- Ardern, C.L., Glasgow, P., Schneiders, A., Witvrouw, E., Clarsen, B., Cools, A., Gojanovic, B., Griffin, S., Khan, K.M., Moksnes, H., Mutch, S.A., Phillips, N., Reurink, G., Sadler, R., Silbernagel, K.G., Thorborg, K., Wangensteen, A., Wilk, K.E., Bizzini, M., 2016. 2016 Consensus statement on return to sport from the First World Congress in Sports Physical Therapy, Bern. *British Journal of Sports Medicine* 50, 853-864.
- Aughey, R.J., 2011. Applications of GPS technologies to field sports. *International Journal of Sports Physiology and Performance* 6, 295-310.
- Bagger, M., Petersen, P.H., Pedersen, P.K., 2003. Biological variation in variables associated with exercise training. *International Journal of Sports Medicine* 24, 433-440.
- Banister, E.W., Calvert, T.W., Savage, M.V., Bach, T.M., 1975. Systems model of training for athletic performance. *Australian Journal of Sports Medicine* 7, 57-61.

- Barreira, P., Robinson, M.A., Drust, B., Nedergaard, N., Raja Azidin, R.M.F., Vanrenterghem, J., 2016. Mechanical Player Load™ using trunk-mounted accelerometry in football: Is it a reliable, task- and player-specific observation? *Journal of Sports Sciences*, 1-8. (Epub ahead of print)
- Barrett, S., Midgley, A., Lovell, R., 2014. PlayerLoad: Reliability, Convergent Validity, and Influence of Unit Position during Treadmill Running. *International Journal of Sports Physiology and Performance* 9, 945-952.
- Barrett, S., Midgley, A., Reeves, M., Joel, T., Franklin, E., Heyworth, R., Garrett, A., Lovell, R., 2016a. The within-match patterns of locomotor efficiency during professional soccer match play: Implications for injury risk? *Journal of Science and Medicine in Sport* 19, 810-815.
- Barrett, S., Midgley, A.W., Towlson, C., Garrett, A., Portas, M., Lovell, R., 2016b. Within-Match PlayerLoad Patterns During a Simulated Soccer Match: Potential Implications for Unit Positioning and Fatigue Management. *International Journal of Sports Physiology and Performance* 11, 135-140.
- Barron, D.J., Atkins, S., Edmundson, C., Fewtrell, D., 2014. Accelerometer derived load according to playing position in competitive youth soccer. *International Journal of Performance Analysis in Sport* 14, 734-743.
- Besier, T.F., Lloyd, D.G., Cochrane, J.L., Ackland, T.R., 2001. External loading of the knee joint during running and cutting maneuvers. *Medicine and Science in Sports and Exercise* 33, 1168-1175.
- Blanch, P., Gabbett, T.J., 2016. Has the athlete trained enough to return to play safely? The acute:chronic workload ratio permits clinicians to quantify a player's risk of subsequent injury. *British Journal of Sports Medicine* 50, 471-475.
- Bland, J.M., Altman, D.G., 2010. Statistical methods for assessing agreement between two methods of clinical measurement. *International Journal of Nursing Studies* 47, 931-936.
- Blickhan, R., 1989. The spring-mass model for running and hopping. *Journal of Biomechanics* 22, 1217-1227.
- Bloomfield, J.P., R., O'Donoghue, P., 2007. Deceleration movements performance during FA Premier League soccer matches. *Journal of Sport and Medicine* 6, 6.

- Bobbert, M.F., Schamhardt, H.C., Nigg, B.M., 1991. Calculation of vertical ground reaction force estimates during running from positional data. *Journal of Biomechanics* 24, 1095-1105.
- Bobbert, M.F., Yeadon, M.R., Nigg, B.M., 1992. Mechanical analysis of the landing phase in heel-toe running. *Journal of Biomechanics* 25, 223-234.
- Bowen, L., Gross, A.S., Gimpel, M., Li, F.X., 2016. Accumulated workloads and the acute:chronic workload ratio relate to injury risk in elite youth football players. *British Journal of Sports Medicine*. (Epub ahead of print)
- Boyd, L.J., Ball, K., Aughey, R.J., 2011. The Reliability of MinimaxX Accelerometers for Measuring Physical Activity in Australian Football. *International Journal of Sports Physiology and Performance* 6, 311-321.
- Boyd, L.J., Ball, K., Aughey, R.J., 2013. Quantifying External Load in Australian Football Matches and Training Using Accelerometers. *International Journal of Sports Physiology and Performance* 8, 44-51.
- Brughelli, M., Cronin, J., 2008. Influence of running velocity on vertical, leg and joint stiffness : modelling and recommendations for future research. *Sports Medicine* 38, 647-657.
- Buchheit, M., Gray, A.J., Morin, J.B., 2015. Assessing Stride Variables and Vertical Stiffness with GPS-Embedded Accelerometers: Preliminary Insights for the Monitoring of Neuromuscular Fatigue on the Field. *Journal of Sports Science and Medicine* 14, 698 - 701.
- Bullimore, S.R., Burn, J.F., 2007. Ability of the planar spring-mass model to predict mechanical parameters in running humans. *Journal of Theoretical Biology* 248, 686-695.
- Busso, T., 2003. Variable dose-response relationship between exercise training and performance. *Medicine and Science in Sports and Exercise* 35, 1188-1195.
- Casamichana, D., Castellano, J., Calleja-Gonzalez, J., San Roman, J., Castagna, C., 2013. Relationship between indicators of training load in soccer players. *Journal of Strength and Conditioning Research* 27, 369-374.
- Cavagna, G.A., 1970. Elastic bounce of the body. *Journal of Applied Physiology* 29, 279-282.

- Cavagna, G.A., Saibene, F.P., Margaria, R., 1964. Mechanical work in running. *Journal of Applied Physiology* 19, 249-256.
- Cavagna, G.A., Thys, H., Zamboni, A., 1976. The sources of external work in level walking and running. *Journal of Physiology* 262, 639-657.
- Chambers, R., Gabbett, T.J., Cole, M.H., Beard, A., 2015. The Use of Wearable Microsensors to Quantify Sport-Specific Movements. *Sports Medicine* 45, 1065-1081.
- Chandler, P.T., Pinder, S.J., Curran, J.D., Gabbett, T.J., 2014. Physical demands of training and competition in collegiate netball players. *Journal of Strength and Conditioning Research* 28, 2732-2737.
- Christina, K.A., White, S.C., Gilchrist, L.A., 2001. Effect of localized muscle fatigue on vertical ground reaction forces and ankle joint motion during running. *Human Movement Science* 20, 257-276.
- Clark, K.P., Ryan, L.J., Weyand, P.G., 2014. Foot speed, foot-strike and footwear: linking gait mechanics and running ground reaction forces. *Journal of Experimental Biology* 217, 2037-2040.
- Clark, K.P., Weyand, P.G., 2014. Are running speeds maximized with simple-spring stance mechanics? *Journal of Applied Physiology* 117, 604-615.
- Clarsen, B., Bahr, R., Heymans, M.W., Engedahl, M., Midtsundstad, G., Rosenlund, L., Thorsen, G., Myklebust, G., 2015. The prevalence and impact of overuse injuries in five Norwegian sports: Application of a new surveillance method. *Scandinavian Journal of Medicine & Science in Sports* 25, 323-330.
- Colby, M.J., Dawson, B., Heasman, J., Rogalski, B., Gabbett, T.J., 2014. Accelerometer and GPS-derived running loads and injury risk in elite Australian footballers. *Journal of Strength and Conditioning Research* 28, 2244-2252.
- Cormack, S.J., Mooney, M.G., Morgan, W., McGuigan, M.R., 2013. Influence of neuromuscular fatigue on accelerometer load in elite Australian football players. *International Journal of Sports Physiology and Performance* 8, 373-378.
- Cormack, S.J., Smith, R.L., Mooney, M.M., Young, W.B., O'Brien, B.J., 2014. Accelerometer load as a measure of activity profile in different standards of netball match play. *International Journal of Sports Physiology and Performance* 9, 283-291.

Coutts, A.J., 2016. Working Fast and Working Slow: The Benefits of Embedding Research in High Performance Sport. *International Journal of Sports Physiology and Performance* 11, 1-2.

Coutts, A.J., Duffield, R., 2010. Validity and reliability of GPS devices for measuring movement demands of team sports. *Journal of Science and Medicine in Sport* 13, 133-135.

Cummins, C., Orr, R., O'Connor, H., West, C., 2013. Global positioning systems (GPS) and microtechnology sensors in team sports: a systematic review. *Sports Medicine* 43, 1025-1042.

Cunniffe, B., Proctor, W., Baker, J.S., Davies, B., 2009. An evaluation of the physiological demands of elite rugby union using Global Positioning System tracking software. *Journal of Strength and Conditioning Research* 23, 1195-1203.

D'Lima, D.D., Patil, S., Steklov, N., Chien, S., Colwell, C.W., Jr., 2007. In vivo knee moments and shear after total knee arthroplasty. *Journal of Biomechanics* 40, S11-S17.

Dalen, T., Jorgen, I., Gertjan, E., Geir Havard, H., Ulrik, W., 2016. Player Load, Acceleration, and Deceleration During Forty-Five Competitive Matches of Elite Soccer. *Journal of Strength and Conditioning Research* 30, 351-359.

Dalleau, G., Belli, A., Bourdin, M., Lacour, J.R., 1998. The spring-mass model and the energy cost of treadmill running. *European Journal of Applied Physiology and Occupational Physiology* 77, 257-263.

Damsgaard, M., Rasmussen, J., Christensen, S.T., Surma, E., de Zee, M., 2006. Analysis of musculoskeletal systems in the AnyBody Modeling System. *Simulation Modelling Practice and Theory* 14, 1100-1111.

Degache, F., Morin, J.B., Oehen, L., Guex, K., Giardini, G., Schena, F., Millet, G.Y., Millet, G.P., 2016. Running Mechanics During the World's Most Challenging Mountain Ultramarathon. *International Journal of Sports Physiology and Performance* 11, 608-614.

Dellaserra, C.L., Gao, Y., Ransdell, L., 2014. Use of integrated technology in team sports: a review of opportunities, challenges, and future directions for athletes. *Journal of Strength and Conditioning Research* 28, 556-573.

- Delp, S.L., Anderson, F.C., Arnold, A.S., Loan, P., Habib, A., John, C.T., Guendelman, E., Thelen, D.G., 2007. OpenSim: open-source software to create and analyze dynamic simulations of movement. *IEEE Transactions on Biomedical Engineering* 54, 1940-1950.
- Dempster, W.T., 1955. Space requirements of the seated operator: geometrical, kinematic, and mechanical aspects of the body with special reference to the limbs. Wright Air Development Center, Wright-Patterson Air Force Base, Ohio.
- Derrick, T.R., 2004. The effects of knee contact angle on impact forces and accelerations. *Medicine and Science in Sports and Exercise* 36, 832-837.
- Derrick, T.R., Caldwell, G.E., Hamill, J., 2000. Modeling the stiffness characteristics of the human body while running with various stride lengths. *Journal of Applied Biomechanics* 16, 36-51.
- Derrick, T.R., Dereu, D., McLean, S.P., 2002. Impacts and kinematic adjustments during an exhaustive run. *Medicine and Science in Sports and Exercise* 34, 998-1002.
- Di Salvo, V., Baron, R., Tschann, H., Calderon Montero, F.J., Bachl, N., Pigozzi, F., 2007. Performance characteristics according to playing position in elite soccer. *International Journal of Sports Medicine* 28, 222-227.
- Dick, R., Hertel, J., Agel, J., Grossman, J., Marshall, S.W., 2007. Descriptive epidemiology of collegiate men's basketball injuries: National Collegiate Athletic Association Injury Surveillance System, 1988-1989 through 2003-2004. *Journal of Athletic Training* 42, 194-201.
- Drust, B., Atkinson, G., Reilly, T., 2007. Future perspectives in the evaluation of the physiological demands of soccer. *Sports Medicine* 37, 783-805.
- Drust, B., Impellizzeri, F., Meyer, T., 2014. Return to play decisions - a highly important albeit unsolved issue. *Journal of Sports Sciences* 32, 1205.
- Düking, P., Hotho, A., Holmberg, H.-C., Fuss, F.K., Sperlich, B., 2016. Comparison of Non-Invasive Individual Monitoring of the Training and Health of Athletes with Commercially Available Wearable Technologies. *Frontiers in Physiology* 7, 71.
- Dutto, D.J., Smith, G.A., 2002. Changes in spring-mass characteristics during treadmill running to exhaustion. *Medicine and Science in Sports and Exercise* 34, 1324-1331.
- Dye, S.F., 2005. The pathophysiology of patellofemoral pain: a tissue homeostasis perspective. *Clinical Orthopaedics and Related Research* 436, 100-110.

- Eggl, P.S., Hunziker, E.B., Schenk, R.K., 1988. Quantitation of structural features characterizing weight- and less-weight-bearing regions in articular cartilage: a stereological analysis of medial femoral condyles in young adult rabbits. *International Journal of Anatomy and Research* 222, 217-227.
- Ehrmann, F.E., Duncan, C.S., Sindhusake, D., Franzsen, W.N., Greene, D.A., 2016. GPS and Injury Prevention in Professional Soccer. *Journal of Strength and Conditioning Research* 30, 360-367.
- Ekstrand, J., Hagglund, M., Kristenson, K., Magnusson, H., Walden, M., 2013. Fewer ligament injuries but no preventive effect on muscle injuries and severe injuries: an 11-year follow-up of the UEFA Champions League injury study. *British Journal of Sports Medicine* 47, 732-737.
- Elfmann, H., 1938. The measurement of the external force in walking. *Science* 88, 152-153.
- Elvin, N.G., Elvin, A.A., Arnoczky, S.P., 2007. Correlation between ground reaction force and tibial acceleration in vertical jumping. *Journal of Applied Biomechanics* 23, 180-189.
- Farley, C.T., Blickhan, R., Saito, J., Taylor, C.R., 1991. Hopping frequency in humans: a test of how springs set stride frequency in bouncing gaits. *Journal of Applied Physiology* 71, 2127-2132.
- Farley, C.T., Gonzalez, O., 1996. Leg stiffness and stride frequency in human running. *Journal of Biomechanics* 29, 181-186.
- Ferrari, A., Cutti, A.G., Garofalo, P., Raggi, M., Heijboer, M., Cappello, A., Davalli, A., 2010. First in vivo assessment of "Outwalk": a novel protocol for clinical gait analysis based on inertial and magnetic sensors. *Medical & Biological Engineering & Computing* 48, 1-15.
- Finch, C.F., Cook, J., 2014. Categorising sports injuries in epidemiological studies: the subsequent injury categorisation (SIC) model to address multiple, recurrent and exacerbation of injuries. *British Journal of Sports Medicine* 48, 1276-1280.
- Finni, T., Hu, M., Kettunen, P., Vilavuo, T., Cheng, S., 2007. Measurement of EMG activity with textile electrodes embedded into clothing. *Physiological Measurement* 28, 1405-1419.

- Forwood, M.R., Parker, A.W., 1991. Repetitive loading, in vivo, of the tibiae and femora of rats: effects of repeated bouts of treadmill-running. *Journal of Bone and Mineral Research* 13, 35-46.
- Foster, C., 1998. Monitoring training in athletes with reference to overtraining syndrome. *Medicine and Science in Sports and Exercise* 30, 1164-1168.
- Fourchet, F., Girard, O., Kelly, L., Horobeanu, C., Millet, G.P., 2015. Changes in leg spring behaviour, plantar loading and foot mobility magnitude induced by an exhaustive treadmill run in adolescent middle-distance runners. *Journal of Science and Medicine in Sport* 18, 199-203.
- Frost, H.M., 1997. On our age-related bone loss: insights from a new paradigm. *Journal of Bone and Mineral Research* 12, 1539-1546.
- Gabbett, T.J., 2010. The development and application of an injury prediction model for noncontact, soft-tissue injuries in elite collision sport athletes. *Journal of Strength and Conditioning Research* 24, 2593-2603.
- Gabbett, T.J., 2013. Quantifying the Physical Demands of Collision Sports: Does Microsensor Technology Measure What It Claims to Measure? *Journal of Strength and Conditioning Research* 27, 2319-2322.
- Gabbett, T.J., Ullah, S., 2012. Relationship between running loads and soft-tissue injury in elite team sport athletes. *Journal of Strength and Conditioning Research* 26, 953-960.
- Gallo, T., Cormack, S., Gabbett, T., Williams, M., Lorenzen, C., 2015. Characteristics impacting on session rating of perceived exertion training load in Australian footballers. *Journal of Sports Sciences* 33, 467-475.
- Gastin, P.B., Mclean, O.C., Breed, R.V.P., Spittle, M., 2014. Tackle and impact detection in elite Australian football using wearable microsensor technology. *Journal of Sports Sciences* 32, 947-953.
- Gaudino, P., Alberti, G., Iaia, F.M., 2014. Estimated metabolic and mechanical demands during different small-sided games in elite soccer players. *Human Movement Science* 36, 123-133.
- Gaudino, P., Gaudino, C., Alberti, G., Minetti, A.E., 2013. Biomechanics and predicted energetics of sprinting on sand: hints for soccer training. *Journal of Science and Medicine in Sport* 16, 271-275.

- Gaudino, P., Iaia, F.M., Strudwick, A.J., Hawkins, R.D., Alberti, G., Atkinson, G., Gregson, W., 2015. Factors influencing perception of effort (session rating of perceived exertion) during elite soccer training. *International Journal of Sports Physiology and Performance* 10, 860-864.
- Girard, O., Brocherie, F., Morin, J.B., Millet, G.P., 2016a. Mechanical alterations during interval-training treadmill runs in high-level male team-sport players. *Journal of Science and Medicine in Sport*. (Epub ahead of print)
- Girard, O., Brocherie, F., Tomazin, K., Farooq, A., Morin, J.B., 2016b. Changes in running mechanics over 100-m, 200-m and 400-m treadmill sprints. *Journal of Biomechanics* 49, 1490-1497.
- Girard, O., Micallef, J.P., Millet, G.P., 2011. Changes in spring-mass model characteristics during repeated running sprints. *European Journal of Applied Physiology* 111, 125-134.
- Girard, O., Millet, G.P., Slawinski, J., Racinais, S., Micallef, J.P., 2013. Changes in running mechanics and spring-mass behaviour during a 5-km time trial. *International Journal of Sports Medicine* 34, 832-840.
- Gomez-Piriz, P.T., Jimenez-Reyes, P., Ruiz-Ruiz, C., 2011. Relation between total body load and session rating of perceived exertion in professional soccer players. *Journal of Strength and Conditioning Research* 25, 2100-2103.
- Hamill, J., Bates, B.T., Knutzen, K.M., Sawhill, J.A., 1983. Variations in ground reaction force parameters at different running speeds. *Human Movement Science* 2, 47-56.
- Hamill, J., Derrick, T.R., Holt, K.G., 1995. Shock attenuation and stride frequency during running. *Human Movement Science* 14, 45-60.
- Haupenthal, A., Ruschel, C., Hubert, M., de Brito Fontana, H., Roesler, H., 2010. Loading forces in shallow water running in two levels of immersion. *Journal of Rehabilitation Medicine* 42, 664-669.
- Highton, J., Mullen, T., Norris, J., Oxendale, C., Twist, C., 2016. Energy Expenditure Derived From Micro-Technology is Not Suitable for Assessing Internal Load in Collision-Based Activities. *International Journal of Sports Physiology and Performance*.

- Hobara, H., Inoue, K., Gomi, K., Sakamoto, M., Muraoka, T., Iso, S., Kanosue, K., 2010. Continuous change in spring-mass characteristics during a 400 m sprint. *Journal of Science and Medicine in Sport* 13, 256-261.
- Hollville, E., Couturier, A., Guilhem, G., Rabita, G., 2015. Minimaxx player load as an index of the center of mass displacement? a validation study, 33rd International Conference of Biomechanics in Sports, Poitiers, France.
- Hopkins, W.G., 1991. Quantification of training in competitive sports. Methods and applications. *Sports Medicine* 12, 161-183.
- Hopkins, W.G., Marshall, S.W., Batterham, A.M., Hanin, J., 2009. Progressive statistics for studies in sports medicine and exercise science. *Medicine and Science in Sports and Exercise* 41, 3-13.
- Hreljac, A., 2004. Impact and overuse injuries in runners. *Medicine and Science in Sports and Exercise* 36, 845-849.
- Impellizzeri, F.M., Rampinini, E., Coutts, A.J., Sassi, A., Marcora, S.M., 2004. Use of RPE-based training load in soccer. *Medicine and Science in Sports and Exercise* 36, 1042-1047.
- Jennings, D., Cormack, S., Coutts, A.J., Boyd, L.J., Aughey, R.J., 2010. Variability of GPS units for measuring distance in team sport movements. *International Journal of Sports Physiology and Performance* 5, 565-569.
- Jensen, B.R., Hovgaard-Hansen, L., Cappelen, K.L., 2016. Muscle Activation and Estimated Relative Joint Force During Running with Weight Support on a Lower-Body Positive-Pressure Treadmill. *Journal of Applied Biomechanics* 32, 335-341.
- Jones, P.A., Herrington, L., Graham-Smith, P., 2016. Braking Characteristics during Cutting and Pivoting in Female Soccer Players. *Journal of Electromyography and Kinesiology*. (Epub ahead of print)
- Jones, P.A., Herrington, L.C., Graham-Smith, P., 2015. Technique determinants of knee joint loads during cutting in female soccer players. *Human Movement Science* 42, 203-211.
- Jung, Y., Jung, M., Lee, K., Koo, S., 2014. Ground reaction force estimation using an insole-type pressure mat and joint kinematics during walking. *Journal of Biomechanics* 47, 2693-2699.

- Kawabata, M., Goto, K., Fukusaki, C., Sasaki, K., Hihara, E., Mizushina, T., Ishii, N., 2013. Acceleration patterns in the lower and upper trunk during running. *Journal of Sports Sciences* 31, 1841-1853.
- Kelly, D., Coughlan, G., Green, B., Caulfield, B., 2012. Automatic detection of collisions in elite level rugby union using a wearable sensing device. *Sports Engineering* 15, 81-92.
- Kelly, S.J., Murphy, A.J., Watsford, M.L., Austin, D., Rennie, M., 2015. Reliability and Validity of Sports Accelerometers During Static and Dynamic Testing. *International Journal of Sports Physiology and Performance* 10, 106-111.
- Kempton, T., Sullivan, C., Bilsborough, J.C., Cordy, J., Coutts, A.J., 2015. Match-to-match variation in physical activity and technical skill measures in professional Australian Football. *Journal of Science and Medicine in Sport* 18, 109-113.
- Ker, R.F., Bennett, M.B., Alexander, R.M., Kester, R.C., 1989. Foot strike and the properties of the human heel pad. *Proceedings of the Institution of Mechanical Engineers, Part H: Journal of Engineering in Medicine* 203, 191-196.
- Kibler, W.B., Chandler, T.J., Stracener, E.S., 1992. Musculoskeletal adaptations and injuries due to overtraining. *Exercise and Sport Sciences Reviews* 20, 99-126.
- King, D.A., Hume, P.A., Milburn, P.D., Guttenbeil, D., 2010. Match and training injuries in rugby league: a review of published studies. *Sports Medicine* 40, 163-178.
- Kjaer, M., Langberg, H., Heinemeier, K., Bayer, M.L., Hansen, M., Holm, L., Doessing, S., Kongsgaard, M., Krogsgaard, M.R., Magnusson, S.P., 2009. From mechanical loading to collagen synthesis, structural changes and function in human tendon. *Scandinavian Journal of Medicine & Science in Sports* 19, 500-510.
- Koning, B.H., van der Krogt, M.M., Baten, C.T., Koopman, B.F., 2015. Driving a musculoskeletal model with inertial and magnetic measurement units. *Computer Methods in Biomechanics and Biomedical Engineering* 18, 1003-1013.
- Lafortune, M.A., 1991. Three-dimensional acceleration of the tibia during walking and running. *Journal of Biomechanics* 24, 877-886.
- Lafortune, M.A., Lake, M.J., Hennig, E.M., 1996. Differential shock transmission response of the human body to impact severity and lower limb posture. *Journal of Biomechanics* 29, 1531-1537.

- Lake, M., Nedergaard, N., Kersting, U., 2014. Using accelerometers in-built into portable GPS units to capture the rapid decelerations needed for turning movements in soccer, World Conference on science and soccer 4.0, Portland, Oregon, USA.
- Lambert, M.I., Borresen, J., 2010. Measuring training load in sports. *International Journal of Sports Physiology and Performance* 5, 406-411.
- Lieberman, D.E., Venkadesan, M., Werbel, W.A., Daoud, A.I., D'Andrea, S., Davis, I.S., Mang'eni, R.O., Pitsiladis, Y., 2010. Foot strike patterns and collision forces in habitually barefoot versus shod runners. *Nature* 463, 531-535.
- Lovell, T.W., Sirotic, A.C., Impellizzeri, F.M., Coutts, A.J., 2013. Factors affecting perception of effort (session rating of perceived exertion) during rugby league training. *International Journal of Sports Physiology and Performance* 8, 62-69.
- Luteberget, L.S., Spencer, M., 2016. High Intensity Events in International Female Team Handball Matches. *International Journal of Sports Physiology and Performance*. (Epub ahead of print)
- Maganaris, C.N., Narici, M.V., Almekinders, L.C., Maffulli, N., 2004. Biomechanics and pathophysiology of overuse tendon injuries: ideas on insertional tendinopathy. *Sports Medicine* 34, 1005-1017.
- Malone, J.J., Di Michele, R., Morgans, R., Burgess, D., Morton, J.P., Drust, B., 2015. Seasonal training-load quantification in elite English premier league soccer players. *International Journal of Sports Physiology and Performance* 10, 489-497.
- Mapelli, A., Zago, M., Fusini, L., Galante, D., Colombo, A., Sforza, C., 2014. Validation of a protocol for the estimation of three-dimensional body center of mass kinematics in sport. *Gait & Posture* 39, 460-465.
- Mathie, M.J., Coster, A.C., Lovell, N.H., Celler, B.G., 2004. Accelerometry: providing an integrated, practical method for long-term, ambulatory monitoring of human movement. *Physiological Measurement* 25, R1-20.
- McLaren, S.J., Graham, M., Spears, I.R., Weston, M., 2016a. The Sensitivity of Differential Ratings of Perceived Exertion as Measures of Internal Load. *International Journal of Sports Physiology and Performance* 11, 404-406.

- McLaren, S.J., Smith, A., Spears, I.R., Weston, M., 2016b. A detailed quantification of differential ratings of perceived exertion during team-sport training. *Journal of Science and Medicine in Sport*.
- McLaren, S.J., Weston, M., Smith, A., Cramb, R., Portas, M.D., 2016c. Variability of physical performance and player match loads in professional rugby union. *Journal of Science and Medicine in Sport* 19, 493-497.
- McLellan, C.P., Lovell, D.I., Gass, G.C., 2011. Biochemical and endocrine responses to impact and collision during elite Rugby League match play. *Journal of Strength and Conditioning Research* 25, 1553-1562.
- McMahon, T.A., Cheng, G.C., 1990. The mechanics of running: How does stiffness couple with speed? *Journal of Biomechanics* 23, Supplement 1, 65-78.
- McMahon, T.A., Greene, P.R., 1979. The influence of track compliance on running. *Journal of Biomechanics* 12, 893-904.
- McMahon, T.A., Valiant, G., Frederick, E.C., 1987. Groucho running. *Journal of Applied Physiology* 62, 2326-2337.
- McNamara, D.J., Gabbett, T.J., Naughton, G., Farhart, P., Chapman, P., 2013. Training and Competition Workloads and Fatigue Responses of Elite Junior Cricket Players. *International Journal of Sports Physiology and Performance* 8, 517-526.
- Meeusen, R., Duclos, M., Gleeson, M., Rietjens, G., Steinacker, J., Urhausen, A., 2006. Prevention, diagnosis and treatment of the Overtraining Syndrome. *European Journal of Sport Science* 6, 1-14.
- Meyer, U., Ernst, D., Schott, S., Riera, C., Hattendorf, J., Romkes, J., Granacher, U., Gopfert, B., Kriemler, S., 2015. Validation of two accelerometers to determine mechanical loading of physical activities in children. *Journal of Sports Sciences* 33, 1702-1709.
- Miller, R.H., Edwards, W.B., Brandon, S.C., Morton, A.M., Deluzio, K.J., 2014. Why don't most runners get knee osteoarthritis? A case for per-unit-distance loads. *Medicine and Science in Sports and Exercise* 46, 572-579.
- Montgomery, P.G., Pyne, D.B., Minahan, C.L., 2010. The physical and physiological demands of basketball training and competition. *International Journal of Sports Physiology and Performance* 5, 75-86.

- Morin, J.B., Dalleau, G., Kyrolainen, H., Jeannin, T., Belli, A., 2005. A simple method for measuring stiffness during running. *Journal of Applied Biomechanics* 21, 167-180.
- Morin, J.B., Jeannin, T., Chevallier, B., Belli, A., 2006. Spring-mass model characteristics during sprint running: correlation with performance and fatigue-induced changes. *International Journal of Sports Medicine* 27, 158-165.
- Morin, J.B., Tomazin, K., Edouard, P., Millet, G.Y., 2011. Changes in running mechanics and spring-mass behavior induced by a mountain ultra-marathon race. *Journal of Biomechanics* 44, 1104-1107.
- Morton, R.H., Fitzclarke, J.R., Banister, E.W., 1990. Modeling Human-Performance in Running. *Journal of Applied Physiology* 69, 1171-1177.
- Mundermann, A., Dyrby, C.O., D'Lima, D.D., Colwell, C.W., Jr., Andriacchi, T.P., 2008. In vivo knee loading characteristics during activities of daily living as measured by an instrumented total knee replacement. *Journal of Orthopaedic Research* 26, 1167-1172.
- Nedergaard, N.J., Robinson, M.A., Eusterwiemann, E., Drust, B., Lisboa, P.J., Vanrenterghem, J., 2016. The relationship between whole-body external loading and body-worn accelerometry during team sports movements. *International Journal of Sports Physiology and Performance*. (Epub ahead of print)
- Nielsen, R.O., Buist, I., Sorensen, H., Lind, M., Rasmussen, S., 2012. Training errors and running related injuries: a systematic review. *International Journal of Sports Physical Therapy* 7, 58-75.
- Nielsen, R.O., Cederholm, P., Buist, I., Sorensen, H., Lind, M., Rasmussen, S., 2013. Can GPS be used to detect deleterious progression in training volume among runners? *Journal of Strength and Conditioning Research* 27, 1471-1478.
- Nigg, B.M., Cole, G.K., Bruggemann, G.P., 1995. Impact forces during heel-toe running. *Journal of Applied Biomechanics* 11, 407-432.
- Nikooyan, A.A., Zadpoor, A.A., 2011. Mass-spring-damper modelling of the human body to study running and hopping--an overview. *Proceedings of the Institution of Mechanical Engineers, Part H: Journal of Engineering in Medicine* 225, 1121-1135.
- Page, R.M., Marrin, K., Brogden, C.M., Greig, M., 2015. Biomechanical and Physiological Response to a Contemporary Soccer Match-Play Simulation. *Journal of Strength and Conditioning Research* 29, 2860-2866.

- Page, R.M., Marrin, K., Brogden, C.M., Greig, M., 2016. The biomechanical and physiological response to repeated soccer-specific simulations interspersed by 48 or 72 hours recovery. *Physical Therapy in Sport* 22, 81-87.
- Pataky, T.C., 2012. One-dimensional statistical parametric mapping in Python. *Computer Methods in Biomechanics and Biomedical Engineering* 15, 295-301.
- Pataky, T.C., Robinson, M.A., Vanrenterghem, J., 2013. Vector field statistical analysis of kinematic and force trajectories. *Journal of Biomechanics* 46, 2394-2401.
- Polglaze, T., Dawson, B., Hiscock, D.J., Peeling, P., 2015. A comparative analysis of accelerometer and time-motion data in elite men's hockey training and competition. *International Journal of Sports Physiology and Performance* 10, 446-451.
- Polley, C.S., Cormack, S.J., Gabbett, T.J., Polglaze, T., 2015. Activity profile of high-level Australian lacrosse players. *Journal of Strength and Conditioning Research* 29, 126-136.
- Prins, J., Cutner, D., 1999. Aquatic therapy in the rehabilitation of athletic injuries. *Clinics in Sports Medicine* 18, 447-461.
- Rabita, G., Couturier, A., Dorel, S., Hausswirth, C., Le Meur, Y., 2013. Changes in spring-mass behavior and muscle activity during an exhaustive run at VO₂max. *Journal of Biomechanics* 46, 2011-2017.
- Raffalt, P.C., Hovgaard-Hansen, L., Jensen, B.R., 2013. Running on a lower-body positive pressure treadmill: VO₂max, respiratory response, and vertical ground reaction force. *Research Quarterly for Exercise and Sport* 84, 213-222.
- Ritchie, D., Hopkins, W.G., Buchheit, M., Cordy, J., Bartlett, J.D., 2016. Quantification of Training and Competition Load Across a Season in an Elite Australian Football Club. *International Journal of Sports Physiology and Performance* 11, 474-479.
- Rowlands, A.V., Stiles, V.H., 2012. Accelerometer counts and raw acceleration output in relation to mechanical loading. *Journal of Biomechanics* 45, 448-454.
- Saunders, J.B., Inman, V.T., Eberhart, H.D., 1953. The major determinants in normal and pathological gait. *The Journal of Bone & Joint Surgery* 35-A, 543-558.
- Scanlan, A.T., Wen, N., Tucker, P.S., Dalbo, V.J., 2014. The relationships between internal and external training load models during basketball training. *Journal of Strength and Conditioning Research* 28, 2397-2405.

- Scott, B.R., Lockie, R.G., Knight, T.J., Clark, A.C., Janse de Jonge, X.A., 2013. A comparison of methods to quantify the in-season training load of professional soccer players. *International Journal of Sports Physiology and Performance* 8, 195-202.
- Setuain, I., Martinikorena, J., Gonzalez-Izal, M., Martinez-Ramirez, A., Gomez, M., Alfaro-Adrian, J., Izquierdo, M., 2016. Vertical jumping biomechanical evaluation through the use of an inertial sensor-based technology. *Journal of Sports Sciences* 34, 843-851.
- Slowman, S.D., Brandt, K.D., 1986. Composition and glycosaminoglycan metabolism of articular cartilage from habitually loaded and habitually unloaded sites. *Arthritis & Rheumatology* 29, 88-94.
- Soligard, T., Schweltnus, M., Alonso, J.-M., Bahr, R., Clarsen, B., Dijkstra, H.P., Gabbett, T., Gleeson, M., Hägglund, M., Hutchinson, M.R., Janse van Rensburg, C., Khan, K.M., Meeusen, R., Orchard, J.W., Pluim, B.M., Raftery, M., Budgett, R., Engebretsen, L., 2016. How much is too much? (Part 1) International Olympic Committee consensus statement on load in sport and risk of injury. *British Journal of Sports Medicine* 50, 1030-1041.
- Swann, A.C., Seedhom, B.B., 1993. The stiffness of normal articular cartilage and the predominant acting stress levels: implications for the aetiology of osteoarthritis. *British Journal of Rheumatology* 32, 16-25.
- Taylor, M.J., Beneke, R., 2012. Spring mass characteristics of the fastest men on Earth. *International Journal of Sports Medicine* 33, 667-670.
- Tran, J., Netto, K., Aisbett, B. and Gustin, P., Year Validation of accelerometer data for measuring impacts during jumping and landing tasks. *In 28th International Conference on Biomechanics in Sports. Marquette, Michigan, USA.*
- Vanrenterghem, J., Gormley, D., Robinson, M., Lees, A., 2010. Solutions for representing the whole-body centre of mass in side cutting manoeuvres based on data that is typically available for lower limb kinematics. *Gait & Posture* 31, 517-521.
- Vanrenterghem, J., Lees, A., Lenoir, M., Aerts, P., De Clercq, D., 2004. Performing the vertical jump: movement adaptations for submaximal jumping. *Hum Mov Sci* 22, 713-727.

- Vanrenterghem, J., Nedergaard, N., Robinson, M., Drust, B., Player load monitoring in running-based team sports: A new framework based on physiological and biomechanical principles of load and adaptation. *Sports Medicine*. (Under Review)
- Vanrenterghem, J., Venables, E., Pataky, T., Robinson, M.A., 2012. The effect of running speed on knee mechanical loading in females during side cutting. *Journal of Biomechanics* 45, 2444-2449.
- Varley, M.C., Fairweather, I.H., Aughey, R.J., 2012. Validity and reliability of GPS for measuring instantaneous velocity during acceleration, deceleration, and constant motion. *Journal of Sports Sciences* 30, 121-127.
- Viru, A., Viru, M., 2000. Nature of training effects, Exercise and sport science. 1st edn. Philadelphia: Lippincott Williams and Wilkins, 67-95.
- Walker, E.J., McAinch, A.J., Sweeting, A., Aughey, R.J., 2016. Inertial sensors to estimate the energy expenditure of team-sport athletes. *Journal of Science and Medicine in Sport* 19, 177-181.
- Weston, M., Siegler, J., Bahnert, A., McBrien, J., Lovell, R., 2015. The application of differential ratings of perceived exertion to Australian Football League matches. *Journal of Science and Medicine in Sport* 18, 704-708.
- Winter, D.A., 2005. Biomechanics and motor control of human movement. 4th edn. John Wiley & Sons, Hoboken, N.J.
- Wundersitz, D.W., Gatin, P.B., Richter, C., Robertson, S.J., Netto, K.J., 2015a. Validity of a trunk-mounted accelerometer to assess peak accelerations during walking, jogging and running. *European Journal of Sport Science* 15, 382-390.
- Wundersitz, D.W., Gatin, P.B., Robertson, S., Davey, P.C., Netto, K.J., 2015b. Validation of a Trunk-mounted Accelerometer to Measure Peak Impacts during Team Sport Movements. *International Journal of Sports Medicine* 36, 742-746.
- Wundersitz, D.W., Gatin, P.B., Robertson, S.J., Netto, K.J., 2015c. Validity of a Trunk-Mounted Accelerometer to Measure Physical Collisions in Contact Sports. *International Journal of Sports Physiology and Performance* 10, 681-686.
- Wundersitz, D.W., Josman, C., Gupta, R., Netto, K.J., Gatin, P.B., Robertson, S., 2015d. Classification of team sport activities using a single wearable tracking device. *Journal of Biomechanics* 48, 3975-3981.

-
- Wundersitz, D.W., Netto, K.J., Aisbett, B., Gatin, P.B., 2013. Validity of an upper-body-mounted accelerometer to measure peak vertical and resultant force during running and change-of-direction tasks. *Sports Biomechanics* 12, 403-412.
- Yang, C.C., Hsu, Y.L., 2010. A Review of Accelerometry-Based Wearable Motion Detectors for Physical Activity Monitoring. *Sensors* 10, 7772-7788.
- Young, C.M., Gatin, P.B., Sanders, N., Mackey, L., Dwyer, D.B., 2016. Player Load in Elite Netball: Match, Training and Positional Comparisons. *International Journal of Sports Physiology and Performance*. (Epub ahead of print)
- Zadpoor, A.A., Nikooyan, A.A., 2010. Modeling muscle activity to study the effects of footwear on the impact forces and vibrations of the human body during running. *Journal of Biomechanics* 43, 186-193.

APPENDICES

Appendix A: Laboratory accelerometers location relative to the GPS device

The purpose of this appendix was to explore the influence of the laboratory accelerometers location relative to the GPS device and the consistently higher values observed for the laboratory accelerometer compared to the GPS integrated accelerometer.

A pilot study was therefore conducted where two tri-axial wireless laboratory accelerometers (518, DTS accelerometer, Noraxon Inc., Scottsdale, USA) were attached to the GPS device, one accelerometer on the anterior side and one on the posterior side of the GPS device. All three accelerometers were positioned within a small pocket of a tight fitted elastic vest of one participant which was asked to complete 6 single leg drop landings from a 50 cm drop height. The two laboratory accelerometers were switched halfway through the pilot testing.



Figure A.1: Pictures of the laboratory accelerometers location on the anterior (picture on the left) and posterior side (picture on the right) of the GPS device.

Resultant peak accelerations were determined for each accelerometer (Table A.1). Though slightly higher accelerations generally were observed for the laboratory accelerometer positioned on the posterior side of the GPS device (Figure A.1), the pilot study showed that the laboratory accelerometer measured higher accelerations than the GPS integrated accelerometer regardless of the laboratory accelerometers position. In addition, the peak accelerations observed in the pilot study for the single leg drop landing were higher than the peak accelerations observed for the running and change in direction

trials in Chapter 2. The laboratory accelerometer was subsequently placed on the posterior side in Chapter 2 to ensure that the GPS device was placed as close as possible to the trunk and similar to its position in the field.

Table A.1: Resultant peak accelerations measured with the GPS integrated accelerometer and the two laboratory accelerometers located on the anterior and posterior side of the GPS device.

	Catapult (g)	Anterior Noraxon (g)	Posterior Noraxon (g)	Difference between the two Noraxon accelerometers (g)
1st trial	5.62	7.56	7.78	0.22
2nd trial	6.43	7.60	8.29	0.69
3rd trial	5.66	6.10	6.54	0.44
4th trial	6.01	8.05	8.43	0.38
5th trial	5.97	8.72	8.52	0.20
6th trial	5.18	6.06	6.20	0.14

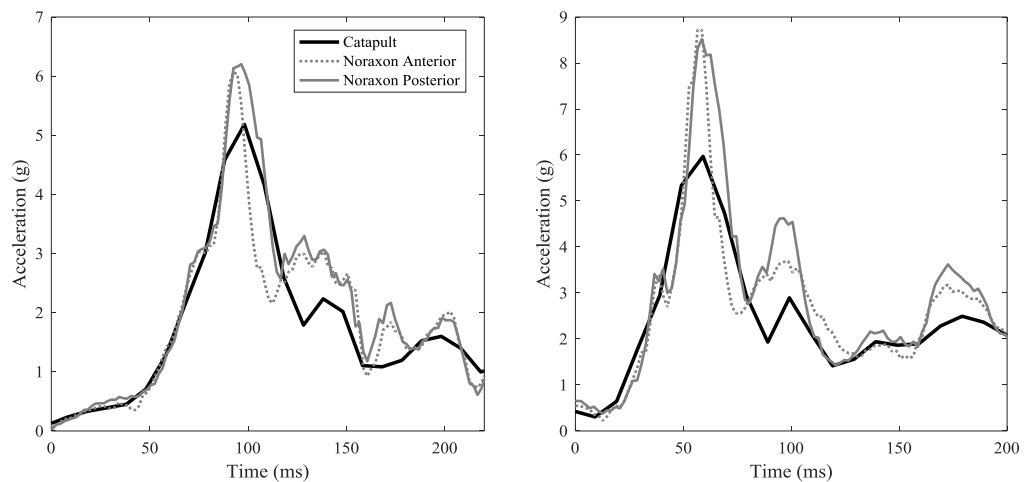


Figure A.2: Two representative examples of the trunk acceleration measured from the GPS integrated accelerometer (Catapult) and the two laboratory accelerometers (Noraxon) from the single leg drop landing.

This pilot study showed a difference in peak acceleration of approximately 0.34 g between the anterior and posterior location. The posterior location could therefore unlikely explain the consistent difference in peak acceleration observed between the GPS integrated accelerometer and laboratory accelerometer observed in Chapter 2.

Appendix B: 1g static accelerometer calibration protocol

The purpose of this appendix was to provide a detailed description of the 1g static accelerometer calibration carried out before and after each data collection. The calibration was performed to ensure the accuracy of the accelerometers. During the calibration protocol the three laboratory accelerometer sensors and the GPS integrated accelerometer described in Chapter 2 were fixed on a flat surface inside a box with double sided tape (Figure B.1). A second GPS integrated accelerometer was also included in the calibration protocol as a reference to the GPS integrated accelerometer used in this thesis.



Figure B.1: Pictures of the three laboratory accelerometers and two GPS integrated accelerometers mounted inside the calibration box used for the 1g static calibration.

The box was carefully rotated through all degrees of freedom, and orientated on the ground to measure acceleration in the positive and negative orientation of the three sensing axis (X, Y, Z). Acceleration data was measured over 20 seconds at each position measuring acceleration due to gravity 1 g or $9.81 \text{ m}\cdot\text{s}^{-1}$ (Figure B.2).

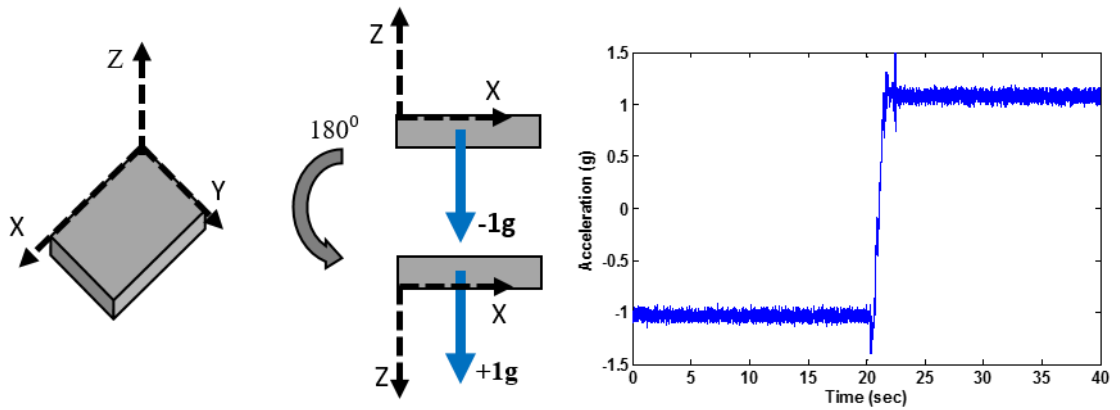


Figure B.2: Illustration of the change in acceleration of 2g when rotating an accelerometer 180° during the static 1g calibration protocol.

The static calibration was used to test the static validity of the individual accelerometers used in this thesis. In addition, the static calibration data before and after each test session was used to investigate the within session and between session static reliability of the different sensors. The sensors dynamic validity and reliability haven not been tested due to the absence of a mechanical shaking device within the department.

Appendix C: Synchronisation of GPS integrated accelerometer

The purpose of this appendix was to explain the method used in this thesis to synchronise the GPS integrated accelerometer with laboratory accelerometers and the ground reaction force measurements. The acceleration data from the GPS integrated accelerometer was continuously collected throughout the entire session (typically around 3 hours). The acceleration data from the trunk-mounted laboratory accelerometer fixed to the GPS device was used to synchronise the acceleration from the GPS integrated accelerometer.

The laboratory accelerometer data was automatically synchronised with the data from the motion capture system through the analog channels of the A/D board. An External trigger was used to trigger and synchronise accelerometer data with motion capture data at the beginning of every trials. The two trunk-mounted accelerometers worn by the participants were tapped three times with a small rubber hammer at the beginning of every trial to create three clear spikes in the anterior/posterior acceleration signal. A customised Matlab code was created to automate the synchronisation of the two accelerometer signals. This basically consisted of two steps: 1) A time synchronisation using the information from the internal clock of the GPS device and the data collection computer and 2) A vector scalar product synchronisation where the signal created from tapping the accelerometers were to improve the time synchronisation. The step by step approach is described below:

Step 1: Time synchronisation

1. The start time of the individual trials were identified in the Catapult data from the QTM (Qualisys Track Manager) file
2. Catapult data from the individual trials were identified as the start time + 25 seconds (the length of the laboratory accelerometer data files), see figure C.1

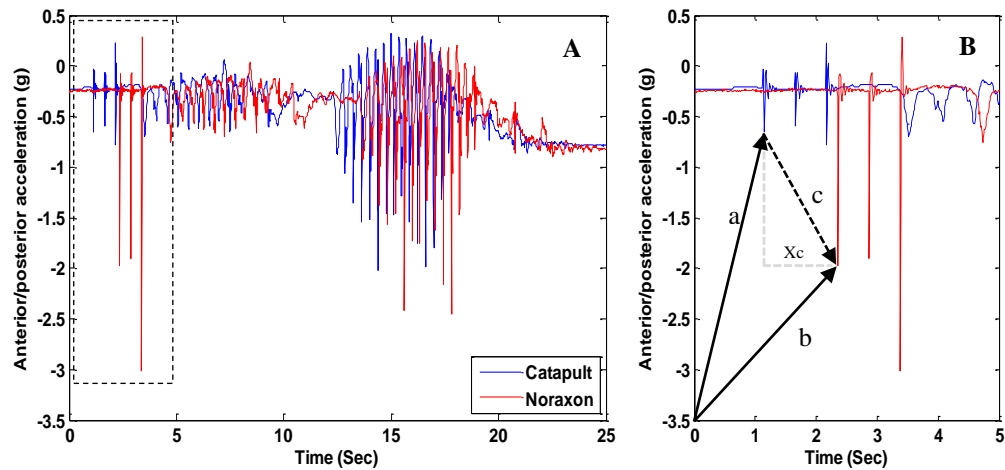


Figure C.1: Time synchronised (A) and vector scalar product synchronisation (B) example from one trial.

Step 2: Vector scalar product synchronisation

1. The first minimum in the accelerometer signal was identify for the two accelerometers (minimum due to the tapping of the accelerometer)
2. Two vectors (a : Catapult vector; b : Noraxon vector) were created from the minimum value and time of the minimum value, see Figure C.1
3. The scalar product of the two vectors was calculated to create a vector (c) between vector a and b . The time difference between the two minimum values were defined as the x-value of vector c (x_c)
4. x_c was used to correct the 25 second time synchronised Catapult signal with the Noraxon signal, see Figure C.2

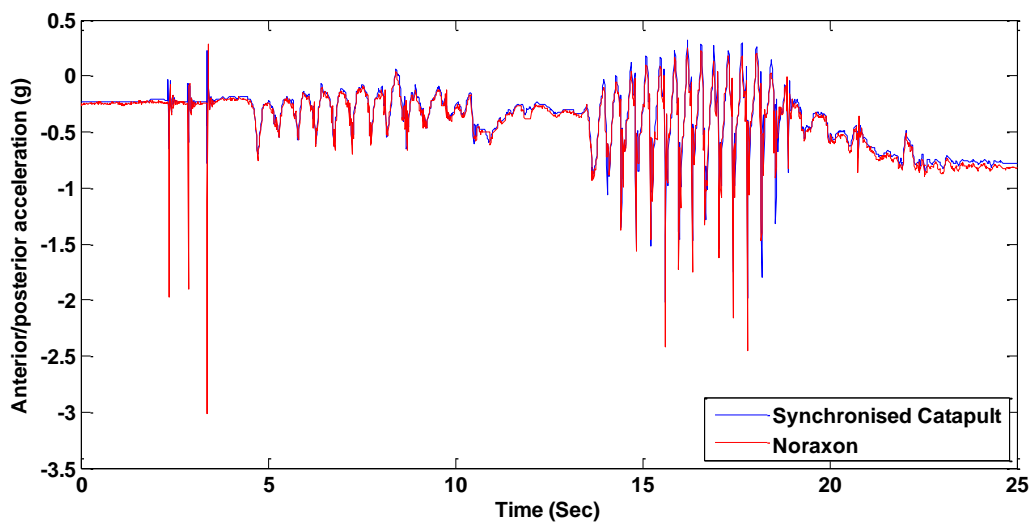


Figure C.2: Synchronised acceleration data from a representative example.

Appendix D: Establishing accelerometer filter cut-off frequency in Chapter 2

The purpose of this appendix was to explore the sensitivity of the filter cut-off frequencies applied to the acceleration signal from the three laboratory accelerometers (Trunk, Pelvis and Tibia) in Chapter 2.

Methods

The laboratory accelerometer data (Trunk, Pelvis and Tibia) from one representative participant for a Run, Cut45 and Cut90 trial with an approach speed of 2 and 5 m·s⁻¹ were used to explore the effect of different filter cut-off frequencies on the acceleration signal and peak acceleration. A 6th order Butterworth low-pass with cut-off frequencies between 20-80Hz were applied to the Trunk and Pelvis data, while cut-off frequencies between 40-100Hz were applied to the Tibia data (Figure D.1). Peak accelerations were calculated as described in Chapter 2 for the individual trials and cut-off frequencies.

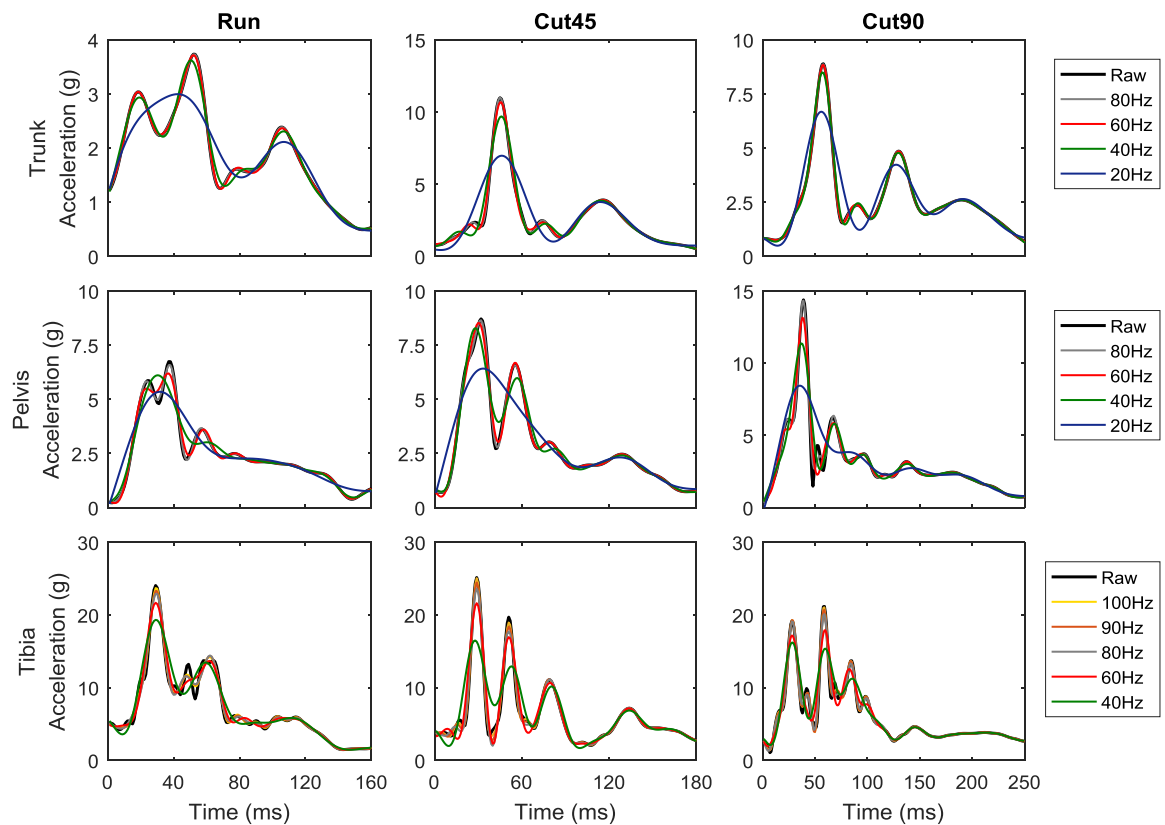


Figure D.1: Resultant acceleration from the Trunk, Pelvis and Tibia for a representative Run, Cut45 and Cut90 trial at 5 m·s⁻¹ with different low-pass filter cut-off frequencies applied to the acceleration signal.

Table D.1: Resultant peak accelerations from the three laboratory accelerometers (Trunk, Pelvis and Tibia) with low-pass filter cut-off frequencies between 20-100Hz applied to the acceleration signal for the Run, Cut45 and Cut90 at 2 and 5 m·s⁻¹.

Trunk	Run		Cut45		Cut90	
	2 m·s ⁻¹	5 m·s ⁻¹	2 m·s ⁻¹	5 m·s ⁻¹	2 m·s ⁻¹	5 m·s ⁻¹
Raw	4.69	3.73	3.83	10.98	3.08	8.89
80Hz	4.68	3.73	3.82	10.99	3.08	8.87
70Hz	4.67	3.73	3.82	10.89	3.06	8.86
60Hz	4.63	3.72	3.81	10.67	3.02	8.84
50Hz	4.56	3.68	3.78	10.35	2.95	8.76
40Hz	4.43	3.62	3.74	9.70	2.84	8.49
20Hz	3.63	2.99	3.21	6.97	2.74	6.68
Pelvis						
Raw	3.38	6.74	3.29	8.71	3.14	14.38
80Hz	3.38	6.58	3.28	8.65	3.14	14.33
70Hz	3.38	6.43	3.28	8.57	3.13	13.84
60Hz	3.36	6.19	3.26	8.52	3.13	13.15
50Hz	3.32	5.97	3.24	8.48	3.11	12.33
40Hz	3.32	6.11	3.18	8.29	3.04	11.37
20Hz	3.01	5.35	2.90	6.42	3.00	8.44
Tibia						
Raw	7.26	24.04	6.79	25.14	5.93	21.18
100Hz	7.26	23.69	6.73	25.05	5.91	21.04
90Hz	7.23	23.29	6.71	24.47	5.92	20.68
80Hz	7.18	22.90	6.68	23.61	5.92	20.12
70Hz	7.11	22.44	6.63	22.73	5.84	19.13
60Hz	7.03	21.67	6.59	21.62	5.63	17.88
40Hz	6.51	19.32	6.51	16.49	5.08	16.20

As illustrated in Table D.1 the lowest filtering cut-off frequencies had a higher effect on the peak accelerations especially for the trials with the fastest approach speed (5 m·s⁻¹). Based on these results and from the cut-off frequencies previously used for body-worn accelerometry during running, cut-off frequencies of 60 Hz for the Trunk and Pelvis data and 90Hz for the Tibia data were applied to the accelerometer data in Chapter 2. These filtering cut-off frequencies were chosen to remove any high-frequency noise in the signal, e.g. from the movement of the accelerometer relative to the segment it was attached to, but at the same time maintain as much of the raw signal as possible.

A fast Fourier analysis would have revealed the frequency content of the acceleration signal from the different accelerometer locations, tasks and intensities and been used as a guidance in choosing the filter cut-off frequency. It was however beyond the scope of this appendix to determine the optimal cut-off frequency as this will dependent on task and intensity as illustrated in this appendix. This makes it very difficult to apply “optimal” filter settings to team sports data from the field. As a consequence, the relationship between peak acceleration from body-worn accelerometers and CoM acceleration explored in Chapter 2 may improve or decrease depending on the filter cut-off frequency applied to the acceleration data.

Appendix E: Definition of the eight natural MSD-model parameters

The purpose of this appendix is to describe how the nine MSD-model parameters presented in Figure E.1 (m_1 , m_2 , x_1 , x_2 , k_1 , k_2 , l_1 , l_2 and c) were transformed into the eight natural model parameters used in this study. The position of m_1 and m_2 (p_1 and p_2), the mass ratio of the lower mass relative to the total body mass (λ), the natural frequencies of upper and lower spring (ω_1^2 and ω_2^2) and the damping ratio (ζ) were defined as describes in Equation E1-E8.

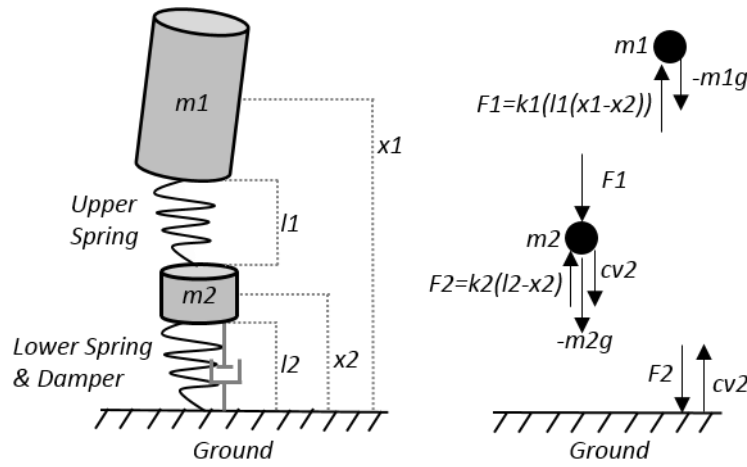


Figure E.1: Illustration of the MSD-model and its free-body diagram.

$$p_1 = x_1 - l_1 - l_2 \quad [\text{Equation E.1}]$$

$$p_2 = x_2 - l_2 \quad [\text{Equation E.2}]$$

$$v_1 = \dot{p}_1 \quad [\text{Equation E.3}]$$

$$v_2 = \dot{p}_2 \quad [\text{Equation E.4}]$$

$$\lambda = \frac{m_1}{m_2} \quad [\text{Equation E.5}]$$

$$\omega_1^2 = \frac{k_1}{m_1} = \frac{(1+\lambda)k_1}{\lambda M} \quad [\text{Equation E.6}]$$

$$\omega_2^2 = \frac{k_2}{m_2} = \frac{(1+\lambda)k_2}{M} \quad [\text{Equation E.7}]$$

$$\zeta = \frac{c}{2\sqrt{k_2 m_2}} \quad [\text{Equation E.8}]$$

Where x_1 and x_2 are the position of the of the upper and lower spring under no external load, l_1 and l_2 are the natural lengths of the upper and lower spring under no external load, k_1 and k_2 are the linear spring constants of the massless upper and lower spring, c is the damping coefficient of the lower spring.

Appendix F: Establishing study specific search parameters

The purpose of this appendix was to clarify how model parameters adopted from Derrick et al. (2000) for running at $3.83 \text{ m}\cdot\text{s}^{-1}$ ($\pm 5\%$) was used in a pilot study to determine the initial search parameters that best represented the types of tasks and approach speeds investigated in Chapter 3.

The model parameters adopted from Derrick et al. (2000) were: p_2 : 0.0074 m; v_{I1} : $-0.73 \text{ m}\cdot\text{s}^{-1}$; v_2 : $-0.66 \text{ m}\cdot\text{s}^{-1}$; k_{I1} : $34100 \text{ N}\cdot\text{m}^{-1}$; k_2 : $78400 \text{ N}\cdot\text{m}^{-1}$; λ : 0.2 and ζ : 0.35. p_{I1} was not presented in the paper by Derrick et al. (2000) and p_{I1} was therefore expected to be twice as long as the position of p_2 . The initial search parameter for p_{I1} was therefore set at 0.015 m for this analysis. The model parameters from Derrick et al. (2000) was used as initial search parameters in a pilot study including the data from all tasks and approach speeds for 4 participants.

The median model parameters obtained from the optimisation routine when the model parameters from Derrick et al. (2000) were used as initial search parameters were as follows: p_{I1} : -0.01 m ; p_2 : 0.00 m ; v_{I1} : $-1.29 \text{ m}\cdot\text{s}^{-1}$; v_2 : $-0.19 \text{ m}\cdot\text{s}^{-1}$; λ : 2.81; ω_{I1}^2 : $336 \text{ N}\cdot\text{m}^{-1}\cdot\text{kg}^{-1}$; ω_2^2 : $3401 \text{ N}\cdot\text{m}^{-1}\cdot\text{kg}^{-1}$; ζ : 0.31. These parameters were used as the initial search parameter for all participants and tasks in Chapter 3.

The same approach was adopted in Chapter 4 to determine accelerometer/MSD-model specific search model parameters. Only difference was that the average model parameters from Chapter 3 were used in the first step, instead of the model parameters from Derrick et al. 2000.

Appendix G: Effect of filter cut-off frequency on accelerometer/MSD-model

The purpose of this appendix was to explore the sensitivity of the filter cut-off frequency applied to the GPS integrated accelerometry and the model parameters from the accelerometer/MSD-model.

Methods

GPS integrated accelerometry from ten participants (age 22 ± 4 years, height 178 ± 8 cm, mass 76 ± 11 kg) were used in this sensitivity analysis to explore the influence of accelerometer filter cut-off frequency on the accelerometer/MSD-model parameters and predicted GRF. A 4th order recursive Butterworth low-pass filter with a cut-off frequency of 5, 10 and 15 Hz respectively were applied to the GPS integrated accelerometry data and used as accelerometer/MSD-model input. The model parameters from the accelerometry with different cut-off frequencies were compared to the model parameters from Chapter 4, where a 20 Hz cut-off was applied to the GPS integrated accelerometer data.

Results

The model parameters from the GPS integrated accelerometer with at filter cut-off frequency at 15 Hz were almost identical with the model parameters from Chapter 4 (20 Hz cut-off frequency). Applying a cut-off frequencies of 5 or 10 Hz generally moved the average model parameters further away from the GRF_{measured} model parameters observed in Chapter 3, though improvements were observed for p_1 , p_2 , v_2 at the Cut90 task when the GPS integrated accelerometer data was filtered with a 5 Hz low-pass filter (Figure G.1).

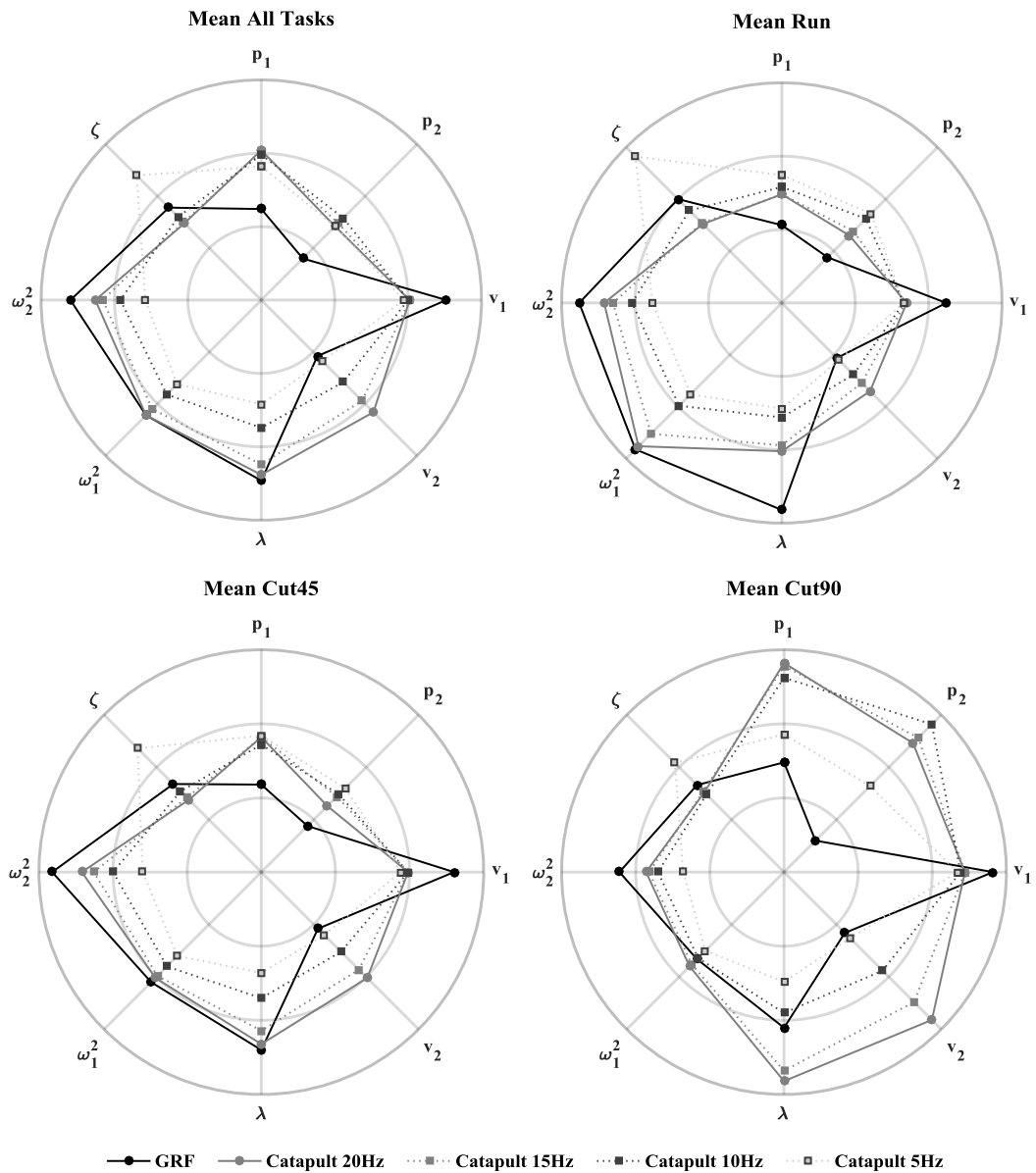


Figure G.1: Polar plots displaying the mean task model parameters (in scaled dimensionless values) for $GRF_{measured}$ (Chapter 3) and the GPS integrated accelerometer (Catapult) with different cut-off frequencies.

The acceleration changed dramatically when the cut-off frequency was lowered and the high frequency in the acceleration signal was removed. Though this enabled the accelerometer/MSD-model to simulate the acceleration patterns with stronger accuracy (Figure G.2) the GRF predictions were still poor regardless of the filter cut-off frequency applied to the GPS integrated accelerometer data.

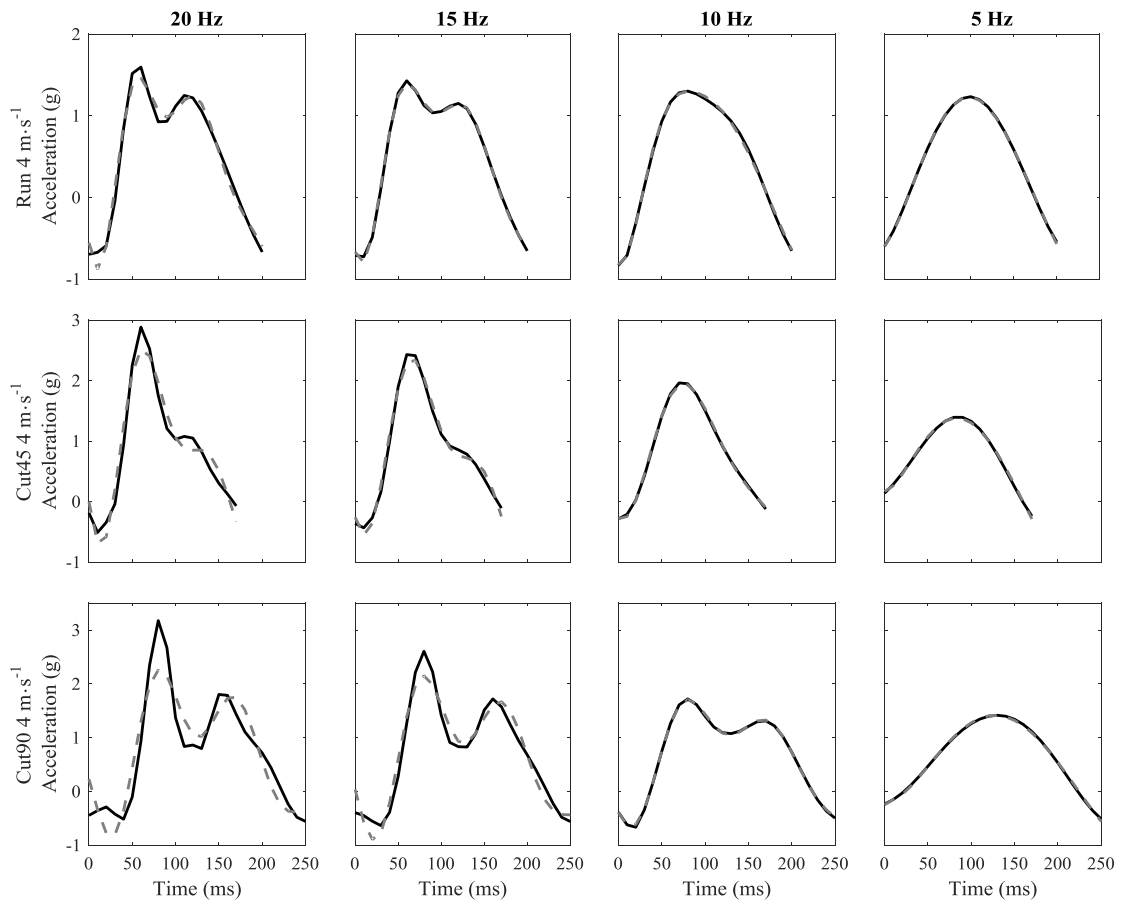


Figure G.2: Representative examples of the of the measured trunk acceleration when different low-pass filter cut-off frequencies were applied to the GPS integrated accelerometer data (black line) and a_1 for the associated acceleration signals (dashed grey line).

Conclusion

Though better MSD-model upper mass acceleration simulations were observed when a low-pass filter with a cut-off frequency at 10 Hz or 5 Hz was applied to the acceleration signal from the GPS integrated accelerometer, it generally did not improve the model parameters or the GRF predictions from the accelerometer/MSD-model.

Appendix H: Laboratory accelerometer as accelerometer/MSD-model input

The purpose of this appendix was to explore the sensitivity of the accelerometer/MSD-model to predict GRF when accelerations from a laboratory accelerometer were used as accelerometer/MSD-model input.

Methods

The acceleration signal from the tri-axial wireless laboratory accelerometer (518, DTS accelerometer, Noraxon Inc., Scottsdale, USA) was used as accelerometer/MSD-model input in this sensitivity analysis. The laboratory accelerometer had an effective sampling frequency of 1000 Hz and was tightly fixated to the posterior side of the GPS device as described in Chapter 2. The laboratory accelerometer data from all participants, tasks and approach speeds were included in this sensitivity analysis of the accelerometer/MSD-model.

Results

The MSD-model was able to simulate the acceleration patterns from the laboratory accelerometer with good to very good accuracy across the different tasks and approach speeds, though a_1 generally underestimating the magnitude of the first peak in the acceleration signal during the stance time (Figure H.1). Nevertheless, poor GRF predictions were observed across tasks and approach speeds from the accelerometer/MSD-model when the acceleration signal from the laboratory accelerometer was used as model input. This was similar to the results observed in Chapter 4 when acceleration data from the GPS integrated accelerometer was used as model input.

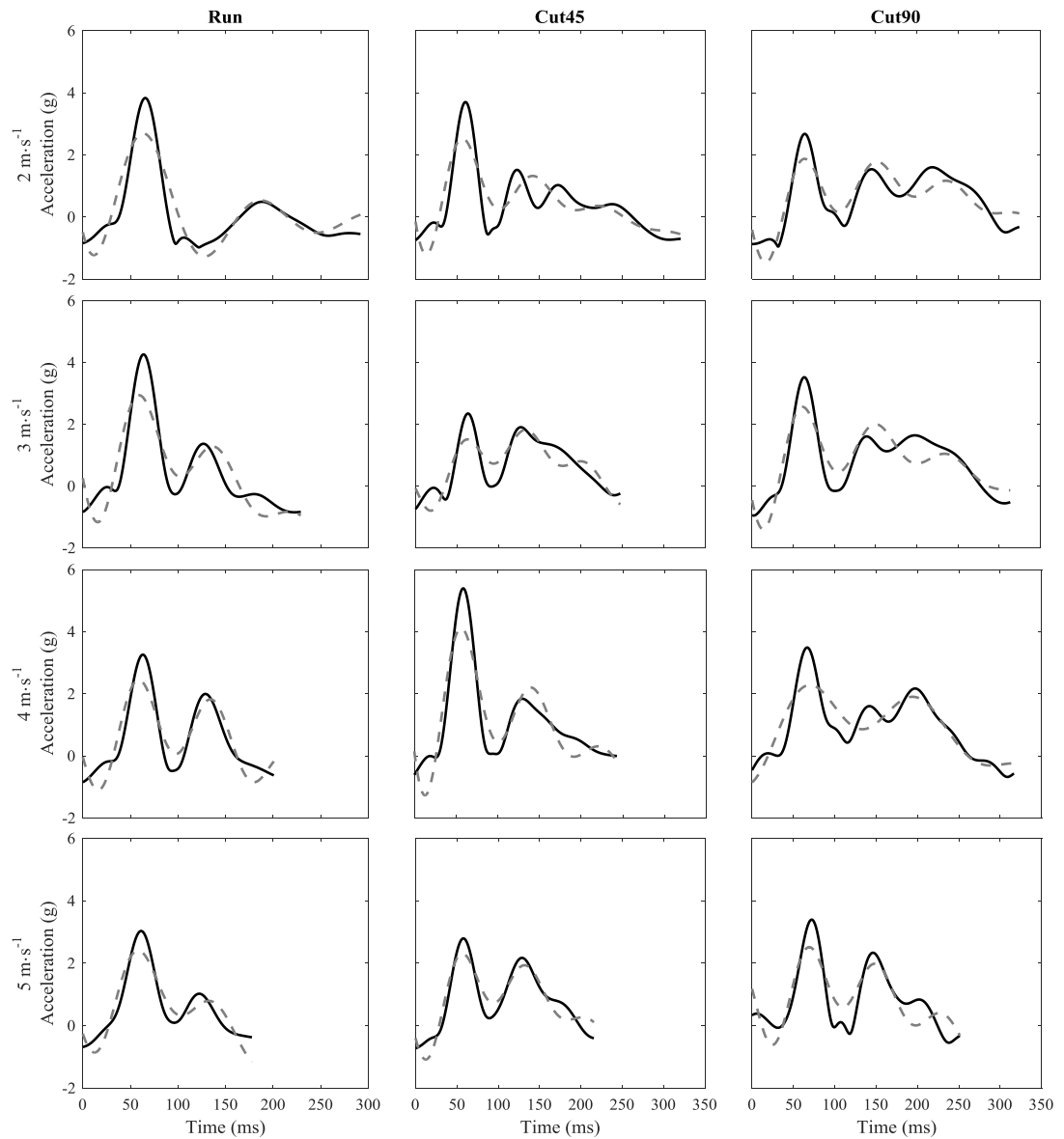


Figure H.1: Representative examples of the measured trunk acceleration from the laboratory accelerometer (black line) and a_1 (dashed grey line).

Model parameter sensitivity analysis

Similar average model parameters were obtained from the laboratory accelerometer data compared to the average model parameters observed in Chapter 4, where GPS integrated accelerometry was used as accelerometer/MSD-model input. Though larger average parameter values were observed for p_1 , p_2 , v_2 and λ across the different tasks and approach speeds (Figure H.2).

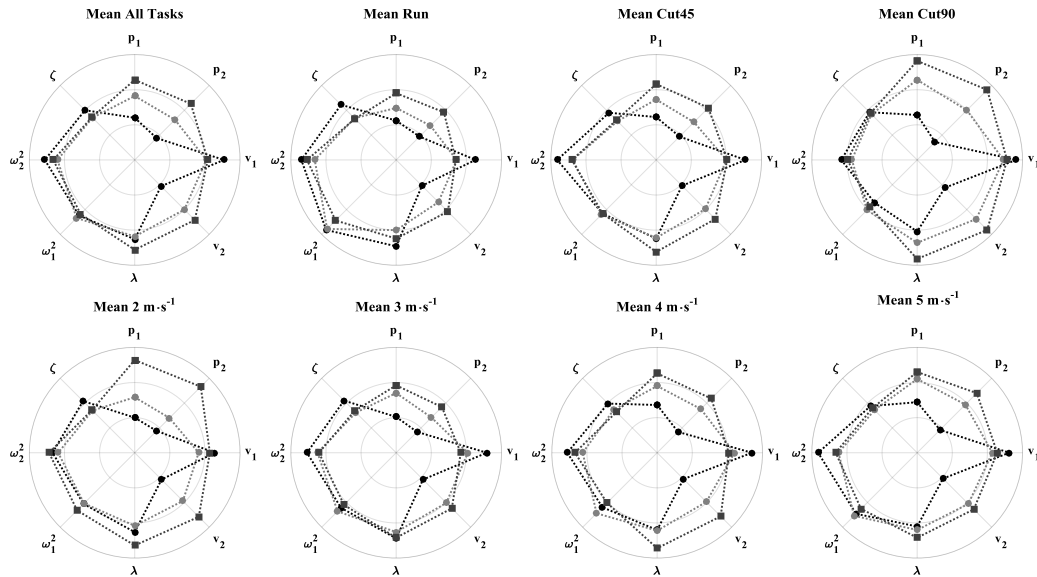


Figure H.2: Polar plots displaying the mean model parameters (in scaled dimensionless values) for the individual conditions. The dark grey squares display the laboratory accelerometer model parameters, the light grey circles display the GPS integrated accelerometer model parameter from Chapter 4 and the black circles display the $GRF_{measured}$ model parameters from Chapter 3.

A weak to moderate relationship (R^2 between 0.01 and 0.61) was observed from the linear regression analysis between the laboratory accelerometer and GRF model parameters (Figure H.3). This range was almost identical with the range observed in Chapter 4, and p_2 (R^2 : 0.22), v_1 (R^2 : 0.61), ω_1^2 (R^2 : 0.37) and ω_2^2 (R^2 : 0.38) again showed the strongest relationship with the GRF model parameters.

To improve the GRF predictions the new model parameter 3 (NP3) approach described in Chapter 4 was adopted to the laboratory accelerometer model parameters, in which p_1 , v_2 , λ and ζ were kept constant and p_2 , v_1 , ω_1^2 and ω_2^2 were recalculated based on the slope of the linear relationship (Figure H.3). Representative examples of $GRF_{modelNP3}$ from the laboratory accelerometer data is displayed in Figure H.4.

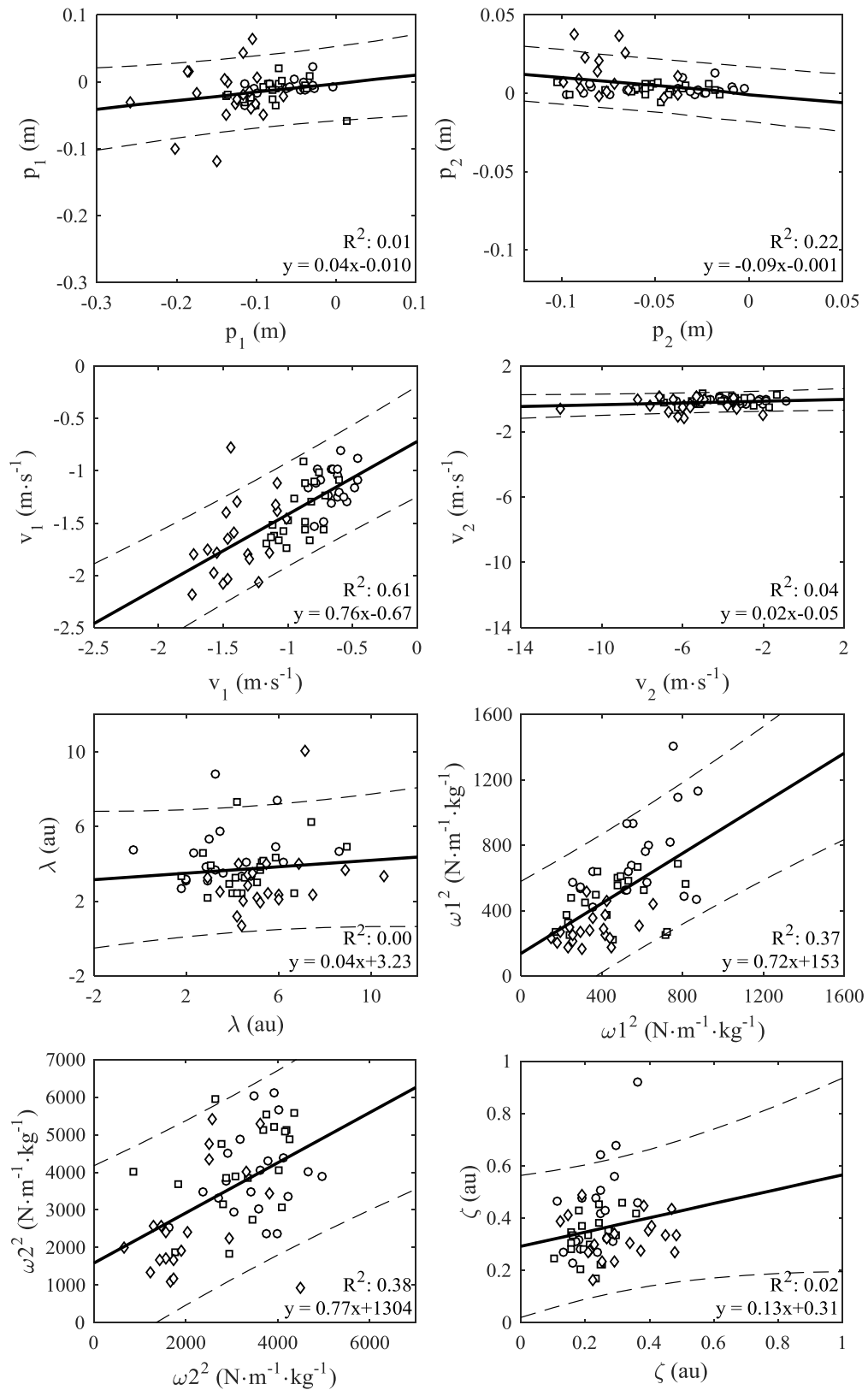


Figure H.3: Linear regression between laboratory accelerometer (horizontal axis) and $GRF_{measured}$ (vertical axis) model parameters. Each circle represents the participants mean within task parameters (Run: circle; Cut45: square and Cut90: diamond). Mean within task parameters outside the 95% prediction interval (dashed line) were not included in the regression analysis.

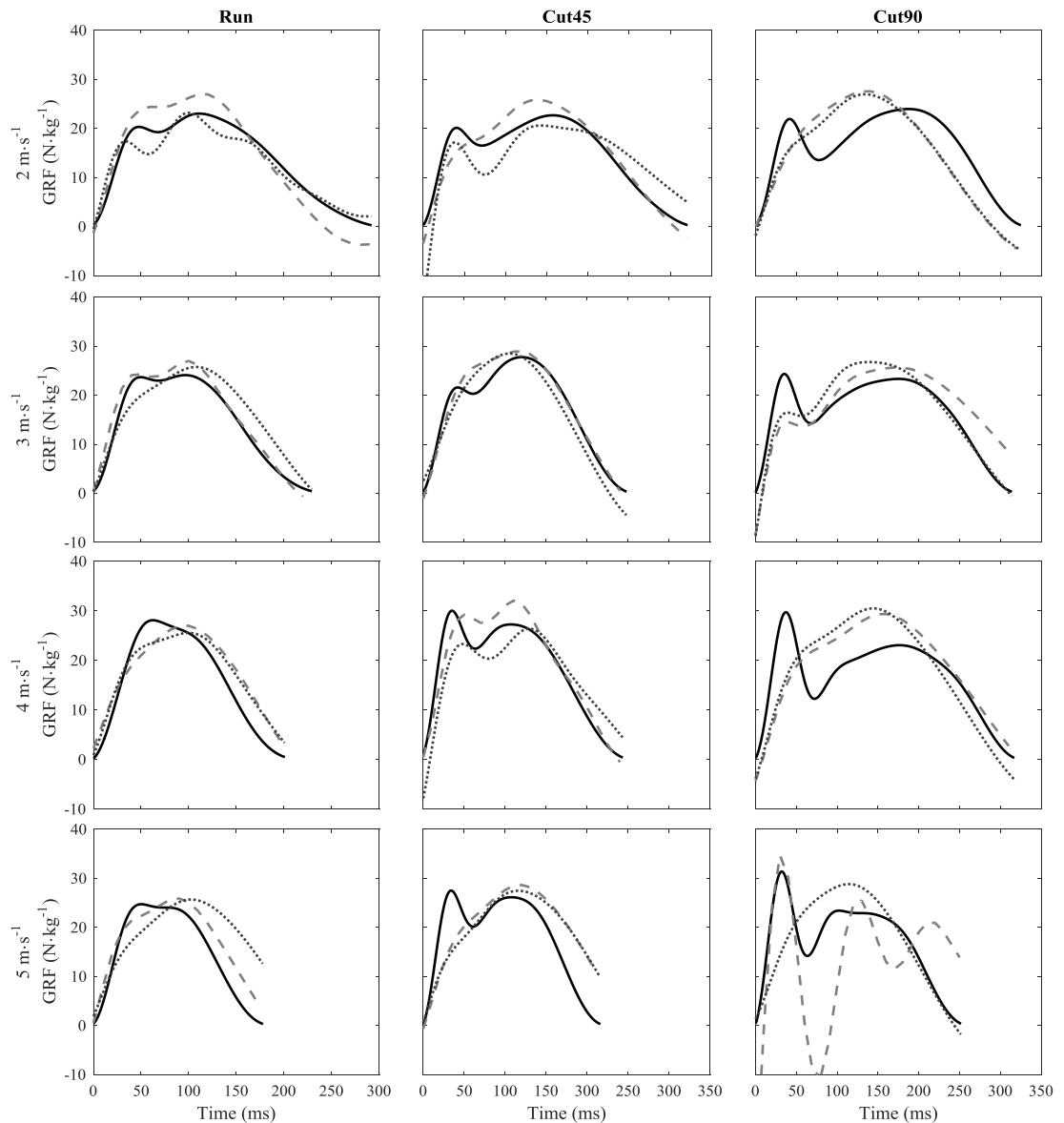


Figure H.4: Representative examples of the $GRF_{measured}$ (black line) and $GRF_{modelNP3}$ when GPS integrated accelerometer data (dashed grey line) and laboratory accelerometer data (dotted grey line) were used as accelerometer/MSD-model input.

Conclusion

The use of a wireless laboratory accelerometer with a higher sampling frequency (1000 Hz) compared to the GPS integrated accelerometer (100 Hz) only had minor influence on the optimised model parameters, the linear relationship with the $GRF_{measured}$ model parameters and therefore did not improve the predicted GRF from the accelerometer/MSD-model.

Appendix I: Acceleration from trunk kinematics as MSD-model input

The purpose of this appendix was to explore the sensitivity of the accelerometer/MSD-model to predict GRF when the vertical accelerations of the participant's trunk segment, obtained from a three-dimensional motion capture system, were used as accelerometer/MSD-model input.

Methods

Three-dimensional trunk kinematics from sixteen participants (age 22 ± 3 years, height 177 ± 8 cm, mass 74 ± 9 kg) were measured with 10 optoelectronic cameras (Qualisys AB, Gothenburg, Sweden) sampling at 500 Hz. The trunk segment was defined from a static measurement as described in (Vanrenterghem et al., 2010) and markers located at C7, Sternum, Xiphoid process and T8 were used to track the movements of the trunk during the different tasks and approach speeds (Figure I.1). Raw marker positions were filtered at 10 Hz using a fourth-order recursive Butterworth low-pass filter in Visual3D (C-motion, Germantown, MD, USA). Vertical trunk acceleration was calculated as the second time derivative of the vertical trunk displacement data in Visual3D for every foot-ground-contact and exported to Matlab, where the vertical trunk acceleration was used as MSD-model input.



Figure I.1: Pictures displaying the marker set used to measure the three-dimensional kinematics of the trunk segment. C7, Sternum, Xiphoid process and T8 (red circles) were used as tracking markers.

Results

The MSD-model was able to simulate the vertical trunk acceleration obtained from trunk kinematics with very good accuracy across tasks and approach speeds (Figure I.2). The simulations were considerably better than the simulations observed when GPS integrated accelerometry was used as model input in Chapter 4. In addition, the measurements reveal a difference between the acceleration signal obtained from trunk kinematics and trunk accelerometry (Figure I.2).

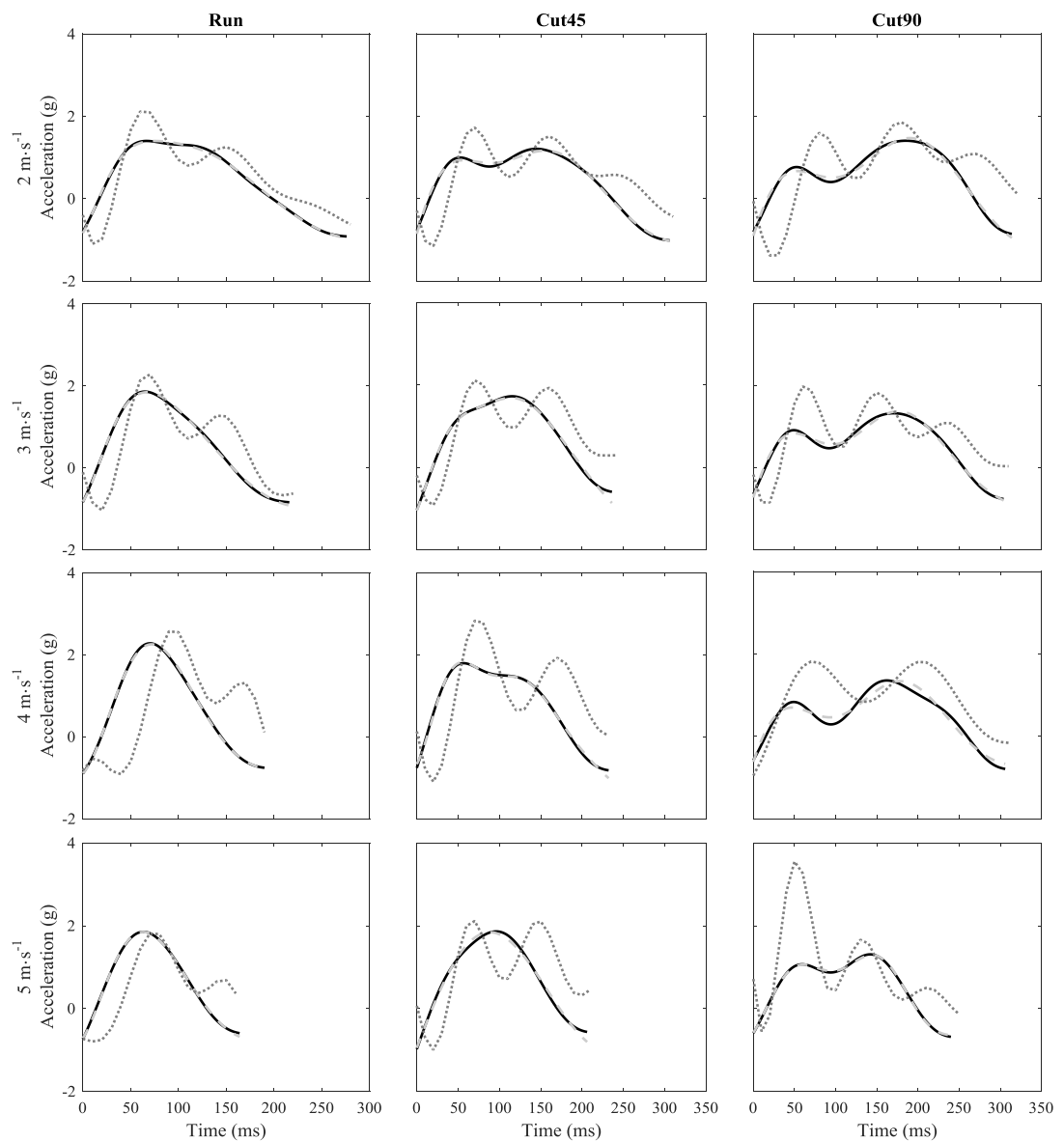


Figure I.2: Representative examples of the vertical trunk acceleration measured from trunk kinematics (black line) and a_1 when trunk kinematics (dashed grey line) and GPS integrated accelerometry (dotted grey line) were used as MSD-model input.

Despite the almost perfect simulations of the measured vertical trunk acceleration, poor to moderate GRF predictions were observed when the model parameters from the optimisation routine were used to calculate GRF_{model} (Figure I.3). Nevertheless, small improvements in the predicted GRF were observed when measured trunk acceleration was used as MSD-model input compared to the predicted GRF observed in Chapter 4.

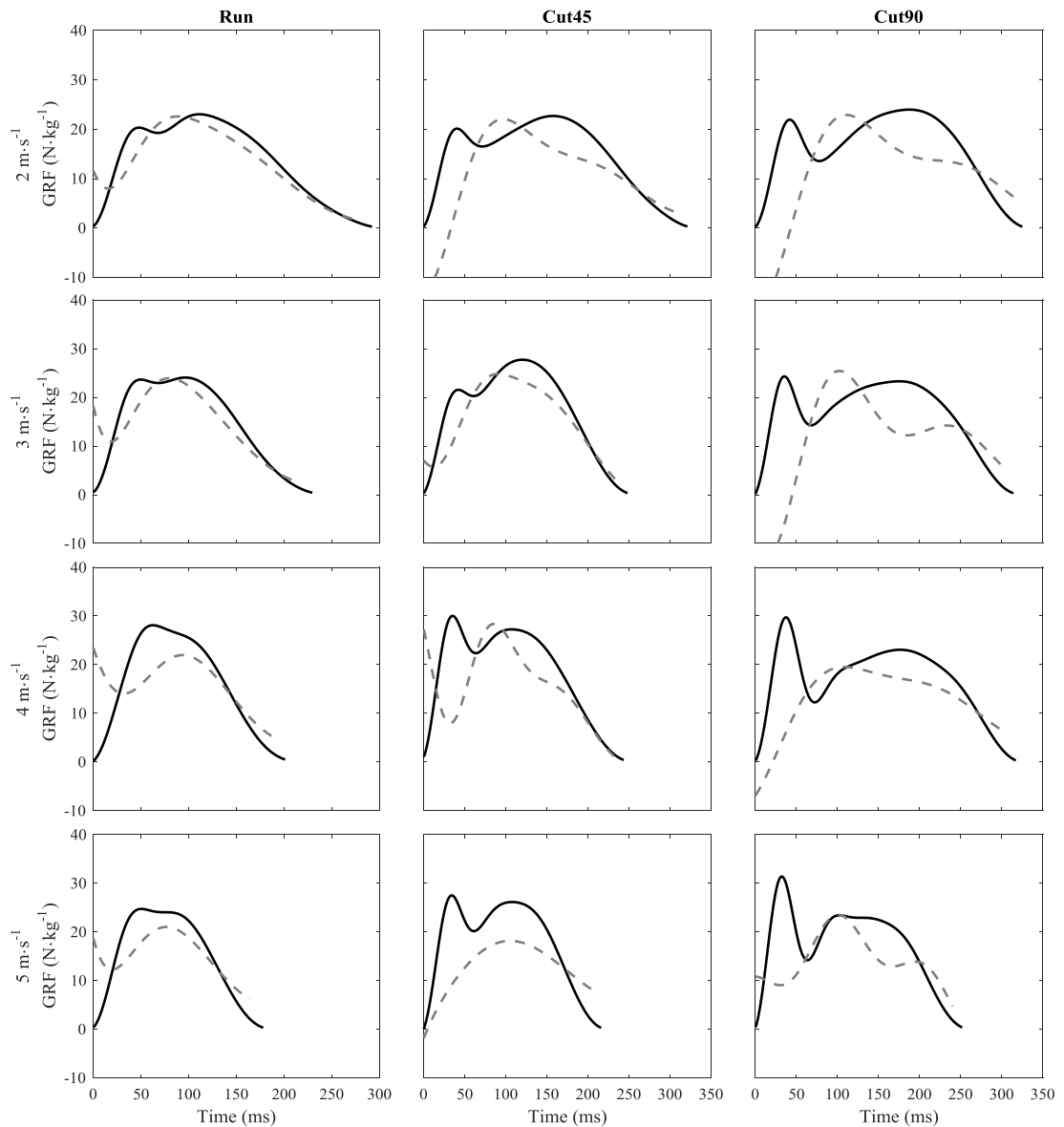


Figure I.3: Representative examples of $GRF_{measured}$ (black line) and GRF_{model} (dashed grey line) when vertical trunk acceleration from trunk kinematics was used as MSD-model input.

Model parameter sensitivity analysis

The average model parameters observed for p_2 , v_2 and ω_1^2 were similar to those observed in Chapter 4, where GPS integrated accelerometry was used as MSD-model input. The average model parameters observed for p_1 and v_2 from the vertical trunk acceleration were however closer to the $GRF_{measured}$ model parameters observed in Chapter 3. In contrast were worse model parameters observed for λ , ω_2^2 and ζ when the vertical trunk acceleration signal was used as MSD/model input compared to the model parameters observed in Chapter 4, see Figure I.4.

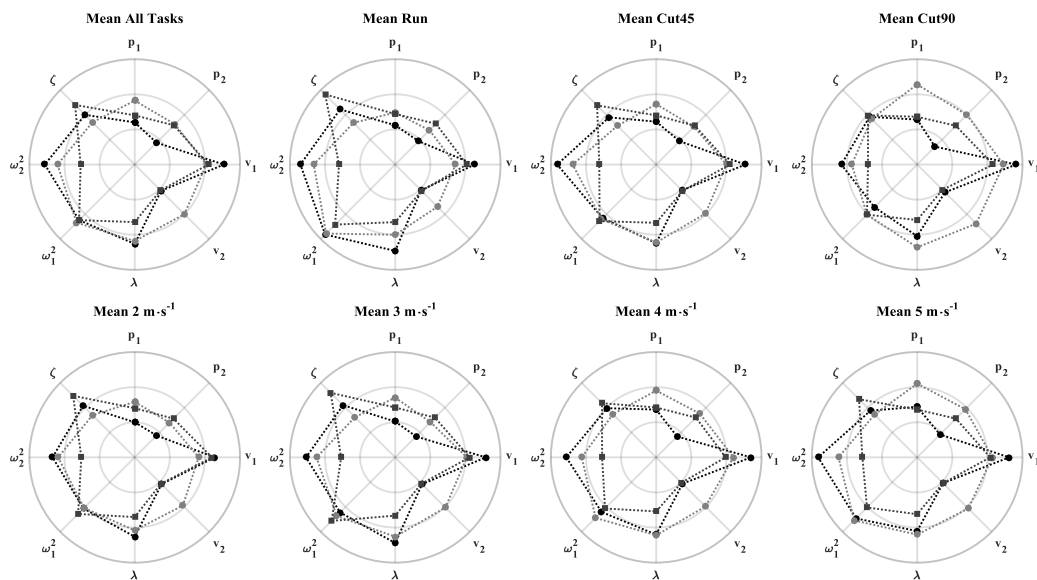


Figure I.4: Polar plots displaying the mean model parameters (in scaled dimensionless values) for the individual conditions. The dark grey squares display the parameters from vertical trunk acceleration, the light grey circles display the GPS integrated accelerometer parameters from Chapter 4 and the black circles display the $GRF_{measured}$ parameters from Chapter 3.

Moderate relationships (R^2 between 0.19 and 0.61) were observed for all model parameters, despite v_2 (R^2 : 0.02), between the vertical trunk acceleration model parameters and $GRF_{measured}$ model parameters from Chapter 3 (Figure I.5). Stronger correlations were especially observed for p_1 , λ and ζ (R^2 between 0.19 and 0.36) compared to the correlations observed in Chapter 4 (R^2 between 0.01 and 0.05).

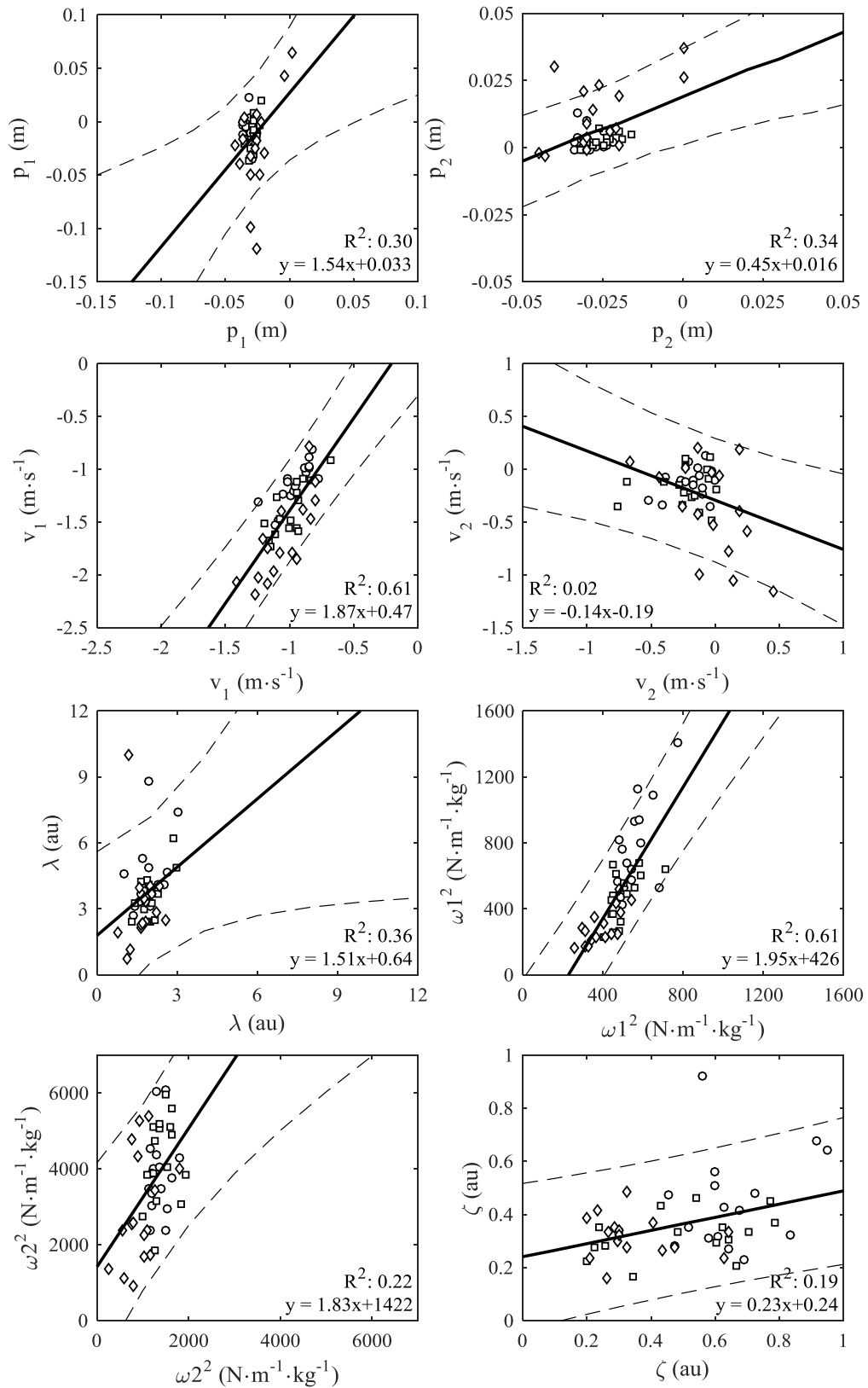


Figure I.5: Linear regression between vertical trunk kinematic (horizontal axis) and $GRF_{measured}$ (vertical axis) model parameters. Each circle represents the participants mean within task parameters (Run: circle; Cut45: square and Cut90: diamond). Mean within task parameters outside the 95% prediction interval (dashed line) were not included in the regression analysis.

New model parameters (NP) were therefore generated by recalculating all model parameters from the slope of the linear regression, despite v_2 which was kept constant. Nevertheless, worse GRF predictions were observed from the new model parameters ($GRF_{modelNP}$) compared to the GRF predictions observed from the model parameters obtained directly from the optimisation routine (GRF_{model}), see Figure I.6.

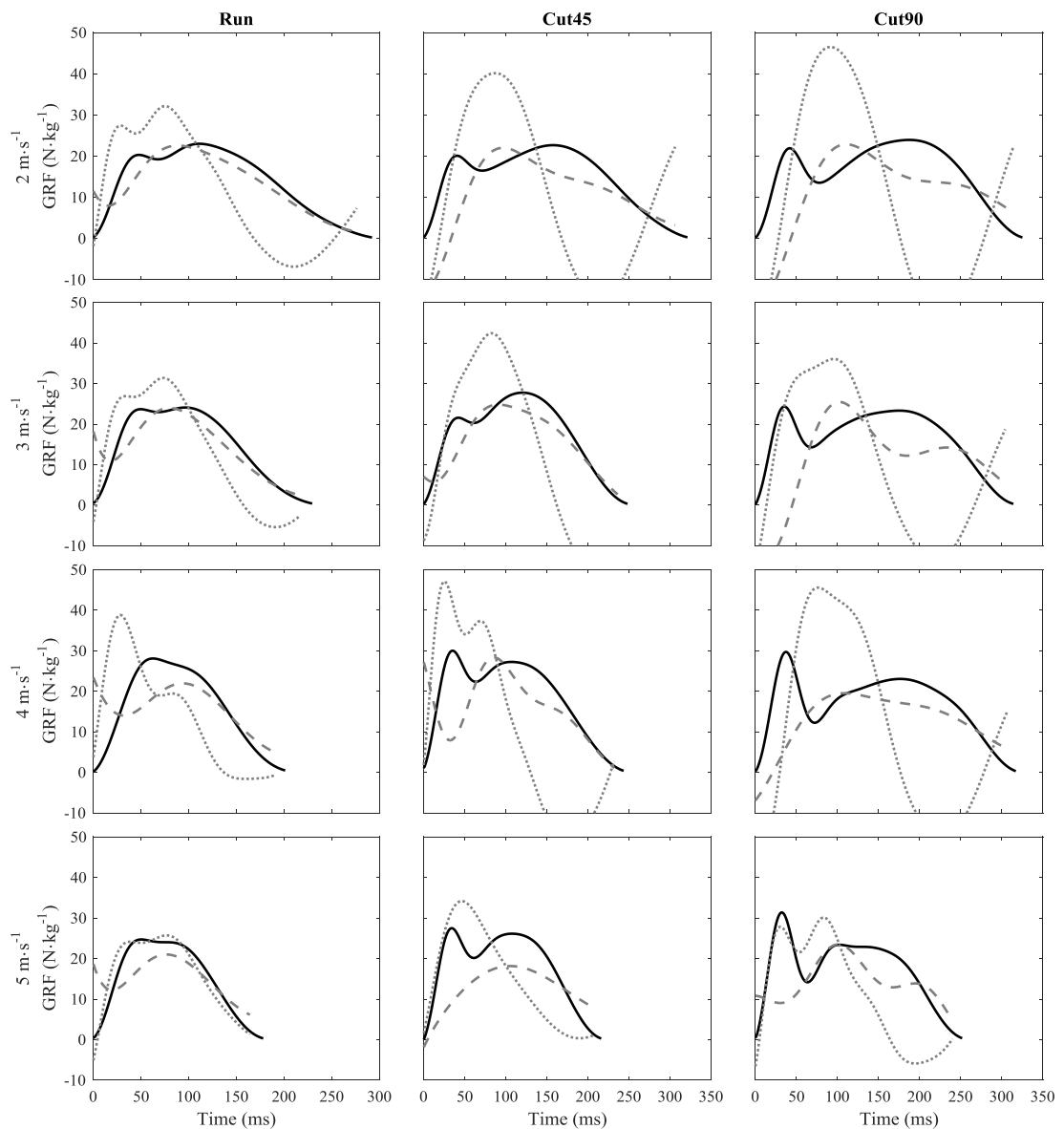


Figure I.6: Representative examples of the $GRF_{measured}$ (black line), $GRF_{modelNP}$ (dotted grey line) and GRF_{model} (dashed grey line) when vertical trunk acceleration measured from trunk kinematics was used as MSD-model input for the difference tasks and approach speeds.

Conclusion

Though better MSD-model upper mass acceleration simulations were observed when vertical acceleration from trunk kinematics was used as MSD-model input compared to Chapter 4. Nevertheless, this generally did not improve the GRF_{model} predictions from the MSD-model. The best GRF_{model} predictions were observed from the model parameters obtained directly from the optimisation routine, whereas worse GRF_{model} predictions were observed when v_2 was kept constant and the other model parameters were recalculating from the slope of the linear regression. Other model parameter combinations might improve the GRF_{model} predictions, but it was beyond the scope of this sensitivity analysis to establish those.

Appendix J: Sensitivity analysis of fixed model parameters on SSE_{GRF}

The purpose of this appendix was to explore the sensitivity of the fixed model parameters and the predicted GRF. In Chapter 4, the fixed model parameters (p_1 , p_2 , v_2 , λ and ζ) were kept constant using the across task average model parameters found in Chapter 3. However, in this sensitivity analysis the fixed model parameters were kept constant using the average task parameters (e.g. average Run parameters for all running trials) or average condition parameters (e.g. average Run at $3 \text{ m}\cdot\text{s}^{-1}$ parameters for all running trials with an approach speed at $3 \text{ m}\cdot\text{s}^{-1}$) values found in Chapter 3.

The results from this sensitivity analysis showed that using average task or condition (task and approach speed) model parameters values as the fixed parameter values when GRF_{model} were calculated from NP3, NP4 or NP5 generally did not improve the GRF_{model} predictions (Figure J.1). In fact, this actually increased the SSE_{GRF} for the Cut90 task and only had minor influence on the predicted GRF for the Run and Cut45. Future study should explore if the use of subject specific model parameters will improve the predicted GRF.

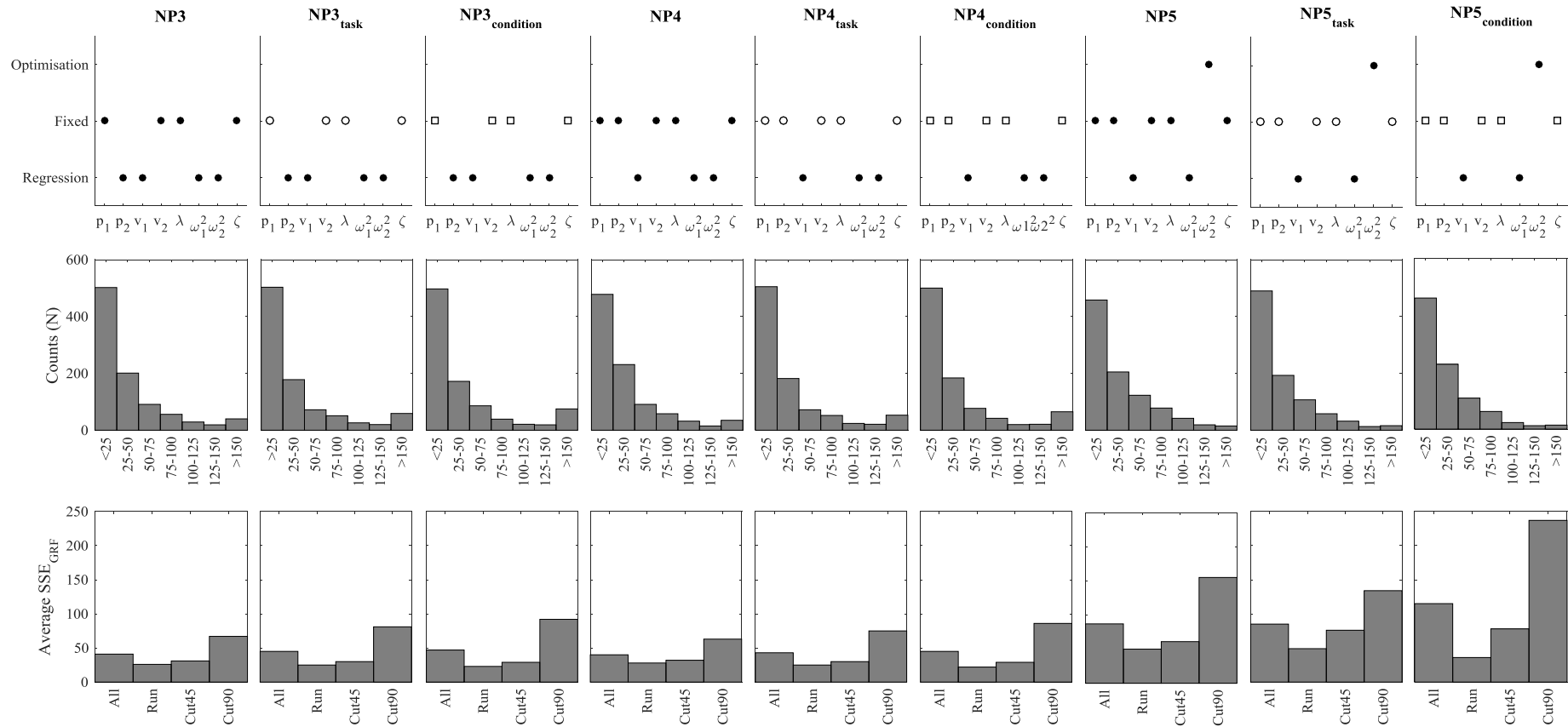


Figure J.1: The top row display the new model parameter combinations (NP), where the open circles indicate that the parameters were kept constant using the average task parameters found in Chapter 3, and the open squares indicate that the model parameters were kept constant using the average parameter value of the individual conditions. The second row display the histograms of the SSE_{GRF} distribution and the bottom row display the average SSE_{GRF} across tasks (All) and for the individual tasks.

Appendix K: Sensitivity analysis of changing $\text{GRF}_{\text{measured}}$ model parameters

The purpose of this appendix was to illustrate the effect of changing the individual $\text{GRF}_{\text{measured}}$ model parameters on $\text{GRF}_{\text{model}}$ and explore whether the effect was dependent on the original GRF pattern.

Four GRP patterns from the same participant and $\text{GRF}_{\text{measured}}$ model parameters from the associated trials were used in this sensitivity analysis. Only one parameter was changed while the other seven model parameters were kept constant, similar to the approach described in Derrick et al. (2000). The change in the individual parameters were based on the mean standard deviations observed in Chapter 3.

This sensitivity analysis clearly showed that the effect of changing the individual model parameters were largely dependent on the original GRF pattern and the stance phase (Figure K.1). v_1 , λ , ω_1^2 , ω_2^2 and ζ were in particular sensitive to small changes in model parameters. The effect of changing two or more model parameters is yet to be established.

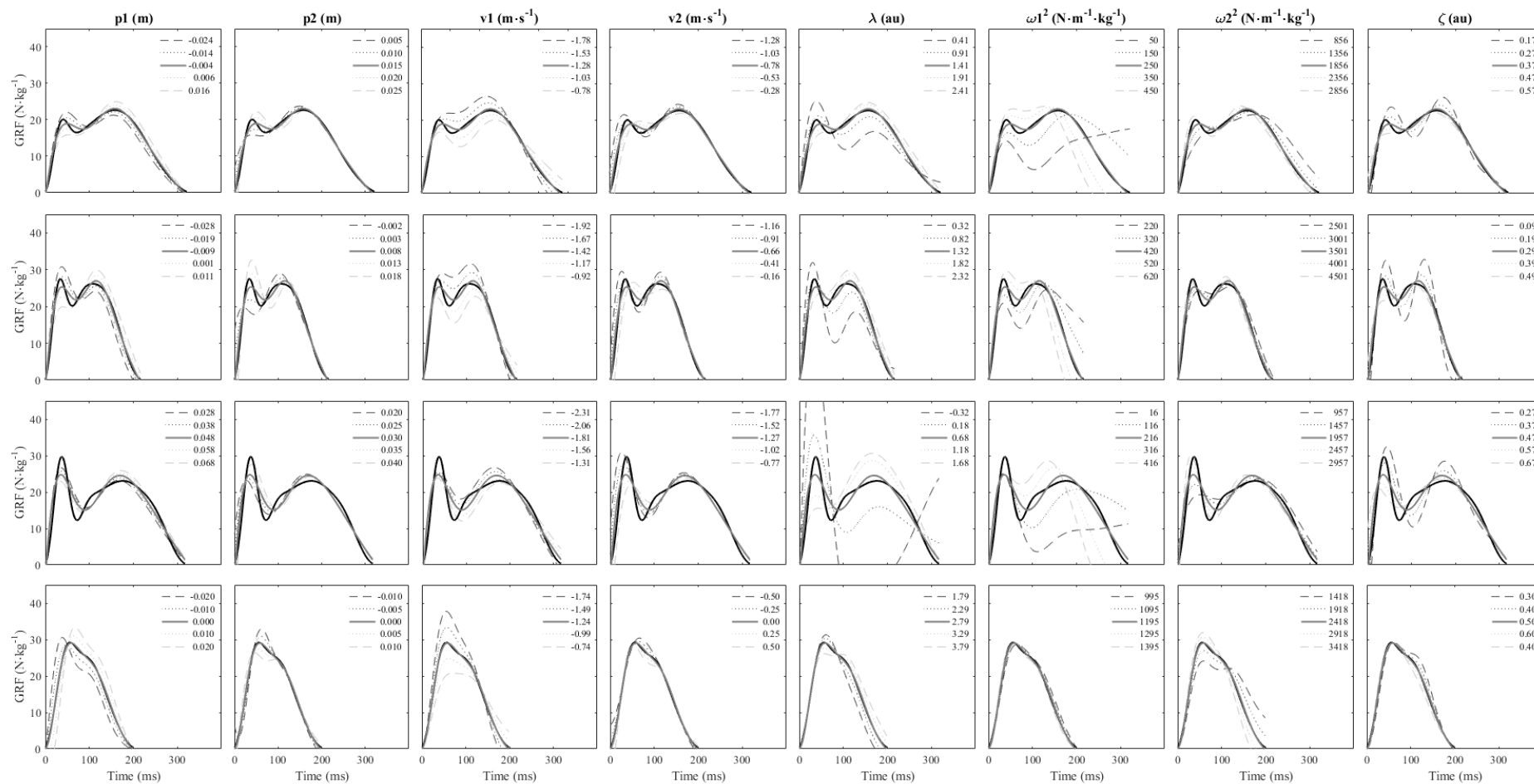


Figure K.1: Displaying the effect of changing one parameter on GRF_{model} for four different GRF patterns from the same participant.

Appendix L: Foot-contact identification from GPS integrated accelerometry

The purpose of this appendix was to explore the variation in acceleration values at touch down and take off from the GPS integrated accelerometers. This is of interest because the novel accelerometer/MSD-model introduced in this thesis are applied to the accelerometer signal from the foot-ground-contact.

The acceleration signal from all participants, tasks and approach speeds from this thesis were used in this explorative sensitivity analysis of the variation in the acceleration signal at touch down and take off. The vertical GRF (20 N threshold) was used to determine the acceleration values at touch down and take off in the resultant gravity corrected acceleration signal measured with the GPS integrated accelerometer (Table L.1).

Table L.1: Mean ± standard deviations of the gravity corrected acceleration values (g) at touch down and take off from the GPS integrated accelerometers.

	Touch down		Take off		Average	
	Mean	SD	Mean	SD	Mean	SD
All tasks	-0.51	0.14	-0.40	0.12	-0.46	0.08
Run	-0.63	0.11	-0.48	0.14	-0.55	0.10
Cut45	-0.47	0.22	-0.35	0.12	-0.41	0.09
Cut90	-0.41	0.21	-0.44	0.19	-0.43	0.02
2 m·s⁻¹	-0.72	0.13	-0.61	0.11	-0.67	0.08
3 m·s⁻¹	-0.59	0.13	-0.43	0.16	-0.51	0.11
4 m·s⁻¹	-0.53	0.18	-0.36	0.16	-0.44	0.12
5 m·s⁻¹	-0.21	0.25	-0.20	0.18	-0.21	0.01
Run 2 m·s⁻¹	-0.79	0.05	-0.71	0.10	-0.75	0.06
Run 3 m·s⁻¹	-0.67	0.15	-0.53	0.19	-0.60	0.10
Run 4 m·s⁻¹	-0.68	0.14	-0.45	0.18	-0.57	0.16
Run 5 m·s⁻¹	-0.36	0.30	-0.25	0.29	-0.30	0.08
Cut45 2 m·s⁻¹	-0.67	0.28	-0.59	0.10	-0.63	0.06
Cut45 3 m·s⁻¹	-0.61	0.17	-0.44	0.17	-0.52	0.12
Cut45 4 m·s⁻¹	-0.51	0.22	-0.28	0.24	-0.39	0.17
Cut45 5 m·s⁻¹	-0.09	0.36	-0.07	0.27	-0.08	0.01
Cut90 2 m·s⁻¹	-0.69	0.17	-0.59	0.14	-0.64	0.07
Cut90 3 m·s⁻¹	-0.55	0.21	-0.48	0.25	-0.51	0.05
Cut90 4 m·s⁻¹	-0.35	0.39	-0.45	0.32	-0.40	0.07
Cut90 5 m·s⁻¹	-0.10	0.33	-0.28	0.17	-0.19	0.13

Though differences were observed in the acceleration values at touch down and take off between the Run (-0.55 ± 0.10 g) and the two change in direction tasks (Cut 45: -0.41 ± 0.09 g; Cut90: -0.43 ± 0.02 g), superior differences were observed between approach speeds. In particular for the $5 \text{ m}\cdot\text{s}^{-1}$ (-0.21 ± 0.01 g) where smaller touch down and take off acceleration values were observed compared to the other approach speeds (-0.67 ± 0.08 g to -0.44 ± 0.12 g).

Applying a threshold to the acceleration signal would be the logical approach to determine the players foot-ground-contact from the GPS integrated accelerometer in the field. Nevertheless, this explorative study indicate that such threshold might be task dependent and surely dependent on the speed which the player is running at. This could have implications on the accelerometer/MSD-model introduced in this thesis, because the acceleration signal will differ depending on the threshold applied to the accelerometer signal. Future studies should therefore explore the sensitive of the foot-ground-contact threshold on the model parameters obtained from the accelerometer/MSD-model.